

ELECTRICAL COMMUNICATION

*Technical Journal of the
International Telephone and Telegraph Corporation
and Associate Companies*

●

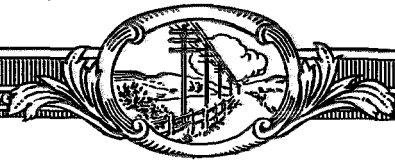
AUTOMATIC HELIARC WELDING
PRODUCTION-LINE PAINTING METHODS
SELENIUM RECTIFIERS FOR CONTACT PROTECTION
REMOTE SIGNALING AND CONTROL OF RAILWAY POWER NETWORKS
ELECTRICAL AND PHYSICAL PROPERTIES OF IN-420 DIELECTRIC
MICROWAVE TECHNIQUE FOR STUDYING DISCHARGES IN GASES
TELEPHONE STATISTICS OF THE WORLD
PROPAGATION OF SPACE-CHARGE WAVES IN ELECTRON BEAMS
THERMAL-VELOCITY SPREAD AND NOISE FIGURE IN TRAVELING-WAVE TUBES
COMPOSITE-DIELECTRIC COAXIAL LINE
LINEAR PASSIVE NONRECIPROCAL MICROWAVE CIRCUIT COMPONENT



Volume 30

JUNE, 1953

Number 2



ELECTRICAL COMMUNICATION

*Technical Journal of the
International Telephone and Telegraph Corporation
and Associate Companies*

H. P. WESTMAN, Editor
J. E. SCHLAJKER, Assistant Editor

EDITORIAL BOARD

H. Busignies H. H. Buttner G. Chevigny E. M. Deloraine W. Hatton B. C. Holding
W. P. Maginnis A. W. Montgomery E. D. Phinney G. Rabuteau N. H. Saunders C. E. Scholz
T. R. Scott C. E. Strong A. E. Thompson A. J. Warner E. N. Wendell H. B. Wood

Published Quarterly by the
INTERNATIONAL TELEPHONE AND TELEGRAPH CORPORATION
67 BROAD STREET, NEW YORK 4, NEW YORK, U.S.A.

Sosthenes Behn, Chairman William H. Harrison, President
Geoffrey A. Ogilvie, Vice President and Secretary

Subscription, \$2.00 per year; single copies, 50 cents

Electrical Communication is indexed in Industrial Arts Index

Copyrighted 1953 by International Telephone and Telegraph Corporation

Volume 30

JUNE, 1953

Number 2

CONTENTS

AUTOMATIC HELIARC WELDING	83
PRODUCTION-LINE PAINTING METHODS	84
<i>By J. T. Pederson</i>	
INVESTIGATION OF THE SELENIUM RECTIFIER FOR CONTACT PROTECTION	96
<i>By H. F. Herbig and J. D. Winters</i>	
REMOTE SIGNALING AND CONTROL OF ELECTRIC RAILWAY POWER NETWORKS	106
<i>By Jacques Van Cauwenberghe</i>	
ELECTRICAL AND PHYSICAL PROPERTIES OF IN-420: A NEW CHLORINATED LIQUID DIELECTRIC	118
<i>By A. J. Warner</i>	
MICROWAVE TECHNIQUE FOR STUDYING DISCHARGES IN GASES	124
<i>By M. A. Lampert and A. D. White</i>	
TELEPHONE STATISTICS OF THE WORLD	129
PROPAGATION OF SPACE-CHARGE WAVES IN INFINITE AND FINITE ELECTRON BEAMS	134
<i>By Philip Parzen</i>	
EFFECT OF THERMAL-VELOCITY SPREAD ON THE NOISE FIGURE IN TRAVELING-WAVE TUBES	139
<i>By Philip Parzen</i>	
COMPOSITE-DIELECTRIC COAXIAL LINE	155
<i>By J. A. Kostriza</i>	
NEW LINEAR PASSIVE NONRECIPROCAL MICROWAVE CIRCUIT COMPONENT	164
<i>By Ladislav Goldstein and M. A. Lampert</i>	
CONTRIBUTORS TO THIS ISSUE	166





Automatic Heliarc Welding

THE frontispiece illustrates an automatic process of welding aluminum as developed by Federal Telephone and Radio Corporation. The process is currently being used in the production of cases for the new army field telephone switchboard.*

The three parts that are welded are shown below. It will be noted that the center partition is slightly larger than the outside dimension of the case. This overhang of the center partition is used as a filler when fusing takes place in the welding operation; no filler rod is therefore needed.

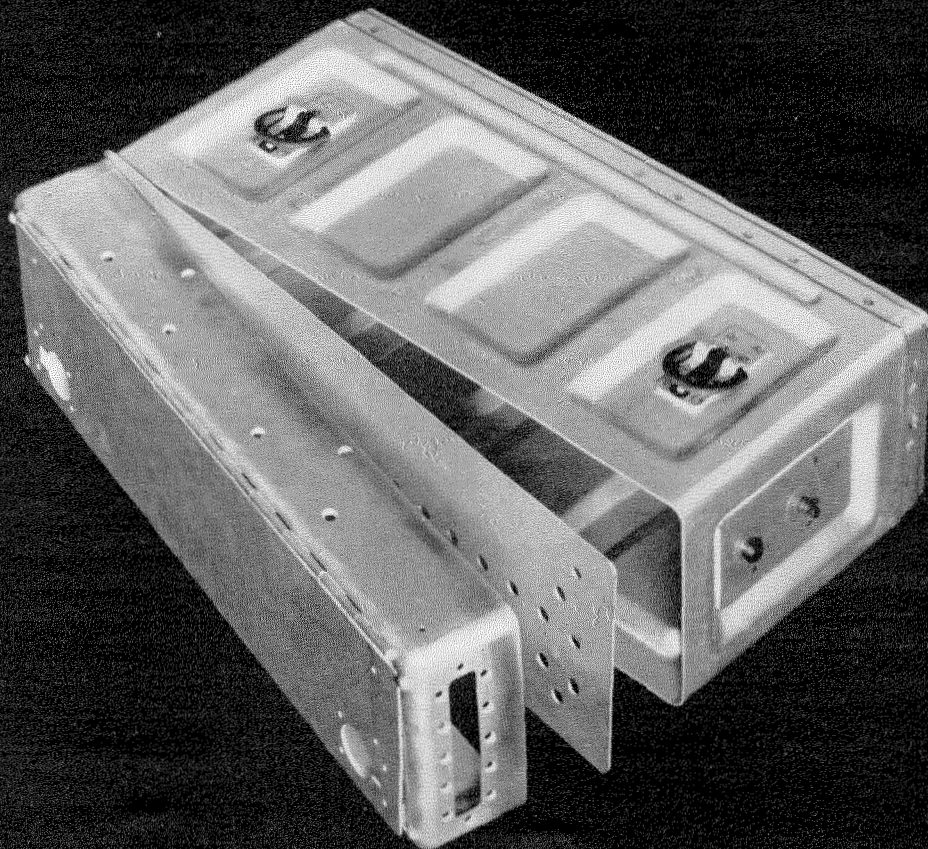
The frontispiece shows the operator observing the flow of metal and adjusting the electrode

while welding the case. The heliarc process is essentially electric-arc welding with the molten metal protected from oxidation by a flow of inert helium gas. The three parts of the case are assembled on the holding fixture, which is an integral part of the machine, and the entire perimeter of the case is then tracked automatically past the welding electrode.

Due to small variations in materials and manufacturing tolerances, the operator must make slight adjustments of the height of the electrode to ensure an unbroken flow of metal while the machine is in operation.

Perhaps the most interesting feature of the process is that despite the sharp turns at the corners of the case, a constant and carefully governed rate of surface speed is maintained past the electrode for the entire welding cycle.

* "Manufacture of a Field Telephone Switchboard," *Electrical Communication*, volume 29, pages 93-107; June, 1952.



Production-Line Painting Methods

By J. T. PEDERSON

The Coolerator Company; Duluth, Minnesota

A PPEARANCE is an important factor in selling a product today. One may wonder what percentage of consumers buy refrigerators, freezers, or automobiles by appearance alone. It would be impossible to arrive at the exact number, but it is known that a large portion of the public buy with their eye.

Besides appearance there are other reasons for applying a good paint finish. Corrosion protection is of primary importance and is only possible through good metal preparation and finishing. The purpose of this article is to describe an automatic production-line painting system incorporating heated-paint sprayers with electrostatic paint-control methods. Before describing the flow of the ware through the production line, some of the more unique features will be taken up.

1. Paint Heating System

Paint heaters are installed on top of the spray booths. These raise the paint to a constant temperature of about 140 degrees fahrenheit (60 degrees centigrade), winter and summer. The system is of a circulatory type, the heated paint circulating back to the heater from the spray gun when the gun is shut off. This assures that a constant supply of heated paint is always at the spray-gun nozzle.

The advantages of this system are numerous. By heating the paint, the amount of thinner required to reduce the paint to a sprayable viscosity is lessened considerably. With less thinner, a heavier coat of paint can be applied without sagging or producing an orange-peel effect. Less thinner also means less time to cure the ware in the ovens, thereby saving fuel. By putting on a heavier coat of paint in one application, better coverage is obtained and also there is a saving in spraying time. The heated paint requires less air pressure for atomization and this reduced pressure lessens overspray paint loss.

Working conditions are improved also, as less thinner is dispersed in the air, and there is less spray fog rebound from the ware.

2. Automatic Spraying System

The spray guns are turned on automatically when the ware is in the correct position for spraying. Some of the guns spray down at the top of the ware while others spray up at the bottom. Still others spray horizontally from arms that reciprocate vertically. The guns are turned on and off by microswitches operated by triggers fastened to the hooks on the conveyor chain. These triggers are set to turn on the proper guns to give the best paint coverage on whatever type of ware may be passing by.

As an example, when painting refrigerator door liners, the guns aimed at the top and bottom do not operate since there is no surface there to be painted. In the case of a refrigerator cabinet, however, all guns would operate to cover the top and bottom of the cabinet as well as its sides. If no ware is hanging on the hook, none of the guns operate.

3. Electrostatic Control of Paint

If the paint particles are sprayed between two electrodes that are negatively charged with 100,000 volts, the particles will acquire a negative electrostatic charge. This negatively charged paint is then attracted to the electrically grounded ware on the conveyor line, since there is an attraction between unlike charges. This system helps save paint since most of the paint that would normally overspray is attracted to the ware. It also helps to control the paint thickness on the surface of the ware. The electrostatic spraying system is used on laminated plastic-impregnated paper objects as well as on metal parts. The plastic parts are made electrically conductive by incorporating graphite in the resin solution from which they are made.

Because of electrostatic attraction, the painted ware will pick up dirt particles very easily; for instance, it can pick the lint from the clothes of a person standing near by. To prevent this, the personnel working in the paint department wear starched white coveralls or coats, and the whole department area is pressurized to keep dirt from

drifting in. Observation windows are provided so that the automatic painting system can be observed without actually entering the spraying booth.

4. Flow of Ware Through Finishing Department

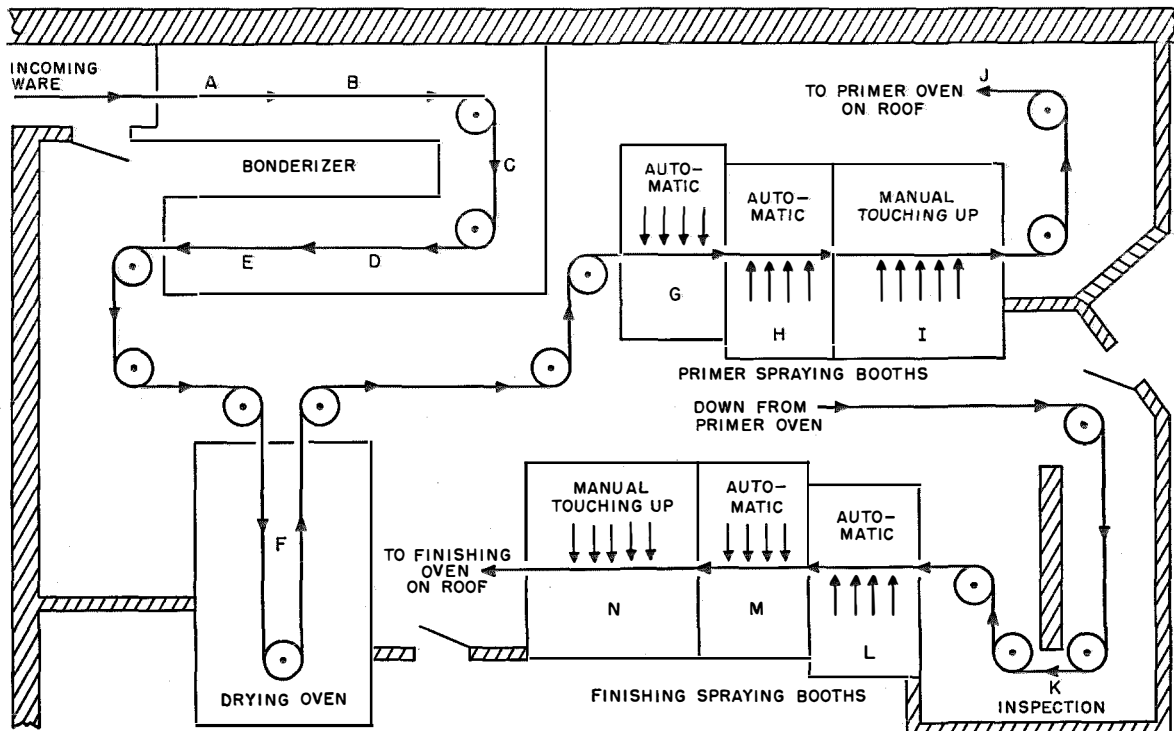
As paint will not adhere properly to an oily, dirty, or moist surface, the preliminary surface preparation is of primary importance. This preparation is called bonderizing. It consists of several stages of spraying systems that wash, rinse, and apply the proper protective coatings before painting. The coating applied in this process not only serves as a bond between metal and paint, but also prevents spreading of rust should the finish be scratched through to the base metal. The importance of a well-prepared surface before painting cannot be over-emphasized. Bonderizing is accomplished in steps *A* through *E* indicated in the drawing below.

After leaving the bonderizer, the part enters the drying oven *F*. It next enters the first automatic primer-spraying booth *G*. Just before it arrives in front of the spray guns, a trigger on the conveyor hook trips the proper microswitch

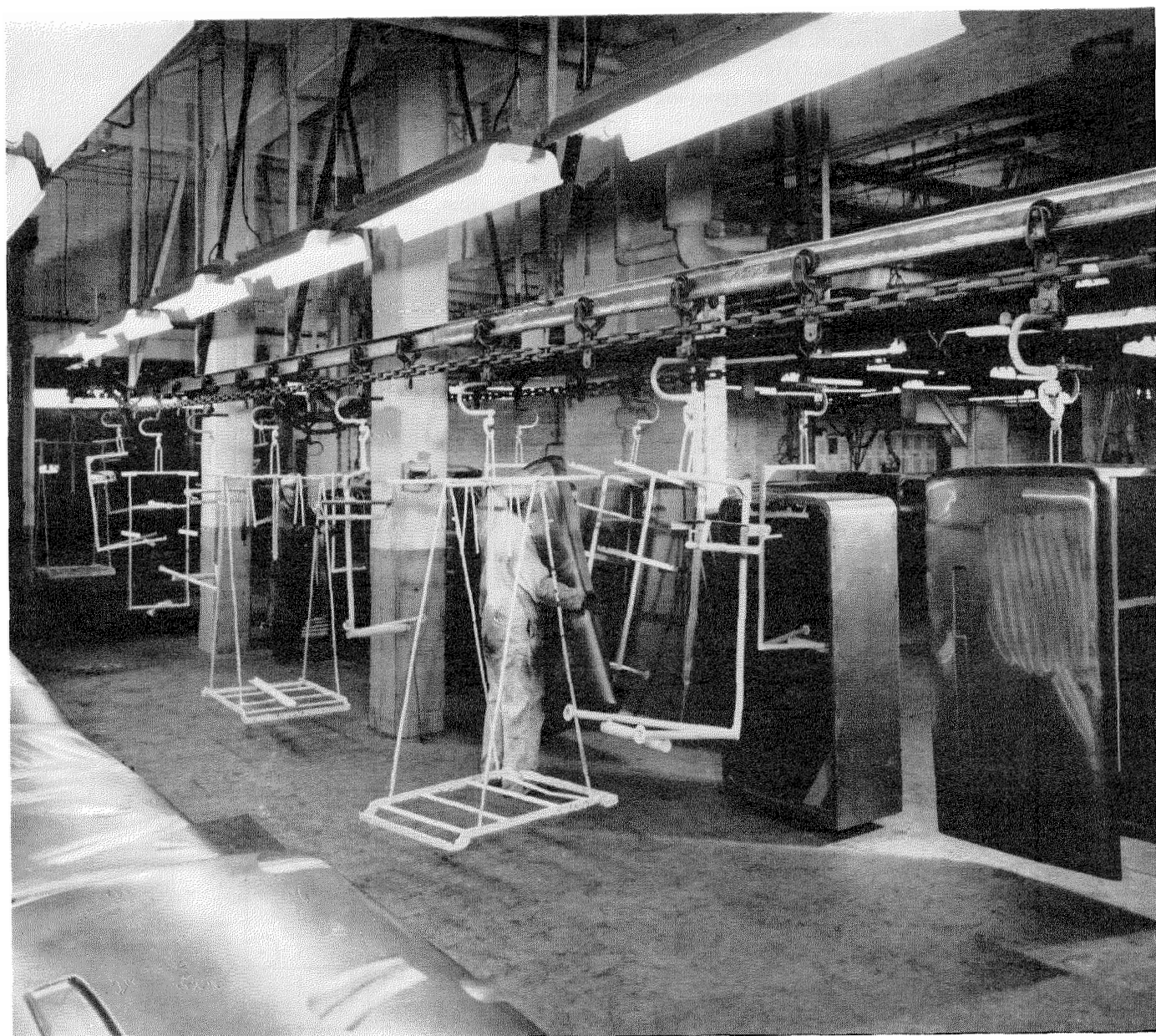
to actuate the automatic spray guns. By starting to spray before the ware is directly in front of the guns, the leading edge is partially covered by paint particles that are electrostatically attracted to it. The reciprocating guns give complete coverage of one side and then as the ware passes by the guns, the trailing edge is partially covered. When the ware is a little past the guns, they turn off.

The ware next enters the second primer-spraying booth *H* where the guns spray from the other side. Here, the leading and trailing edges are completed, and the other side of the cabinet is covered. In the primer-reinforcing booth *I* some areas may be given additional coverage manually. The ware then goes up to the roof to the primer oven *J*, where it is baked.

After baking, at *K* it is inspected, sanded, and wiped free of dust with a tack rag, (a cloth coated with a semidrying varnish that leaves the cloth tacky enough to pick up all dust). In three booths, *L*, *M*, and *N*, identical to the primer booths, the finish coat is applied. The ware then goes to the finishing oven where it is again baked. The last step is a careful inspection before sending the painted ware on to the assembly line.

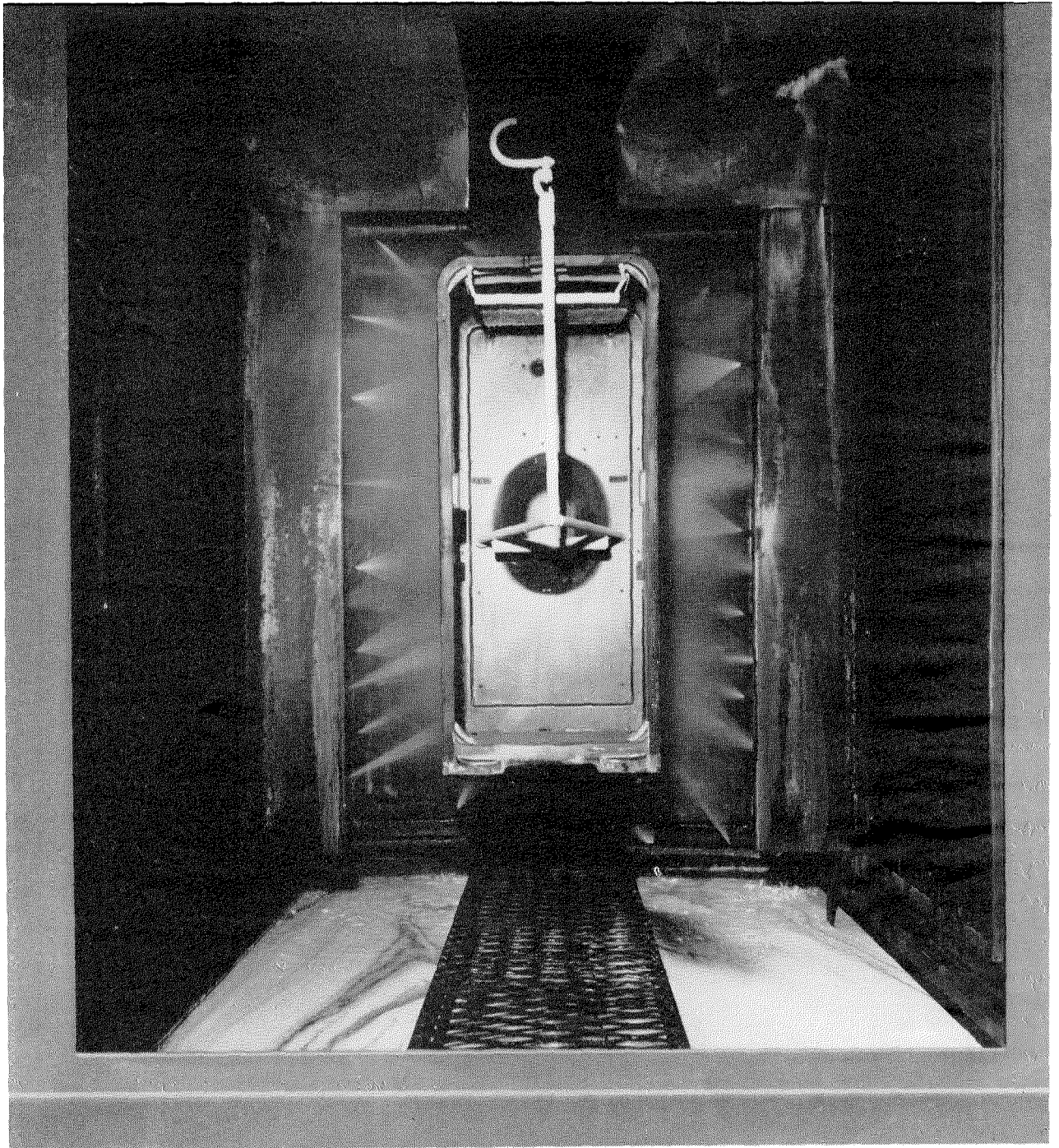


Arrangement of production-line painting system at The Coolerator Company in Duluth, Minnesota.



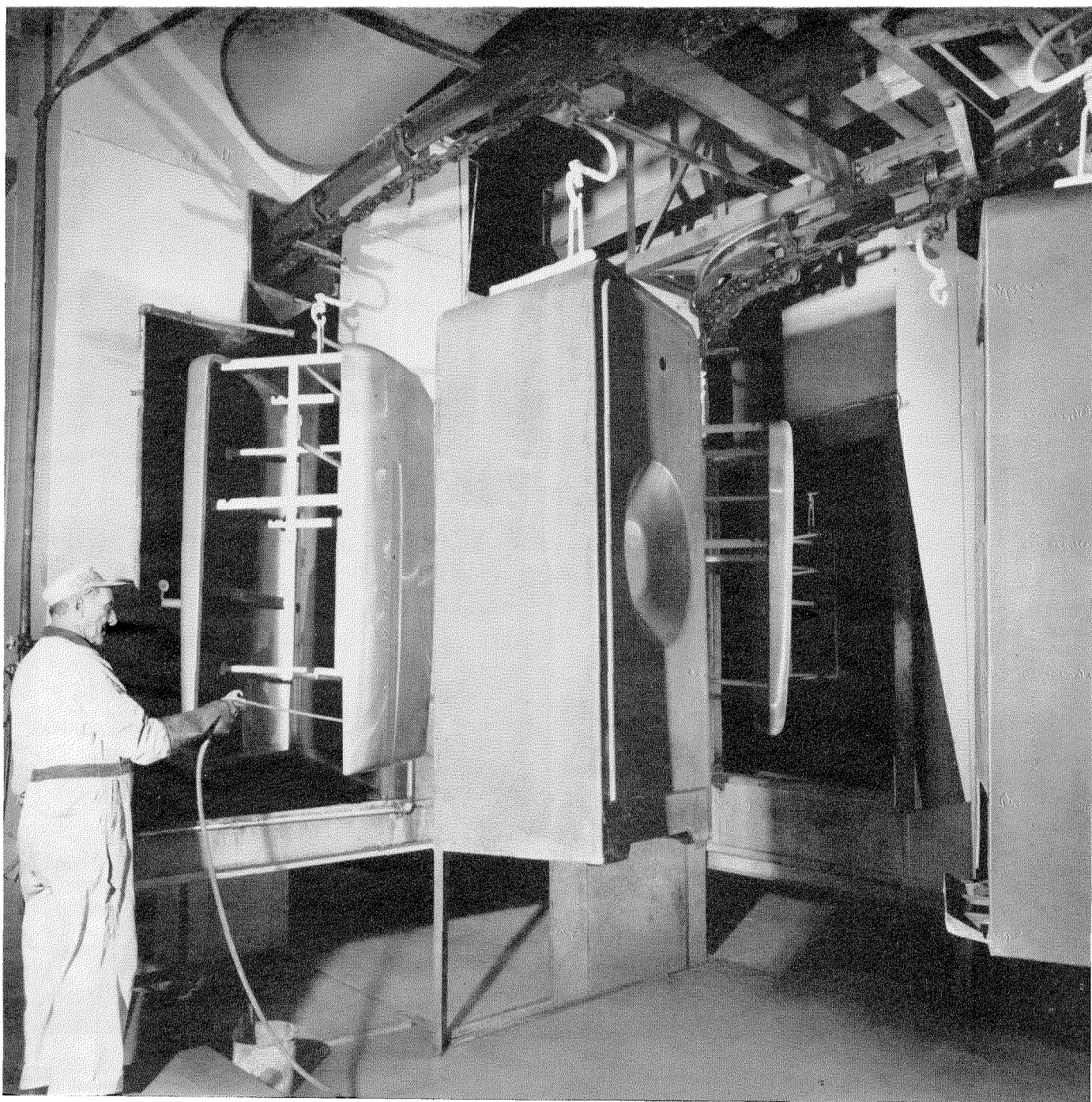
1. After all metal work is finished, refrigerator parts are hung on the conveyor chain that will carry them through the painting department. Note that different types of parts may be next to each other on the conveyor, and each will receive proper paint coverage for its type.

2. The ware entering the bonderizer is sprayed from all sides to assure good chemical preparation of the metal before painting. Various cleaning and phosphatizing chemicals are sprayed on, alternating with rinses.

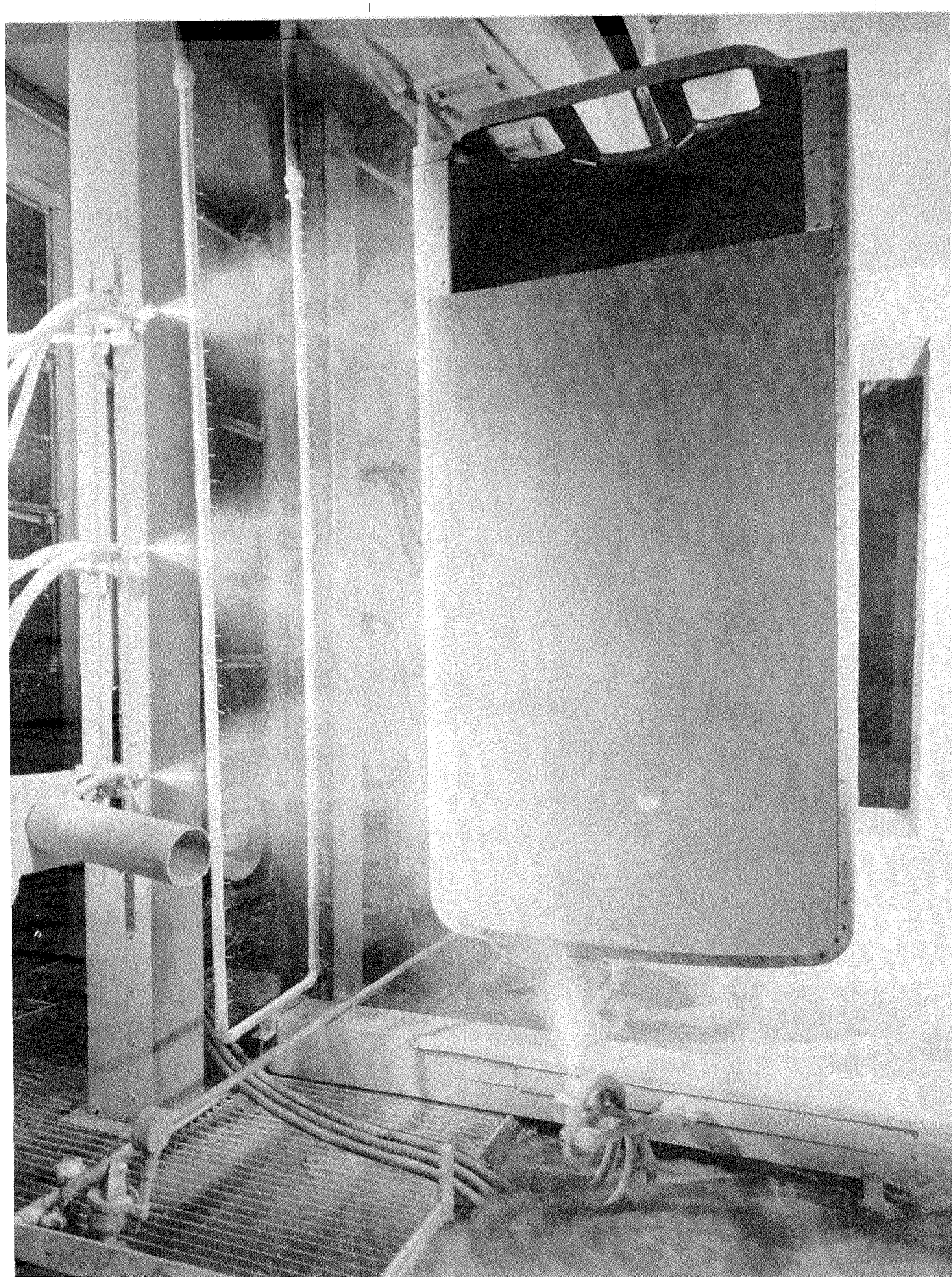


3. Below, excess solution is blown from the ware by means of an air hose as it leaves the bonderizer at the left. It will next enter the drying oven in the right background.

4. On the opposite page is shown the alley in the center of the bonderizer booths; an operator takes samples of the solutions for control tests.



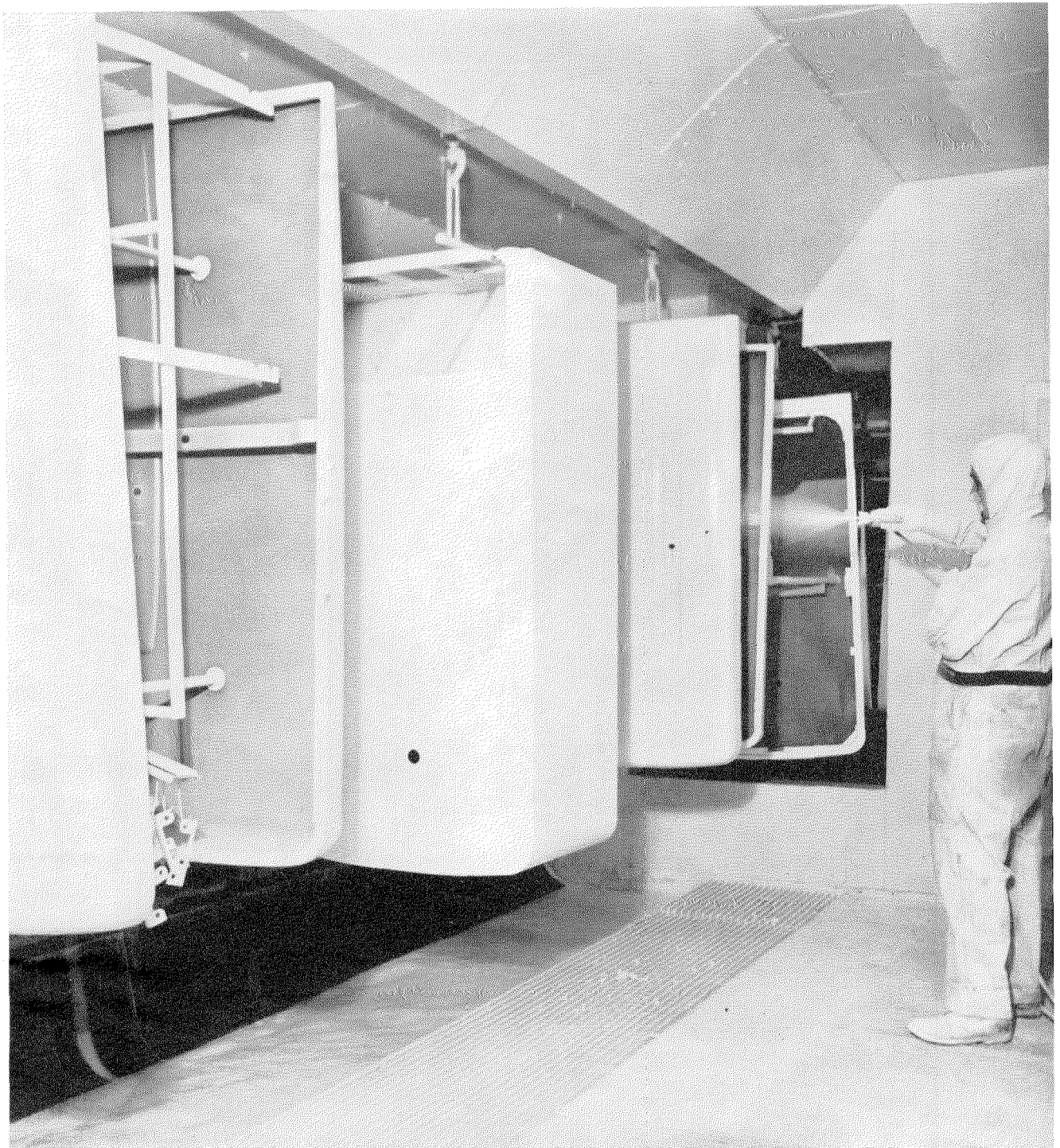




5. Paint leaving the guns on the reciprocating arms at the left passes between the two bars with ionizing points. The bars give the paint particles an electrostatic charge that attracts them to the object being painted.

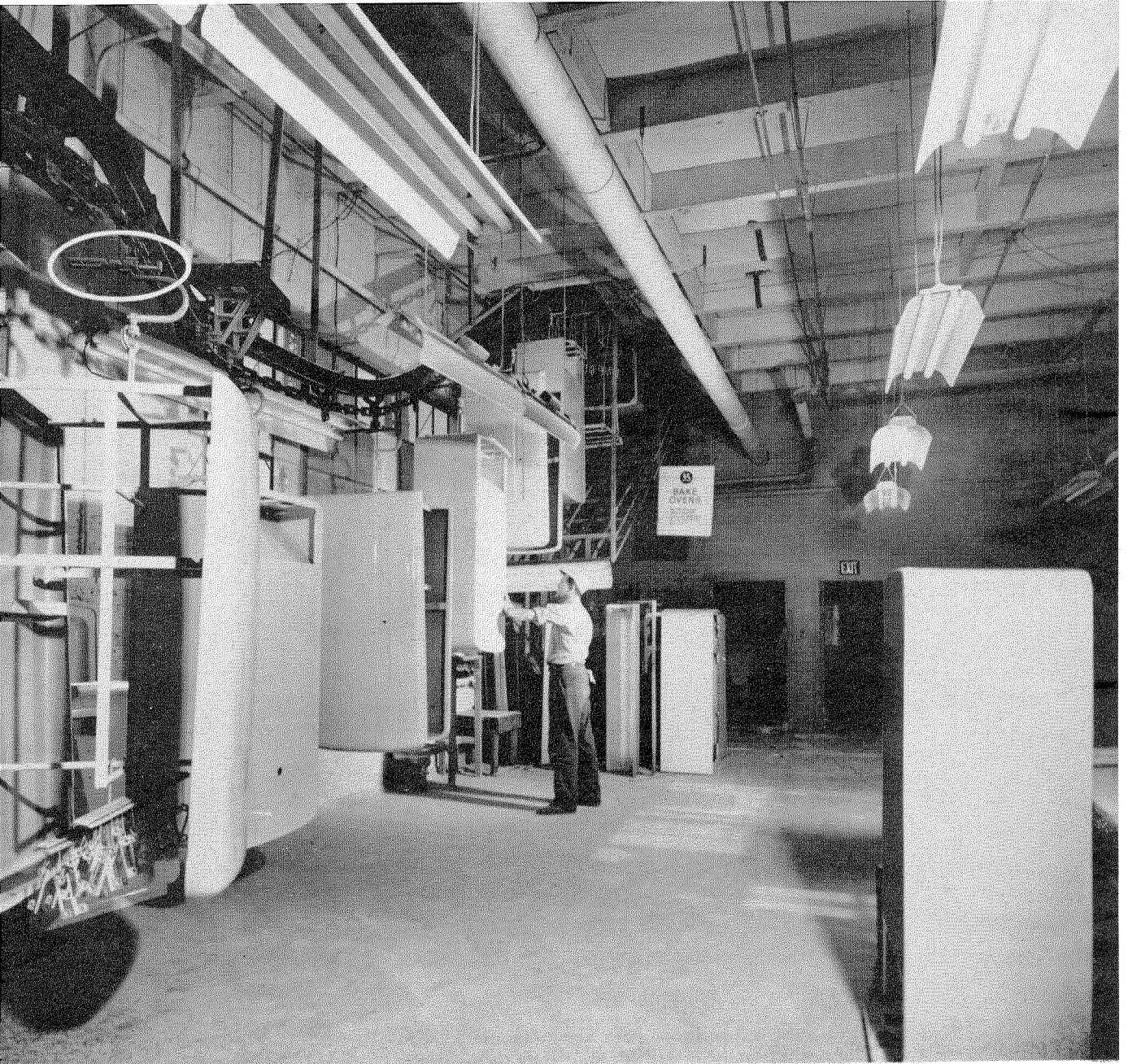


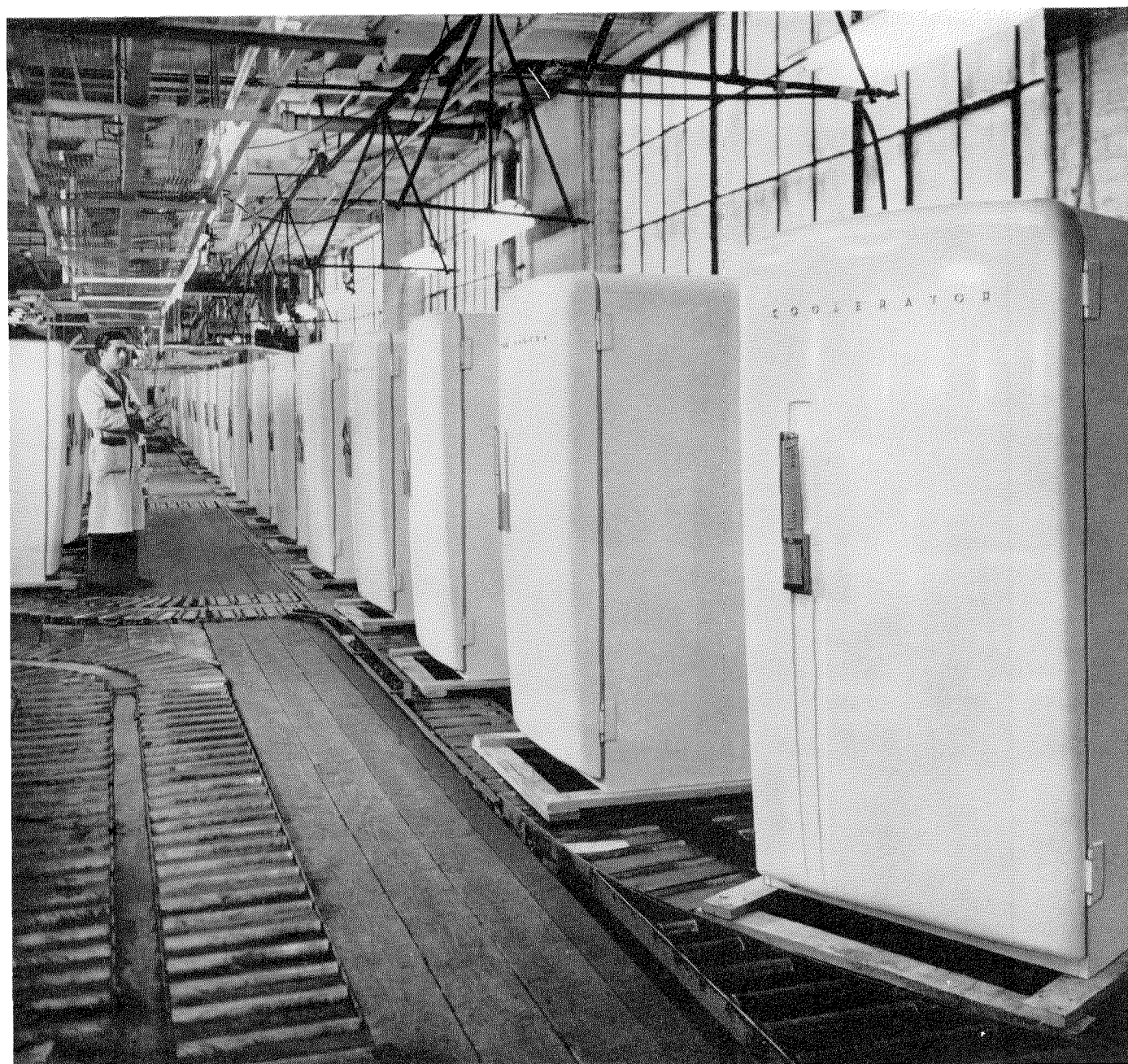
6. The author at the controls of one of the two 100,000-volt power packs that supply the electrostatic charge in the paint-spraying booths.



7. In the manual touching-up booth, the enamel paint coat is reinforced along the edges after it has passed through the two automatic booths.

8. Refrigerator parts being inspected after coming down from the finishing oven on the roof. Defective parts are removed for refinishing at the right. A trigger arm that starts the electrostatic reciprocating spray guns is encircled. The setting of each arm depends on the particular shape of the object to be painted, and varies the number of spray guns that operate.

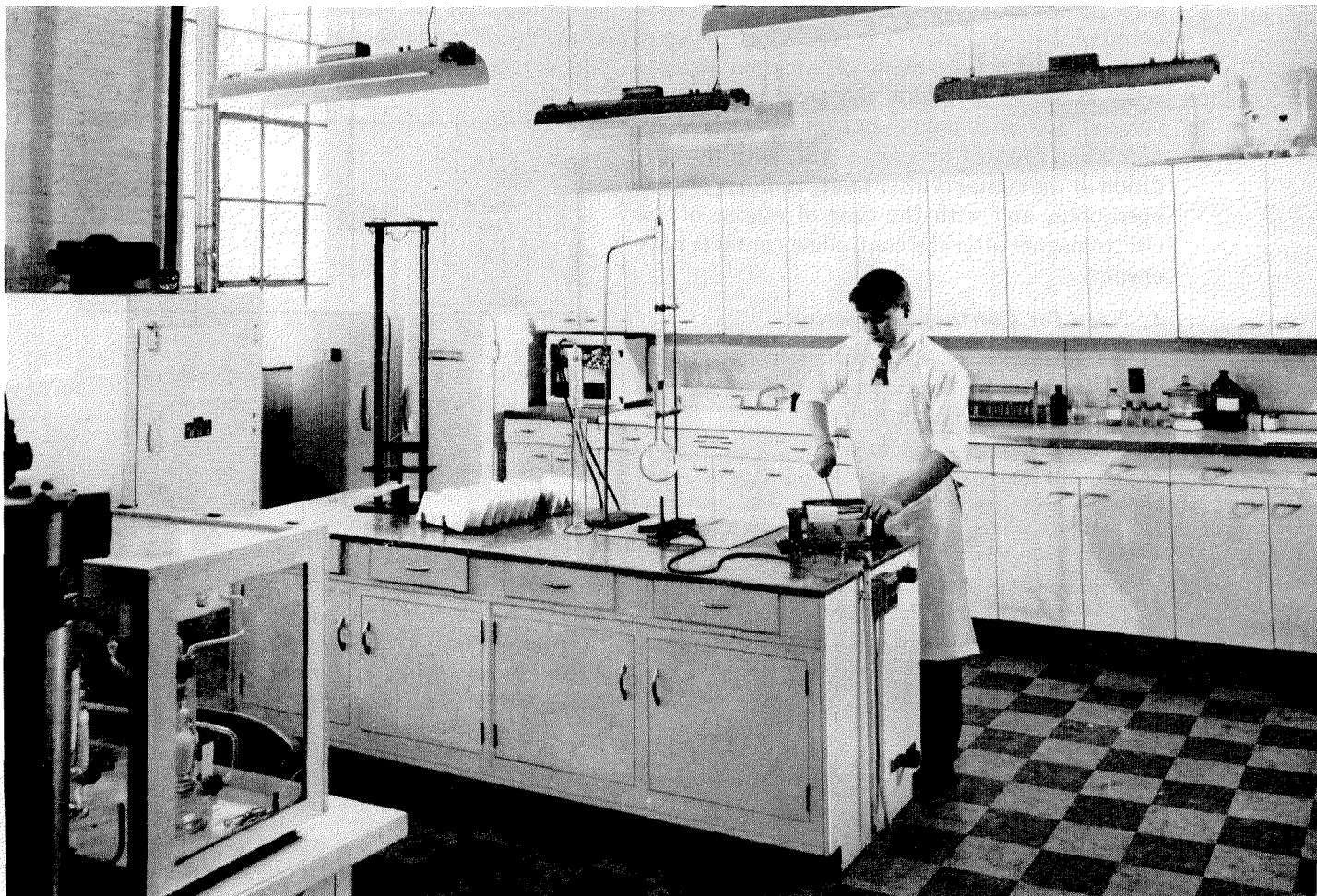




9. A row of finished refrigerators after assembly and final inspection. These will next be crated for shipment to the dealer.

The present trend in household refrigerators provides a separate low-temperature freezing compartment at the top.

10. Below, a laboratory technician tests a paint sample for adhesion by bending it around a conical mandrel. A tray of painted test panels may be seen on the table to the right of the "guillotine" that is also used to test the adhesion of the enamel finish to the metal.



Investigation of the Selenium Rectifier for Contact Protection*

By H. F. HERBIG and J. D. WINTERS

Federal Telecommunication Laboratories, Incorporated; Nulley, New Jersey

A VOLTAGE surge suppressor is described comprising selenium rectifier cells connected in series (in opposed relation) whereby the resulting resistance is high at low voltages and low at high voltages.

This combination of rectifiers, when used for electrical-contact protection, results in an excellent arc-suppressing device that does not materially affect the release time of the shunted electromagnet.

The history of selenium rectifiers is well known and has been published in its various aspects in a number of articles.¹ The primary use of selenium rectifiers has been in the rectification of alternating current for power applications. Among the special applications, particularly in the telephone field, selenium rectifiers have been used as contact protectors.

This paper deals with an application of the selenium rectifier for contact protection in such a manner as to overcome the defect of excessively slow release of shunted electromagnets. This is accomplished by shunting the electromagnet with a novel arrangement of selenium rectifier cells. It deals also with the peak voltage developed across contacts controlling electromagnets when shunted by such a unit, with the condition of the contacts after many millions of such operations, and with the time of release of the electromagnet after the controlling contacts have opened.

1. Need for Contact Protection

The operation of a modern telephone office depends upon the positive operation of millions of electrical contacts.

A 10,000-line office may handle an average of 50,000 calls daily, which runs the number of yearly contact operations into the billions. The operation for the bulk of the contacts varies from 50,000 to 15,000,000 annually.²

* Reprinted from *Transactions of the American Institute of Electrical Engineers*, volume 70, part 2, pages 1919-1923; 1951.

¹ H. K. Henisch, "Metal Rectifiers," Oxford University Press; London, England, 1949; pages 131-155.

² P. W. Swenson, "Contacts," *Bell Laboratories Record*, volume 27, pages 50-53; February, 1949.

Contact erosion is the cause of many circuit failures in telephone offices and in many systems using relays and switches for controlling electrical circuits. Erosion is due to arcing between a pair of contacts and usually results in the loss of material from one contact and the distribution of the lost material on or adjacent to the other contacts. A badly eroded contact often causes snagging and sometimes mechanical locking. This results in circuit failures that are reflected in higher maintenance cost and inferior service. The control of contact erosion is a major problem for the telephone companies in extending contact life. This control of erosion is accomplished by the use of a suitable contact protector.²

The criterion of a good spark suppressor is that it affects the operation of the associated circuit to a minimum degree while giving good protection to the controlling contacts at the same time. In the case of contacts controlling electromagnets, the spark-suppressing device should have little effect on the release time of the controlled electromagnet and should extend the dependable life of the contact many times at the lowest

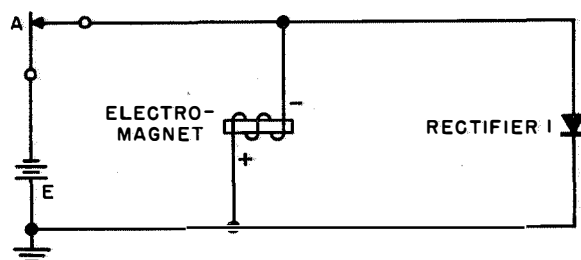


Figure 1—Conventional method of using the selenium rectifier as a spark suppressor.

possible cost. The suppressor circuit components should be dependable and require no attention over extended periods.

At the same time, ease of replacement and low cost also are important factors.

At present, the most generally accepted method of contact protection is the use of a suitable capacitor and resistor in series, this combination being either in parallel with the coil or the con-

tacts. However, their initial cost and installation make their extensive use prohibitive and such protection is provided only for critical cases. The modern trend is toward the development of an inexpensive protector of small size that may be used extensively. The nearest approach to this is now being carried out in Sweden where the Telephone Administration is going "all out" for complete contact protection.

2. Methods of Using Selenium Rectifiers for Contact Protection

The conventional method of using the selenium rectifier as a spark suppressor is shown in Figure 1. When contact *A* is closed, there will be little current flowing through the rectifier due to its high reverse resistance. When contact *A* is opened, the induced electromotive force will maintain the current flow through the coil in the same direction, and the open contact will be shunted by the low forward resistance of the rectifier. This low-resistance shunt will eliminate arcing at the contact but has the effect of prolonging the release time of the electromagnet. After contact *A* opens, and assuming that arcing does not occur, it is known that the time for the current in the coil to fall to a percentage of its initial value is given by

$$t = - \frac{L}{R_L + r} \log_e \frac{i}{I},$$

where

R_L = coil resistance

r = forward resistance of rectifier

L = coil inductance

t = time for current to fall to i

I = steady-state current through the coil (neglecting the small current through the reverse resistance of the rectifier)

i = current at time t .

The voltage V induced on opening the contact is given by:

$$V = -L \frac{di}{dt} = (R_L + r) I \exp - \frac{R_L + r t}{L}.$$

The maximum value of V occurs at the instant the contact opens, or when $t = 0$, and is given by the following equation:

$$V_{\max} = I(R_L + r) = E + Ir,$$

where E = supply voltage as shown in Figure 1.

The increase of the voltage across the contact is directly proportional to the rectifier resistance. An increase in rectifier resistance will reduce the release time but will increase arcing.

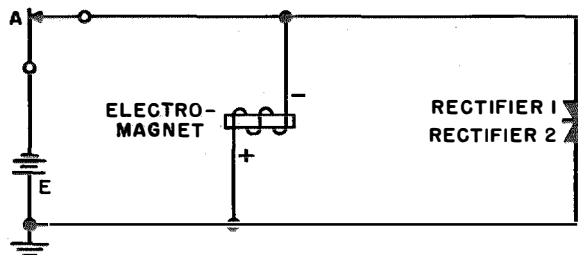


Figure 2—Method of improving the release time by adding a second rectifier.

This conflict between arc suppression and required release time may be resolved by the introduction of a voltage-dependent resistance. If the resistance is low at high voltage, arcing will be eliminated; if the resistance is high at low voltage, improved release time will result. Such an element is obtained when a rectifier is added to the circuit as shown in Figure 2.

It may be seen from Figure 2, that when contact A is closed, rectifier 1 blocks the current flow from battery E and forces practically all of the current through the electromagnet. When contact A is opened, the self-induction of the electromagnet causes a reversal of current flow through the rectifiers, and rectifier 2 blocks the current flow resulting from the collapsing field of the electromagnet. However, the reverse resistance of rectifier 2 is greatly reduced as the voltage rises and the peak voltage at the open contact does not rise to the ionizing potential.

3. Observation of Arcing at Relay Contacts and Methods of Arc Suppression

The voltage at the contact versus the time of collapse of the magnetic field was observed oscillographically by means of the circuit-shown in Figure 3. The transient was photographed with and without contact protection using inductive

loads typical of those existing in telephone central offices. Peak voltages and release times are tabulated in Table 1.

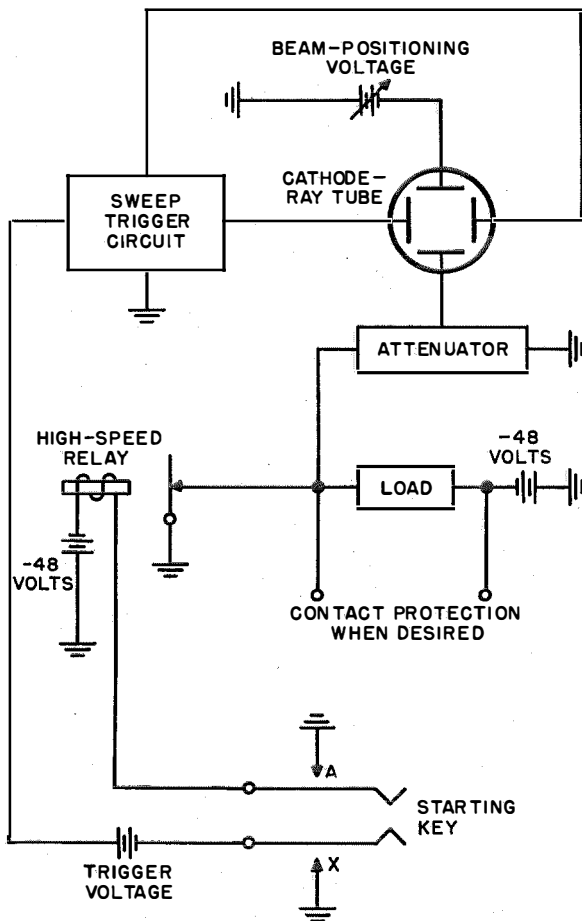


Figure 3—Method of determining voltage at relay contacts. X makes before A breaks.

Sparking at an unprotected relay contact controlling a clutch magnet may be seen in Figure 4. The horizontal line indicates closed con-

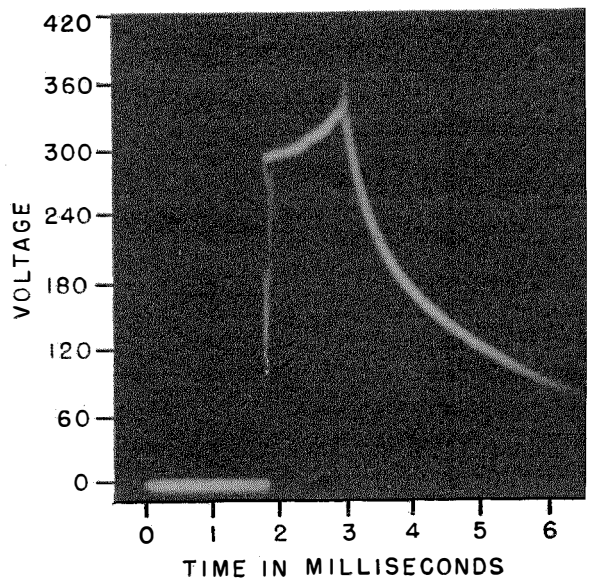


Figure 4—Voltage at unprotected relay contacts controlling a clutch magnet.

tacts. The steep vertical rise occurs at the instant the contacts separate. It may be noted that the voltage rises almost instantly to a value of 300 volts at which value sparking starts. The gradual upward sloping line indicates the duration of the glow. The sharp vertical rise at the end of this sparking line indicates the instant at which the glow extinguishes due to the increased separation of the contacts. From this peak value,

TABLE 1

PEAK VOLTAGES AND RELEASE TIMES FOR ELECTROMAGNETS WITH DIFFERENT TYPES OF CONTACT PROTECTION

Contact Protection	Telephone Clutch Magnet*			Telephone Relay†		
	Release Time in Milliseconds	Peak Voltage at Contact in Volts	Figure Number	Release Time in Milliseconds	Peak Voltage at Contact in Volts	Figure Number
Three $\frac{3}{8}$ -Inch-Diameter Cells (Figure 1)	4.0	83	—	55.0	57	8
Two $\frac{3}{8}$ -Inch-Diameter Cells (Figure 2)	1.3	180	6	12.0	150	7
Three 1-Inch Square Cells (Figure 2)	1.3	192	—	10.9	169	—
Silicon-Carbide Varistor	1.3	210	—	12.8	140	11
0.5 Microfarad + 510 Ohms	—	arcing	—	10.9	160	9
0.1 Microfarad + 510 Ohms	—	arcing	—	7.9	259	10
Unprotected	1.0	400 to 900	4	7.6	450 to 750	5

* $L = 0.485$ henry, $R = 164$ ohms, $I = 0.293$ ampere.

† $L = 3.45$ henries, $R = 1650$ ohms, $I = 0.029$ ampere.

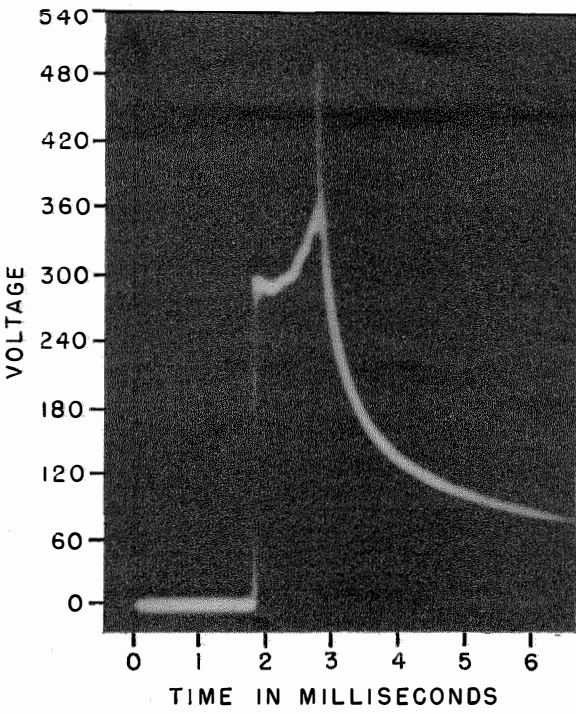


Figure 5—Voltage at unprotected relay contacts controlling a telephone relay.

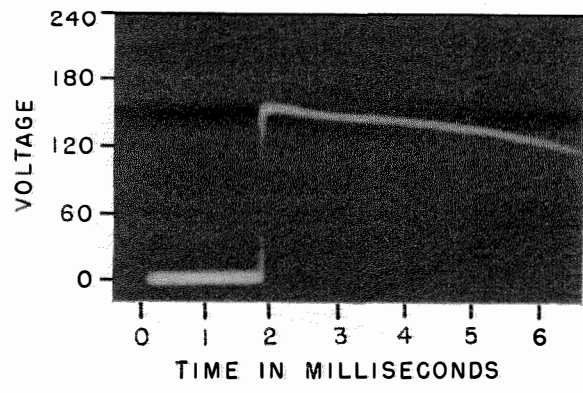


Figure 7—Voltage at rectifier-protected contacts controlling a telephone relay. Protection as shown in Figure 2.

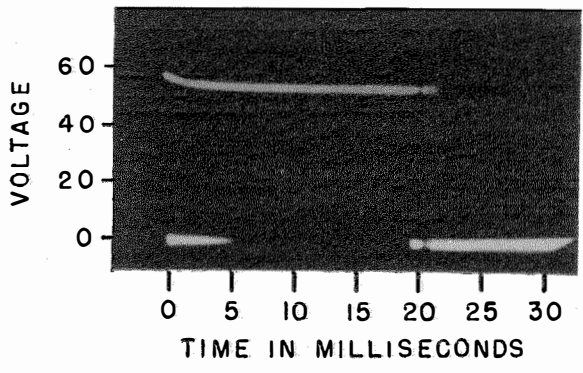


Figure 8—Voltage at rectifier-protected contacts controlling a telephone relay. Protection as shown in Figure 1.

the voltage falls exponentially to the supply potential.

Figure 5 shows the curve for contacts controlling a telephone relay and is similar to Figure 4 with the exception that there is less stored energy in the relay as represented by the shorter duration of the glow.

The selenium rectifiers used for protection of relay contacts are basically combinations of $\frac{9}{32}$ -inch-diameter cells. The arrangement used

consists of two groups of two cells connected in opposition as shown in Figure 2. Therefore, the reverse resistance of two cells is in series with the forward resistance of the other two cells. The voltage at the contact versus the time of collapse of the magnetic field is shown in Figure 6 for the clutch magnet and in Figure 7 for the telephone relay.

The effect of the spark-suppressor unit on voltage is to limit the peak voltage to approximately 180 volts in the case of the clutch magnet, and to 150 volts for the telephone relay.

Figure 8 shows the results obtained with three $\frac{9}{32}$ -inch-diameter cells connected across the load, as shown in Figure 1. The voltage rise is limited to approximately 60 volts with the telephone relay, but the release time is extended six times.

The results obtained by using resistor-capacitor spark-suppressor units may be seen in Figures 9 and 10. When capacitors are used, it is necessary to provide a suitable series resistance to

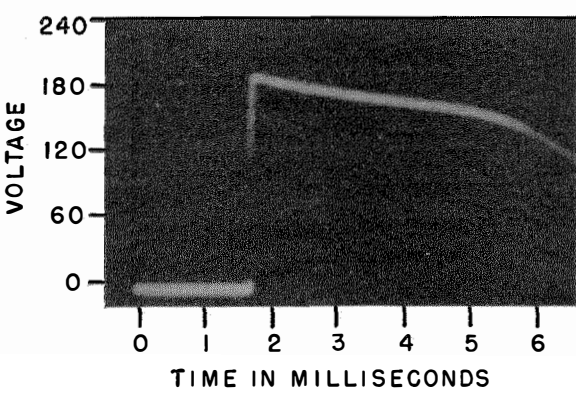


Figure 6—Voltage at rectifier-protected relay contacts controlling a clutch magnet. Protection as in Figure 2.

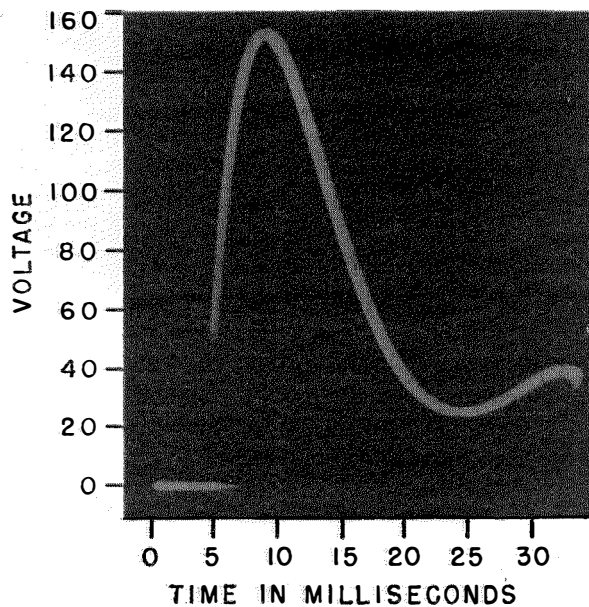


Figure 9—Voltage at resistor-capacitor-protected contacts controlling a telephone relay (510 ohms and 0.5 microfarad).

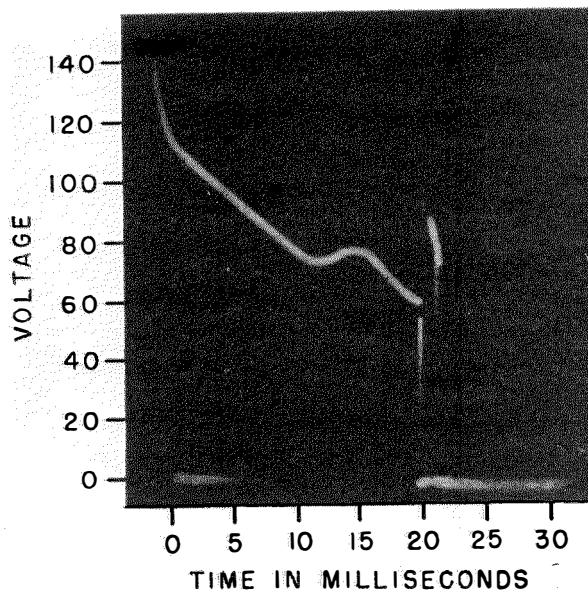


Figure 11—Voltage at silicon-carbide-varistor-protected contacts controlling a telephone relay.

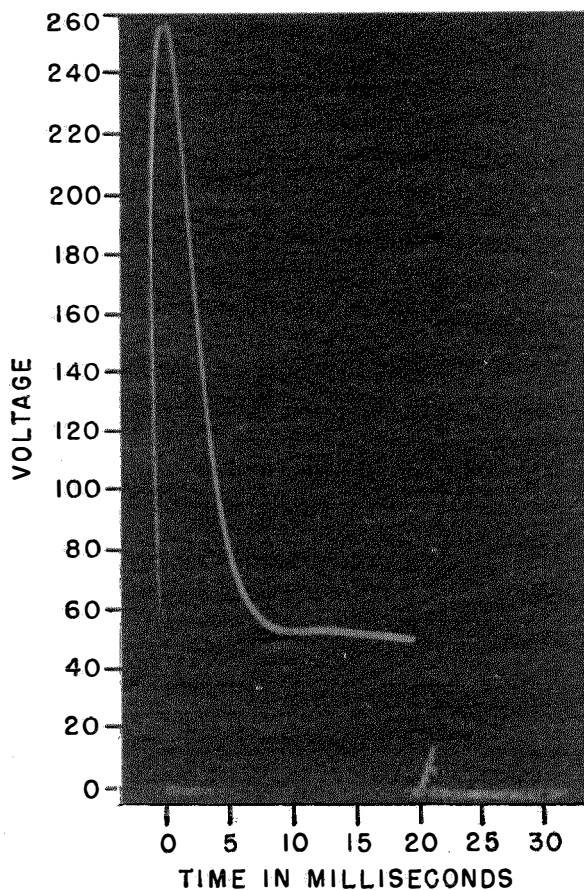


Figure 10—At left, voltage at resistor-capacitor-protected contacts controlling a telephone relay (510 ohms and 0.1 microfarad).

limit the charge and discharge currents that occur during the switching operations. Otherwise, contact burning can occur on initial closure and on immediate reclosure that might result from contact bounce. This is not a problem where selenium rectifiers or silicon-carbide varistors are used because they offer very high resistance to current flow at voltages of 50 volts or less. On closure, the contacts are firmly engaged before the current can build up through the coil to the steady-state value.

The effect on the voltage at the contact when a silicon-carbide varistor is used may be seen in Figure 11. Silicon-carbide-varistor protection gives rise to a transient of a type similar to that shown in Figures 6 and 7, which are for selenium-rectifier protection.

4. Reverse-Resistance Characteristics of Selenium Rectifiers

The reverse-resistance-versus-voltage characteristic of the $\frac{3}{32}$ -inch-diameter cells is of considerable interest, particularly at voltages that

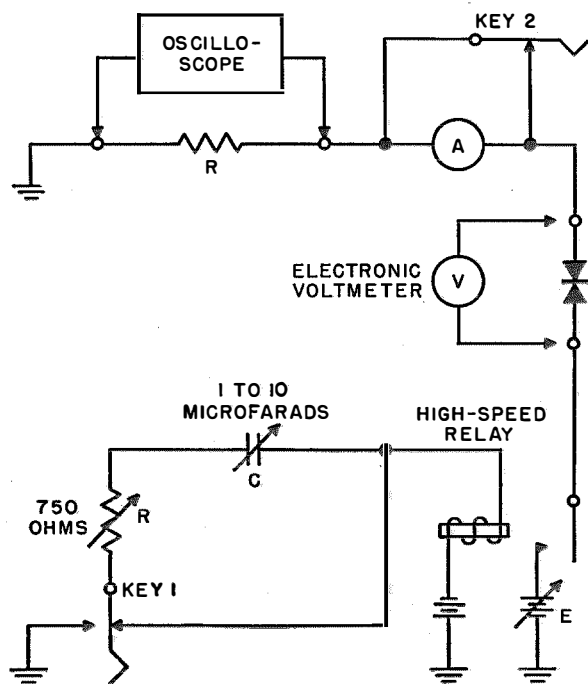


Figure 14 illustrates a family of these reverse-resistance-voltage characteristics. For voltages greater than 50 volts, readings were taken with an oscilloscope with voltage applied for approximately eight milliseconds. For voltages lower than 50 volts, the voltage was applied long enough to read a moving-coil instrument.

The reverse-resistance-versus-voltage characteristics for typical two-cell units, shown in Figure 13, were measured according to Figure 12 and the results plotted in Figure 14. Curves A and B are typical for unaged 2-cell units of $\frac{9}{32}$ -inch diameter. Curve A corresponds to the characteristic for rectifier 1 and curve B for rectifier 2. Reference to Figure 13 shows that rectifier 1 normally blocks the supply voltage.

Curves C , D , and E represent the characteristics for 2-cell units of this type after 50,000,000 operations over a period of six months. Curve C

Figure 12—Method of obtaining reverse-resistance-versus-voltage characteristic of selenium rectifiers.

exceed the direct-current rating of the cells. In order to simulate load conditions, the rectifiers were stressed with a voltage lasting 8 milliseconds. A circuit such as shown in Figure 12 is convenient for such measurements. The time constant may be adjusted for the desired duration of the voltage.

Relays and clutch magnets typical of the inductive loads found in telephone central offices were operated with combinations of back-to-back selenium rectifiers as spark suppressors. Life tests were conducted in order to determine the effect on the electrical characteristics of the rectifiers, and to evaluate the degree of protection afforded the contacts. Figure 13 shows life-test operating conditions.

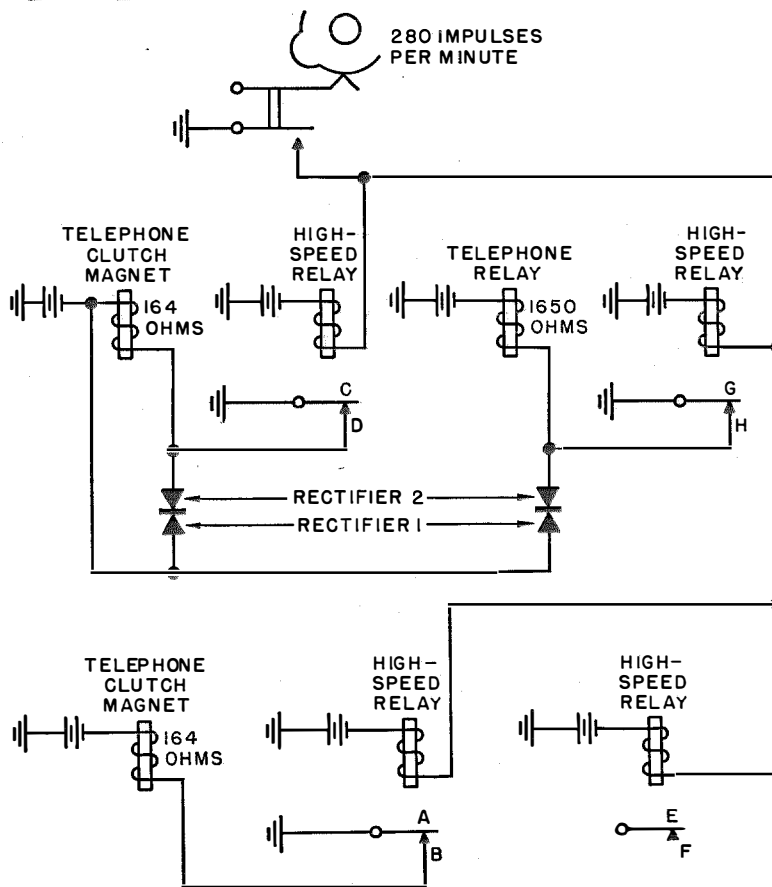


Figure 13—Circuit for life-testing spark-suppression units and contacts. The batteries denote a common 48-volt direct-current source.

represents the typical decrease of reverse resistance with aging which is a well-known characteristic of selenium rectifiers.

Curve *E* represents the characteristic of rectifier 2 with a clutch magnet as the load as shown

that above 50 volts, the change of resistance is less than for the rectifier combination. It should also be noted that the silicon-carbide varistor has a lower resistance at 50 volts, which means greater current drain and increased power dissi-

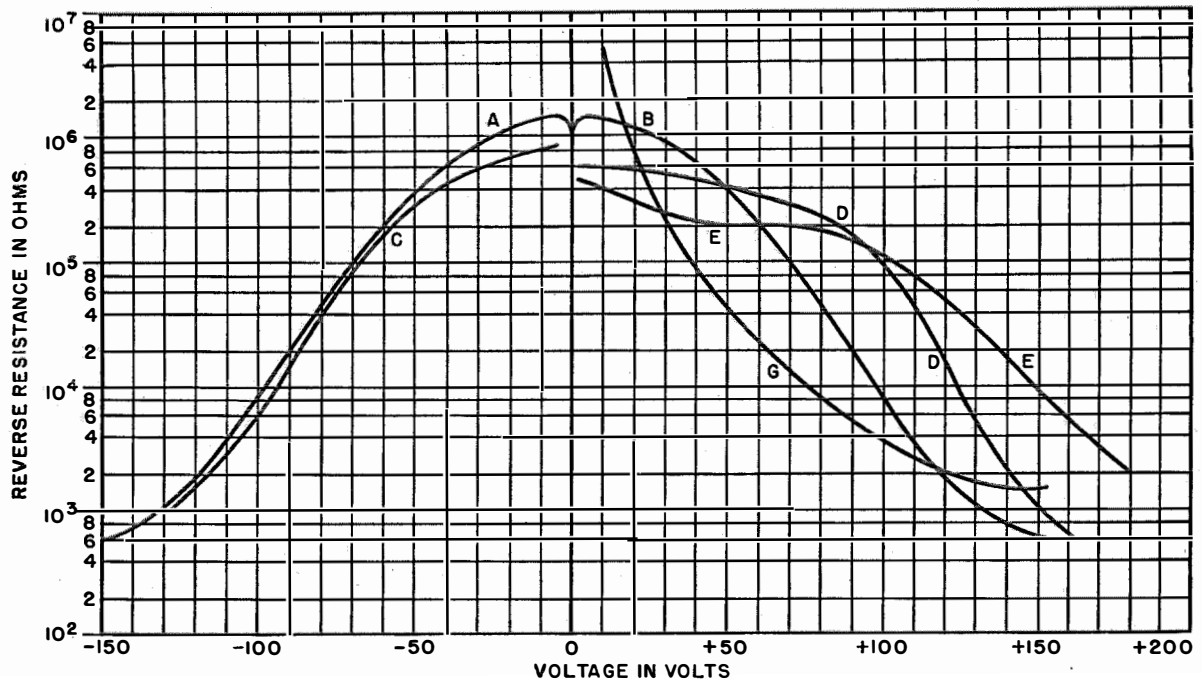


Figure 14—Family of reverse-resistance-versus-voltage characteristics of spark-suppression units.

in Figure 13. The resistance drops at a slower rate. The effect of this is to decrease the release time of the load magnet, but the peak voltage at the contacts rises correspondingly. However, this does not materially affect the unit as a spark suppressor. The peak voltage is still held well below 200 volts.

Curve *D* shows a similar effect as curve *E* but to a lesser degree due to a relay load instead of a clutch magnet.

The increase in reverse resistance described above in curves *D* and *E* is related to the forming process. Higher reverse voltages have the effect of raising the back resistance and prevent the rectifiers from deteriorating as they sometimes do when the current flows in one direction only.

Curve *G* is the characteristic for a silicon-carbide varistor. This varistor is one chosen as being suitable for contact protection with telephone relays and is shown for direct comparison with the rectifier combination. It should be noted

that the silicon-carbide characteristic is concave upwards as opposed to the rectifier combination is obviously less desirable from the point of view of maintaining favorable release times consistent with good spark protection.

5. Mechanism of Rectifier Breakdown

Rectifier breakdown, that is the tendency for the forward and reverse resistances to equalize, is always associated with excessive temperature. If the high voltage stress is not applied long enough for the temperature to rise excessively, and the duty cycle is not excessive, the rectifier will not be injured. The maximum period for which the rectifier can stand an excessive electric stress is dependent upon the effective heat capacity of the cell and the ambient temperature. This period must be determined empirically for the particular application, since efforts to gen-

eralize these relationships have not been successful.

6. Photomicrographs of Relay Contacts After Life Test

Reference to Figure 13 will show the circuit conditions under which the contacts shown in the photomicrographs were operated. The contact metal is 99-percent palladium. The physical dimensions of the contact are shown in Figure 15.

The contacts shown in Figure 16A and B were unprotected with the clutch magnet as a load. After 1,300,000 operations, the back contact had eroded through to the relay spring. In this case the armature A was positive with respect to the back contact B, and the transfer of the metal was from negative to positive. CD and GH in Figure 16 show rectifier-protected contacts that were operated with the clutch magnet and the telephone relay, respectively, as loads. The total number of operations was 50,000,000. The improvement over the unprotected case is of the order of 100 to 1. It is interesting to observe that the back contact and armature contact are eroded to the same extent. The transfer of metal from one contact to the other is not in evidence.

In order to judge how much of the erosion is due to mechanical wear alone, see contacts E and F in Figure 16. These contacts were operated 50,000,000 times but interrupted no current.

7. Dimensions and Mountings

For applications where 50-volt direct-current power supplies are used, and the loads are of the same order as discussed above, the $\frac{9}{32}$ -inch cells are satisfactory. Their small size and light weight enable them to be mounted directly across coil terminals. Drillings and mountings are not required because the lead out wires are sufficiently strong to support the unit. They may be mounted in the same manner as the familiar radio-type resistor. The physical dimensions may be seen in Figure 17. The weight is approximately 0.09 ounce (2.6 grams).

8. Conclusions

Contact erosion in the sense that metal is lost from one contact and deposited on the mating contact seems to be eliminated. This is important from the standpoint of reducing snagging. When contacts retain their original shape, minimum readjustment is necessary.

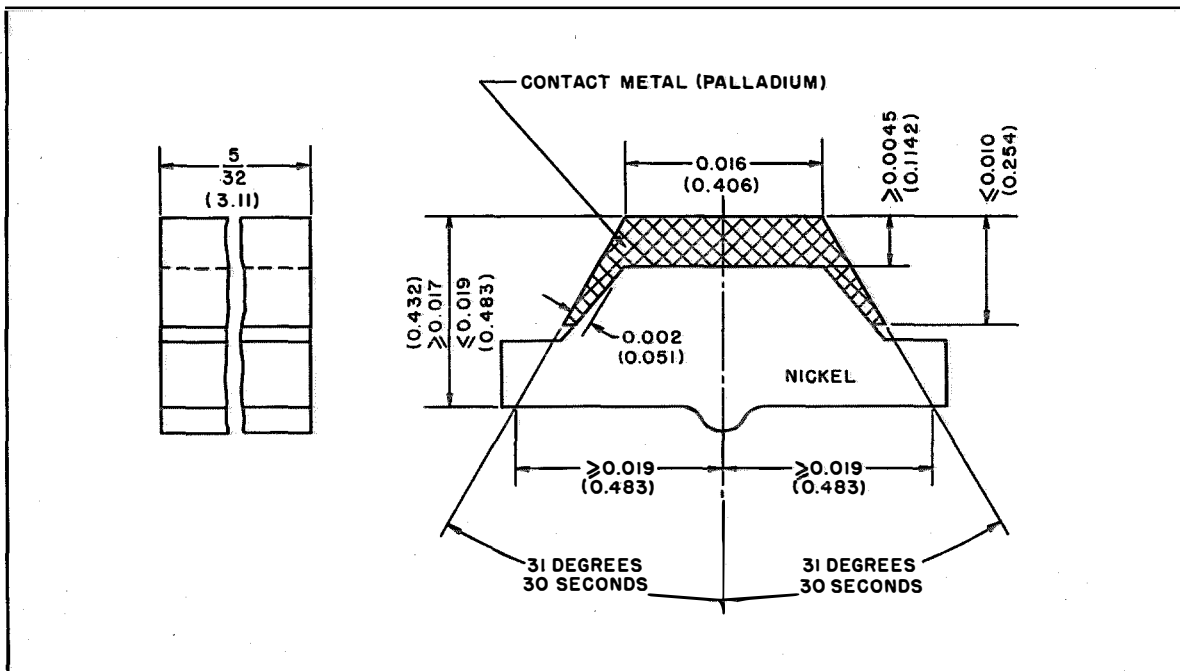
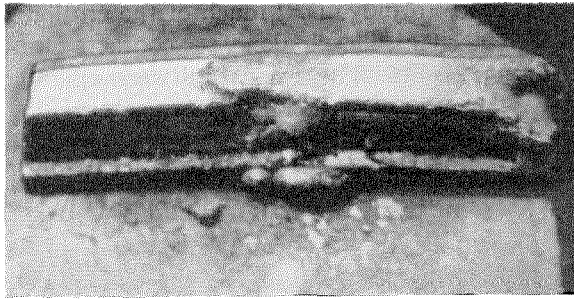
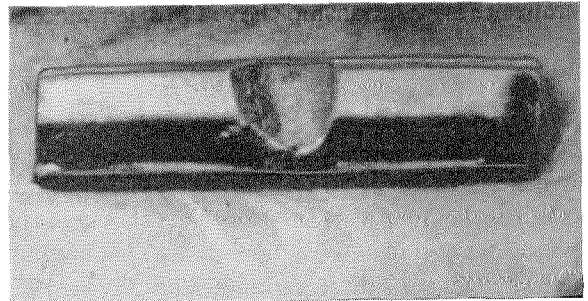


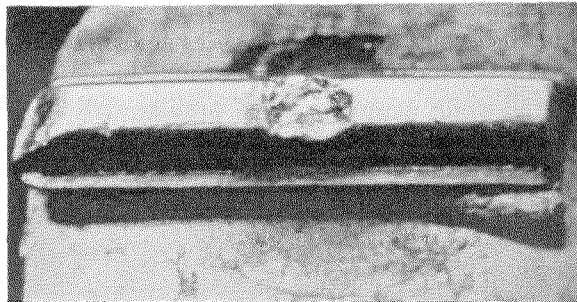
Figure 15.—Structure of relay contact. Dimensions are in inches (millimeters).



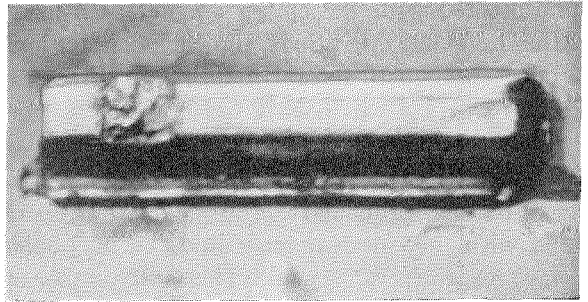
A



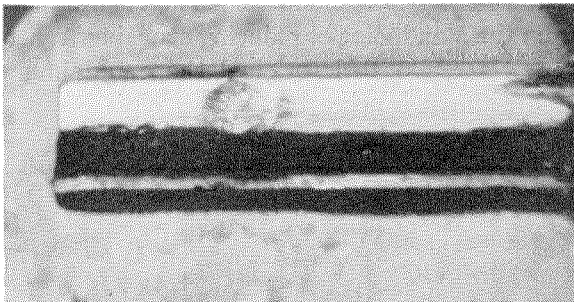
B



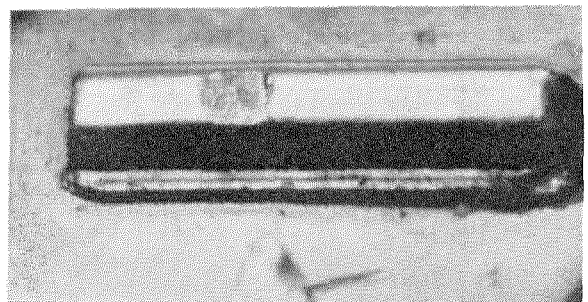
C



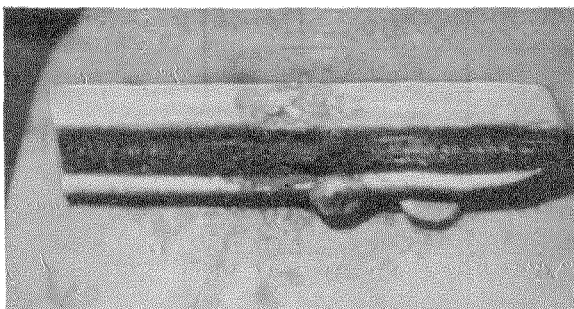
D



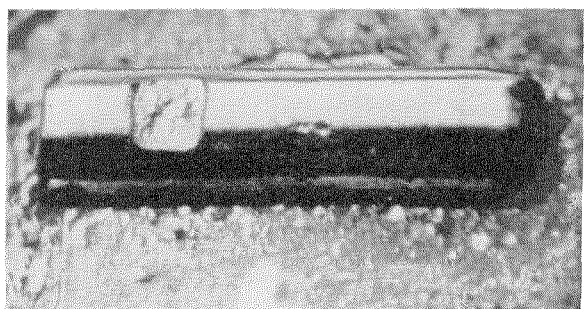
E



F



G



H

Figure 16—The letters correspond to the contacts labeled in Figure 13. *A* and *B*, unprotected contacts after 1,300,000 operations with clutch magnet as load. *C* and *D*, rectifier-protected contacts after 50,000,000 operations with clutch magnet as load. *E* and *F*, mechanical wear of contacts after 50,000,000 operations with no current. *G* and *H*, rectifier-protected contacts after 50,000,000 operations with telephone relay as load.

Satisfactory release time or rate of decay of current is obtained by the addition of a second rectifier as shown in Figure 2. The rectifier com-

dependability over extended periods without attention, makes them most desirable circuit elements.

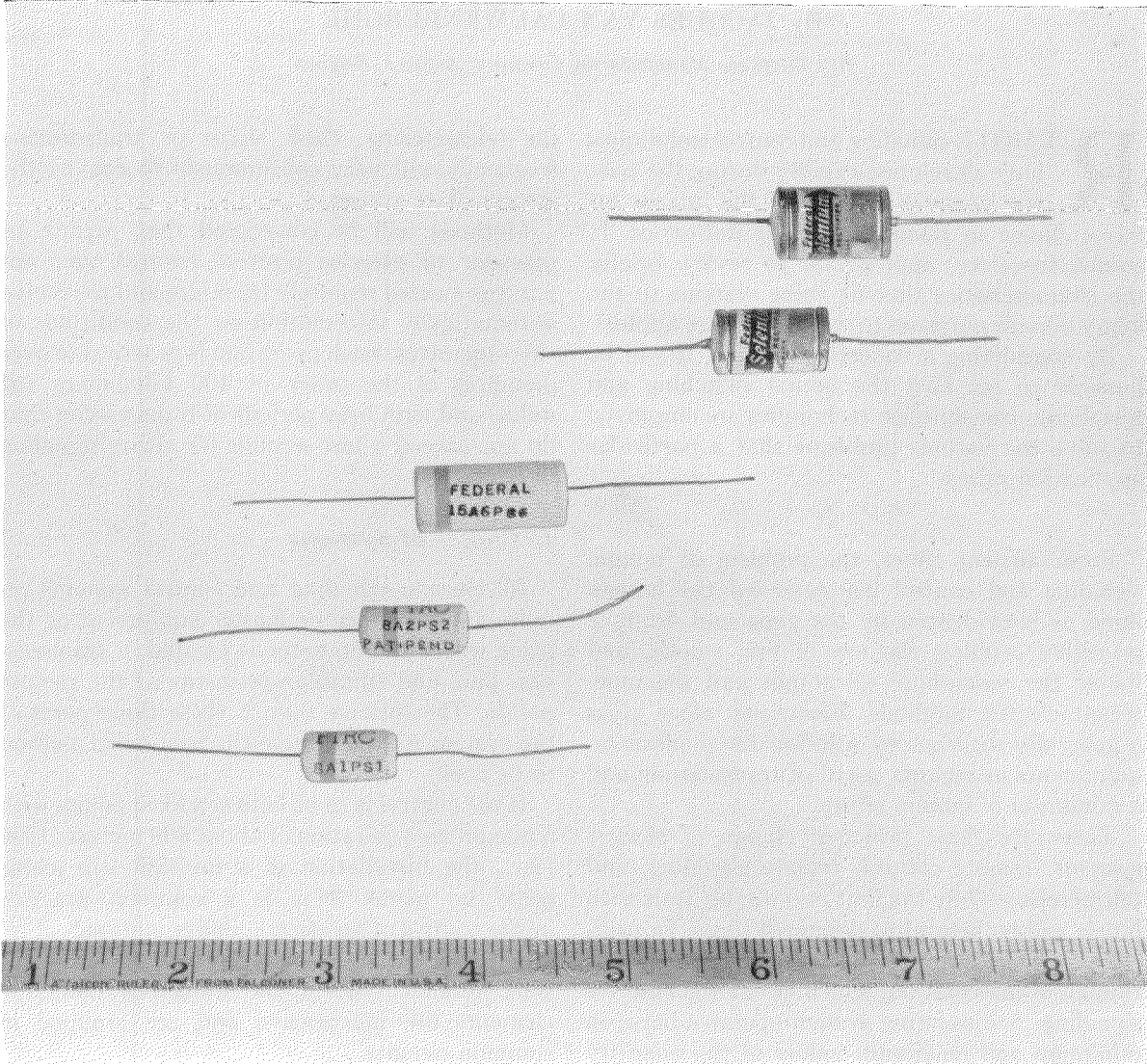


Figure 17—Physical dimensions of rectifier contact protectors.

ination compares very favorably with other known methods of contact protection with respect to peak voltage and timing characteristics.

Selenium rectifiers are inexpensive and are known to have an almost indefinite life. The contact-protection units are simple to mount and, furthermore, it is not necessary to observe polarity when wiring. This, together with their

Power consumption is small when it is desired to connect the unit in parallel with the contacts to be protected.

The use of selenium rectifiers as voltage-surge suppressors is not limited to telephone applications. Cells ranging in area from a quarter of a square inch to thirty square inches may be arranged in series-parallel combinations as the application warrants.

Remote Signaling and Control of Electric Railway Power Networks

By JACQUES VAN CAUWENBERGHE

Bell Telephone Manufacturing Company; Antwerp, Belgium

REMOTE signaling and control techniques have developed rapidly during the past few years as a result of the intense interest shown in them by various industries. It seems, therefore, appropriate to review briefly the characteristics that fit these systems to the many diverse purposes to which they are applied.

By considering a concrete example, it will be possible to see how the actual switching and telephonic transmission techniques are employed to solve the various problems that a particular application raises.

. . .

From ancient times, the problem of remote signaling and control has occupied the human mind as is evidenced by the gong and drum of primitive peoples; the use of fire, smoke, and flares; the semaphore telegraph; and the more recent electric methods. Electricity alone gives a generally satisfactory solution for modern requirements as regards speed of transmission and a minimum of human effort.

There are three principal classes of electric systems: remote control, remote signaling, and telemetering. Only the first two will be dealt with but it will be helpful to define all three. In principle, telemetering is characterized by continuity of information, which is not the case for signaling. A measuring system operates between minimum and maximum values of the quantity to be measured and provides an indication proportional to the instantaneous value. Signaling, however, indicates the position of a piece of apparatus, which changes relatively infrequently from one to another of a limited number of positions. Remote control would be the method used to change the operating position of the piece of apparatus.

Logically, signaling and remote control occur in a discontinuous manner often by the transmission of impulses having constant frequency and shape. If, for some reason, impulses are used

for telemetering, their shape or transmission frequency will vary continuously to convey the intermediate values.

Methods will be considered that permit an operator to exercise positive control over apparatus located remotely from him and to receive automatically information on the conditions of this apparatus. Such operation is practicable over distances of the order of 100 kilometers (62 miles) and with brief periods of transmission that do not exceed a few seconds for either signaling or control.

1. Choice of Systems

All electric signaling and control systems require a supervisory or master equipment at the place where the operator is located, a transmission line, and suitable apparatus at the remote points. The relative cost of these three parts of the system will determine the particular method to be used.

If the control is to be between fixed points with a maximum separation of about 400 meters (1300 feet), the installation of a multiple-wire cable could be made. This is a common practice in the control of an electric power station.

A fire-detecting installation will be economically feasible only if the numerous detecting elements are inexpensive and are grouped in common circuits.

Another comparable arrangement would concern the remote control of a public lighting system. A single pair of wires would pass through the numerous lighting points. Control would be exercised by transmitting a very simple code such as impulses of varying polarity or by applying or removing a voltage from the line. The controlling units must, of course, be simple and inexpensive. In some cases, it may not be practicable to provide special conductors and the operation must be performed by sending the control signals over the lighting mains themselves; either by a

direct current superimposed on the line between ground and neutral or by voice frequencies.

The most difficult cases are those in which there are a number of distant centers, each containing several important pieces of apparatus that must be controlled individually. If the distance from the supervisory to the remote points is large, the cost of transmission means becomes a significant factor; in this case it is justified to complicate the terminal equipment if this permits a reduction in the cost of the aforementioned transmission means. This type of centralized control can be quite complex and will be considered in detail.

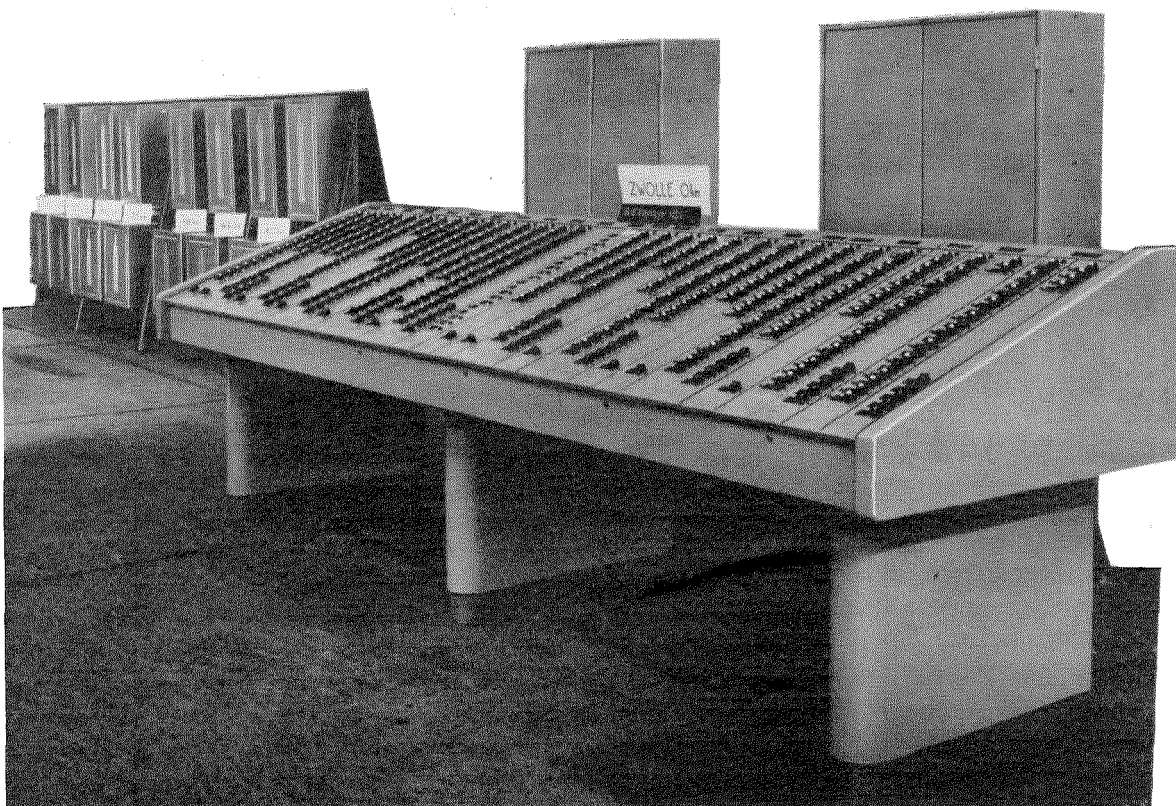
2. Rapidity and Means of Transmission

In the majority of cases, the orders to be transmitted do not require instantaneous execution. Similarly, some seconds delay can be tolerated between a change in the distant apparatus and

the reporting of that change to the operator. This tolerance of time may be used conveniently to increase the information-carrying capacity of the transmission channels by allotting a longer time to the message, thus increasing the information per message and permitting a reduction in the number of transmission channels required. Each control or signaling message will be translated into a code consisting of a series of successive impulses of one or more types at the transmitting end and will be decoded for display or operation at the receiving end.

If several stations are distributed along a common transmission line, the code will contain a preliminary signal to designate the particular station involved.

Impulses are considered to be of different types when they have different forms or characteristics or when they are transmitted through different channels.



One of the control and signaling desks for the Zwolle master station is in the foreground with the associated relay cabinets behind it. The equipment that goes in 7 of the substations is shown in the left background.

In all messages, consideration must be given to the relation among the number of types of impulses, length of the code corresponding to the message, load on the transmission channel, duration of the transmission period, and cost of the apparatus. By adding types of impulses, the length of the code and, hence, the duration of the transmission period are reduced but at the cost of more-involved apparatus for encoding and decoding.

Types of impulses to be used would depend substantially on the means of transmission available. A telephone line of physical conductors can be used very simply by transmitting impulses of one of two polarities, that is, wire *A* may be positive and wire *B* negative for one polarity with the arrangement reversed for the other polarity. It could also be used for transmitting alternating-current impulses of one or more frequencies spaced up to the higher-frequency limit of the line, which might normally be around 2500 or 3200 cycles per second. Very often, impulses are used to modulate carrier frequencies outside the voice spectrum to avoid disturbance of an already-existing voice transmission. Impulses may also be transmitted at radio frequencies with, of course, substantially higher cost of terminal equipment.

A train-dispatching system has been put in service using a code that is characterized by the transmission of exactly 17 pulses for each message. Different messages result from pauses that are inserted in the series of pulses. As an example, there may be three impulses, a pause, seven impulses, a pause, and seven more impulses, making a total of 17 impulses. A wide range of messages is therefore possible and an interruption in transmission or an extraneous disturbing signal will be evident by an incorrect total number of impulses in the series.

In the control of public lighting, where a common channel carries the control impulses to all lamps, the number of impulses may be varied. Three impulses may be used to switch on the lights, four will reduce the lighting to a half-value, five impulses may extinguish the lights, etc.

A simple method of selecting one of a number of telephones on a common line as used by railways is to vary the number and length of the impulses transmitted to the various receiving stations.

The remote operation of a complex and important installation such as an electric substation

requires a rapid means of transmission and one having a much greater reliability and accuracy than stated above.

Transmission reliability cannot be based on the stability of the transmission line because parasitic impulses may be induced in the line or the transmission may be interrupted briefly, both conditions would result in a distortion of the message. As in military services, the reliability of the message is made to depend on the manner in which it is encoded and decoded.

To fulfill these requirements, a system has been developed using an impulse train of constant length but containing two different types of impulses. The length of each impulse and the space between adjacent impulses are the same.

The adoption of a constant number of impulses for each message immediately permits mutilated messages to be discarded. For similar reasons, it is best to avoid systems in which the length of the impulse also is significant. In addition, care has been taken to design a code system that can be verified on reception.

By using impulses having durations and intensities of the order of those used on telegraph circuits, it is possible to make use of all the transmission knowledge developed in the telegraphic field and to obtain maximum speed of transmission at distances without being dangerously influenced by neighboring circuits. On a normal telephone circuit, each type of impulse may be transmitted either as direct current or as one of the 24 voice frequencies spaced 120 cycles apart that are commonly used for voice-frequency telegraph channels. If the circuit is to be used simultaneously for telephony, that service must be protected from the pulses.

The spacing of 120 cycles between the telegraph frequencies limits the number of impulses that can be transmitted per second; to avoid cross talk, the frequency spectrum for each signal must not extend more than 60 cycles from the signaling frequency. If an impulse is to be transmitted without excessive distortion, the fundamental and third harmonic of the pulse frequency must be transmitted. It is evident, therefore, that in such a system, not more than 20 impulses should be transmitted per second. To obtain additional reliability, this number is reduced to 10 or 15 impulses per second, which would be 20 to 30 bauds when expressed in telegraphic language.

When several stations are distributed along the same transmission line, a third type of impulse, which may be transmitted by a pair of wires or by an additional voice frequency, is generally required to prevent interference between the transmissions of the various stations.

3. Cost

Although this system permits transmission over high-voltage power lines and often uses alternating-current pulses to meet particular requirements, most remote signaling and control installations utilize direct-current impulses transmitted over telephone circuits. This permits the use of relatively inexpensive transmitting and receiving equipment operating from an ordinary storage battery, making the system independent of mains-supply failures.

To assure reliable operation at low cost, simple robust keys are provided for the operators, the equipment is controlled through metal or

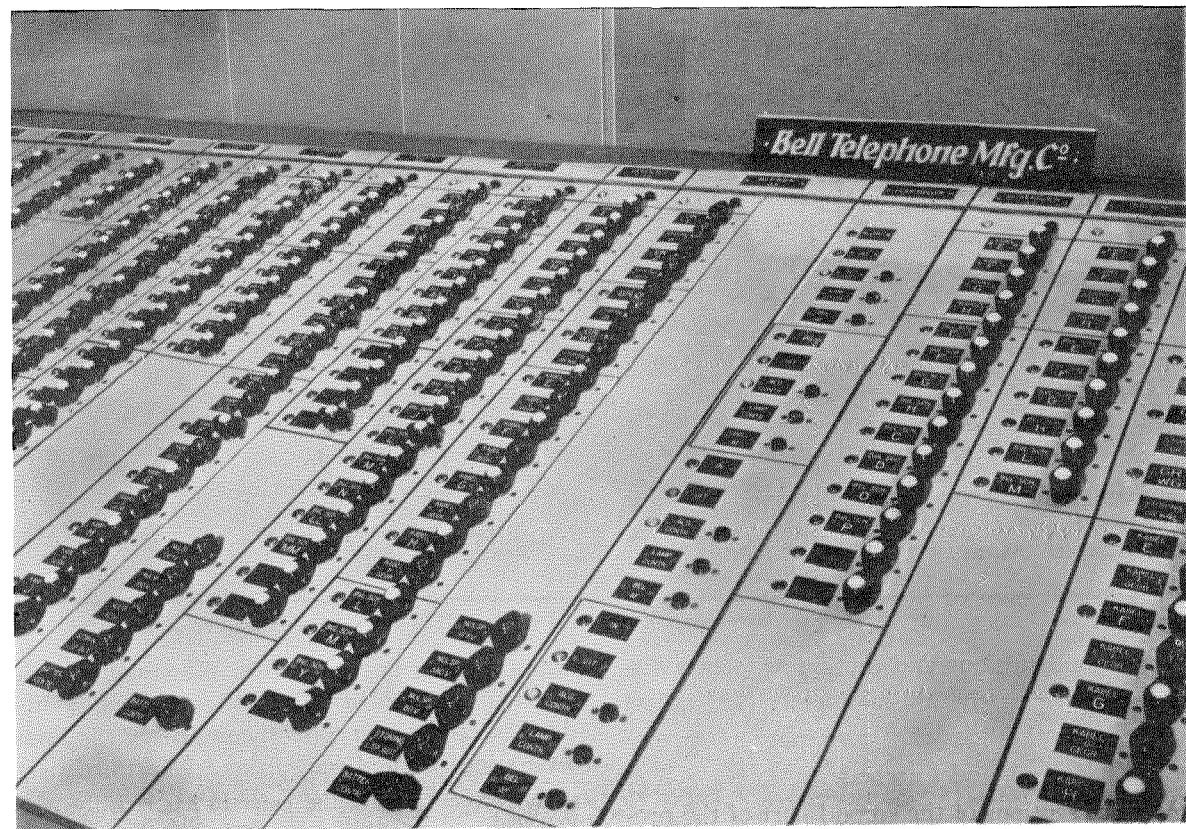
A close-up of the control desk showing the double-motion keys with combined signal lamps. The desk is 4 meters (13 feet) long.

mercury contacts of ample dimensions, and the intervening relays are of well-proved telephone design protected by shockproof dust-tight covers.

4. Dutch Electrified Railway Network

The electrification of the Dutch Railways was started before the war and is now in process of being completed. Power is supplied at 1500 volts direct current and this relatively low value together with a heavy density of traffic has necessitated the erection of many power substations with a consequent large number of track sections. To avoid maintaining supervisory personnel at each of these points, to increase the rapidity with which control actions may be taken, and to improve the coordination of the operation of these stations, it was decided to centralize the supervision and control of the stations in the northern part of the country at Zwolle. This may be seen in Figure 1. Previous experience had been gained in remotely controlling a substation at Sterksel from Eindhoven.

The first part of the program was completed and put in operation early in 1951. It provides for signaling and remote control from Zwolle of



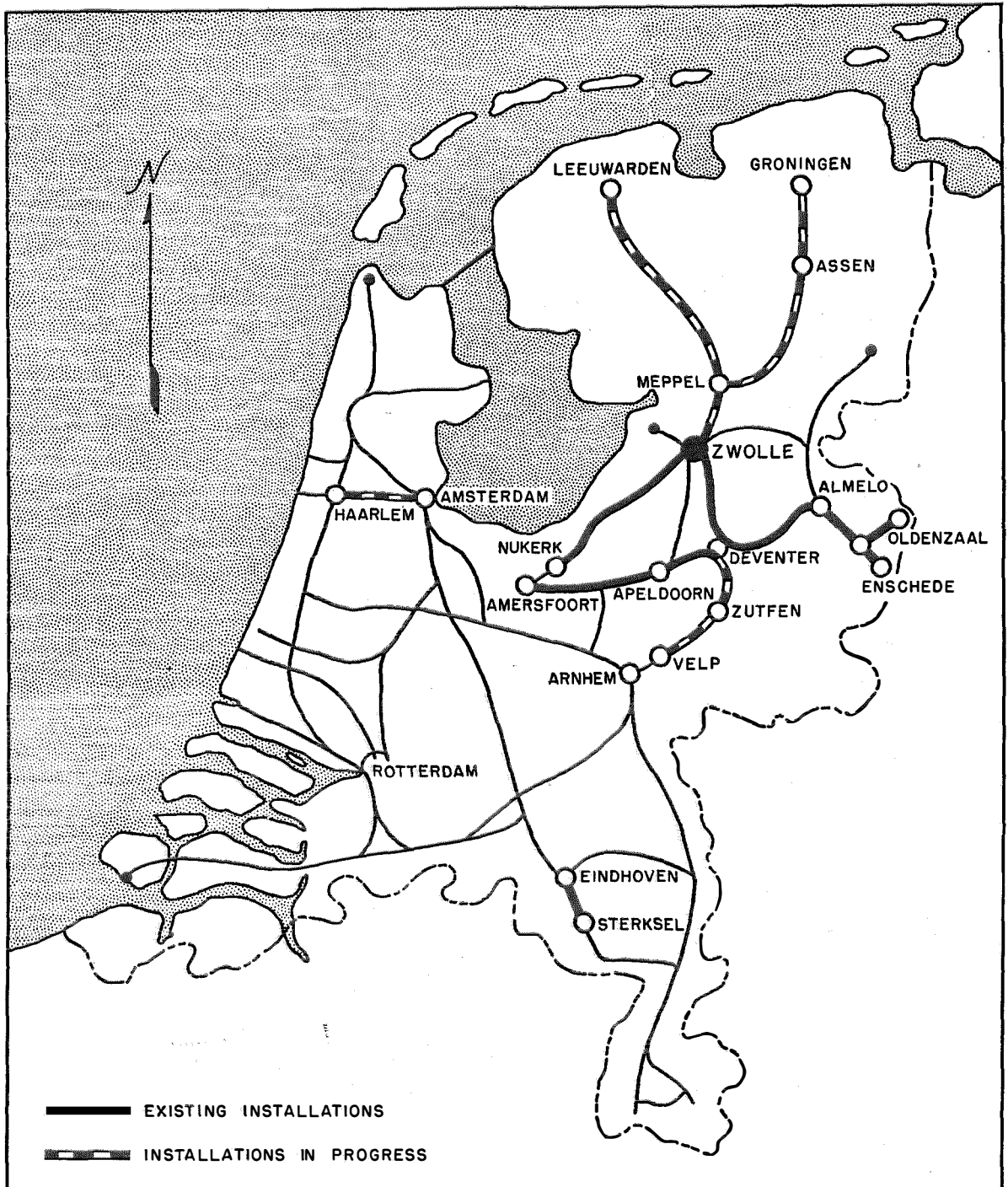


Figure 1—Dutch railway network showing the progress as of January 1, 1952, in remote signaling and control.

22 power substations and sectioning points distributed over nearly 200 kilometers (125 miles) of tracks on the lines that terminate at Amersfoort, Oldenzaal, and Enschede.

Various sections of the second part of the pro-

gram are being put in service. When completed, there will be 34 substations and sectioning points added to the Zwolle control comprising the lines to Groningen and Leeuwarden.¹ The third part

¹This second part of the program has recently been completed.

of the program will add nine more substations on the line to Arnhem; these installations have been ordered recently.

In addition, two substations on the Amster-

are needed, additional units have been provided. Provision has been made for additional needs at each station and to permit increasing the number of stations by about 30 percent.

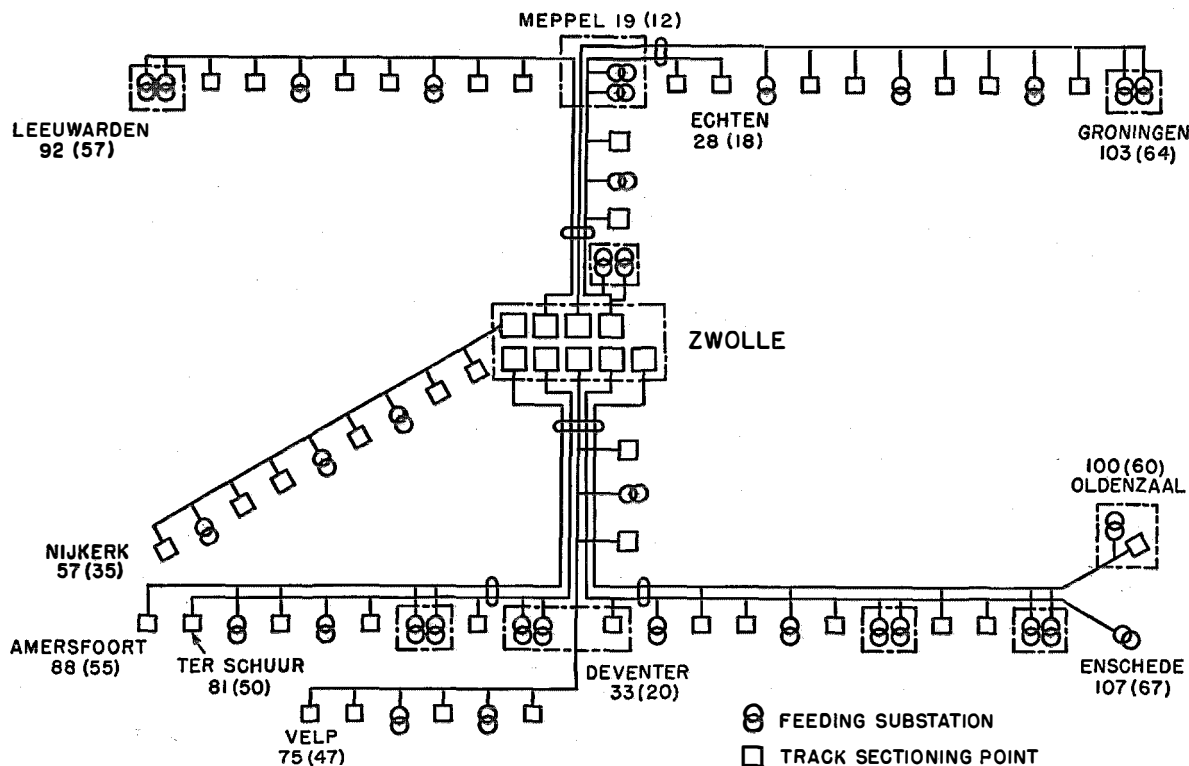


Figure 2—Remote-control network showing in block-diagram form the apportioning of the 9 channels. Distances from Zwolle are indicated in kilometers (miles).

dam-Haarlem line have been modified to permit remote control from Amsterdam.

About half of the installation centered in Zwolle has been placed in service. On completion, the system will permit the recording at this central point of the condition of about 1350 pieces of apparatus, of which some 700 will be controlled remotely. These equipments are distributed among 65 substations or sectioning points. They are distributed in five different directions of approximately 100 kilometers (62 miles) each.

To allow simultaneous and independent control in each of the directions and of neighboring stations as well, a distribution system having nine independent channels is planned as may be seen in Figure 2.

The substation equipment has been standardized and where greater facilities than normal

5. Installation

The equipment installed at Zwolle is mounted in a few cabinets and in a control desk as is indicated in Figure 3. Each substation is equipped with a transmitting apparatus and a contacting-relay box to control the equipment under supervision.

The signaling and control system is operated in each station from a 48-volt storage battery under floating charge. This insures service in case of a breakdown of the power network itself.

6. General Operation

Without the remote-control and signaling installation, the chief operator at Zwolle would require a group of telephone operators who would be constantly in communication with a foreman

at each of the 65 distant stations. The foreman would report all operations taking place and would execute orders given to him by the telephone operator. The remote-control installation permits the telephone operators and foremen to be dispensed with and the chief operator is able alone to supervise the distant installations with greater rapidity and fewer errors than would occur under the above system.

The system operates as though it were under the control of a well-trained corps of invisible personnel. The following description is worded as if 1350 vigilant, accurate, rapid, and invisible attendants were available for each operation that may be required in reporting the condition

free and would engage it to prevent any other center from using the line while he needed it. He would then seek authorization from Zwolle to transmit and by code would have each member of his staff signal the condition of each piece of apparatus at this center.

On the completion of the entire message, the invisible telephone operator at Zwolle verifies that the name of the transmitting center has been clearly given, checks the exact number of impulses received to ascertain that the coded messages have not been distorted, displays on the controller's desk the present condition of each piece of apparatus at this center, and draws the attention of the controller to the recent

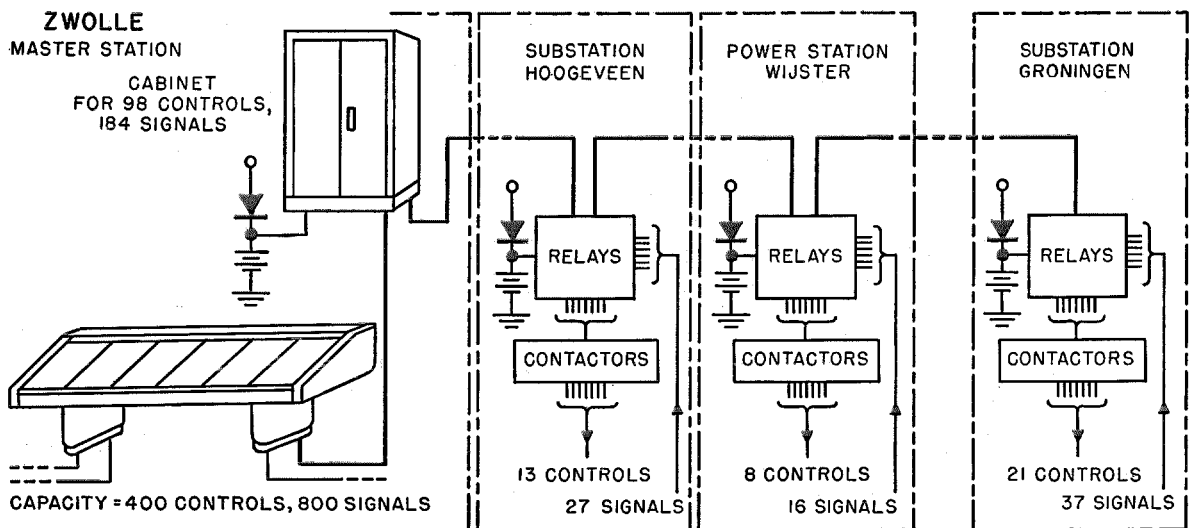


Figure 3—Diagram of the control and signaling channel between Zwolle and Groningen.

or controlling the operation of each of the 1350 pieces of apparatus located in the various stations. There would be an invisible foreman in charge of each of the 65 centers reporting to Zwolle and nine invisible telephone operators in readiness at Zwolle. During periods of inactivity, these invisible operators would rest—there would be no consumption of power by the apparatus.

7. Signaling

If circuit switch 18 at the third station were suddenly to release, invisible attendant 18 would inform the equally invisible foreman, who would ascertain if the telephone line to Zwolle were

release of switch 18 by producing an audible signal. In the meantime, the communication line to the reporting center is freed and made available for other transmissions.

All these operations require not more than four seconds. If, however, a message is not clear, the invisible telephone operator refuses to display the information, so informs the controller, and requires him to order a repetition of the message.

The controller, on receiving the information from the telephone operator, can silence the alarm bell only by placing a key corresponding to switch 18 of the third center in the RELEASED position, which not only silences the bell but extinguishes a lamp incorporated in the key itself.

8. Remote Control

If the controller desires to reclose power switch 18 of the third center, he places the corresponding key in the SWITCH ON position and depresses this key for an instant. The invisible telephone operator is thereby called and after verifying that the communication channel is free, engages it and transmits the code that connects him to center 3. The invisible attendants at each piece of equipment are silenced except the one for switch 18—who is called to attention and is obliged to signal his readiness to receive orders. His message might be read, "I, number 18 of center 3, am waiting for an order; my switch is at present in the OFF position."

At the completion of this message, the attendant of switch 18 will be connected directly to the corresponding key at the controller's desk in Zwolle to await an order.

The invisible telephone operator then verifies whether the repeated code message is identical to that originally sent and whether the invisible attendant reporting is definitely the one associated with the particular apparatus for which a change in condition may be needed. The telephone operator having verified these things, authorizes the controller at Zwolle to depress the key a second time, which initiates the desired action on the part of the invisible attendant of switch 18. When this operation has been carried out, the invisible attendant disconnects himself from the line and the foreman reports to the Zwolle controller the complete condition of the whole center. This entire process requires approximately 12 seconds.

If any of the verifications of the code messages do not tally, any possibility of control action is stopped and an alarm is given so that the contents of the messages may be checked. Until the operator depresses the control key for the second time, he is at liberty to make any change considered desirable in the control instructions.

Usually, these systems are designed to make this second operation of the key unnecessary, the tally between original and repeated messages automatically initiating the control action. But, at the request of the railway people, the double action was incorporated to ensure the full attention of the control operator.

As installed, telephone service is not provided

over the same wires that are used for remote control. The design is such, however, that by the use of additional relays such operation can be included.

9. Equipment and Line

As may readily be seen, some parts of the equipment are common and are independent of the number of signaling or controlled apparatus. Other parts are directly proportional to the number of such apparatus.

As the individual equipment is most numerous, it must be kept to a minimum for economic reasons and be of simple structure to avoid maintenance problems. At the master control station, there are a combined signaling and control key and a relay for each piece of equipment to be remotely controlled. At the substation, an individual relay is required for each component for which signaling is required. Where remote control is applied, two additional mercury-type relays are needed for each piece of apparatus.

The common equipment consists of relays and selectors acting as distributors to connect the relays of the individual pieces of equipment to the common relays.

The line consists of two pairs of wires in a telephone cable. One of these pairs transmits the direct-current polarized impulses in both directions. The other pair is used only for blocking other stations from access to the line while one station is transmitting. This is done by applying a suitable potential to the line. While it is possible to provide this service without using a pair of wires just for blocking, for a given speed of operation, this second pair ensures greater operating reliability.

10. Operating Description

10.1 SIGNALING

The signaling system is based on the synchronous rotation of two selectors, one of which is located at the substation and the other at the control station.

The selectors are of the step-by-step type in which rotating wipers sweep over a series of terminals establishing electric connections successively to each terminal. There may be several levels of such terminals each with its own wiper. To insure that the selector in the control station and the corresponding one in the substation move

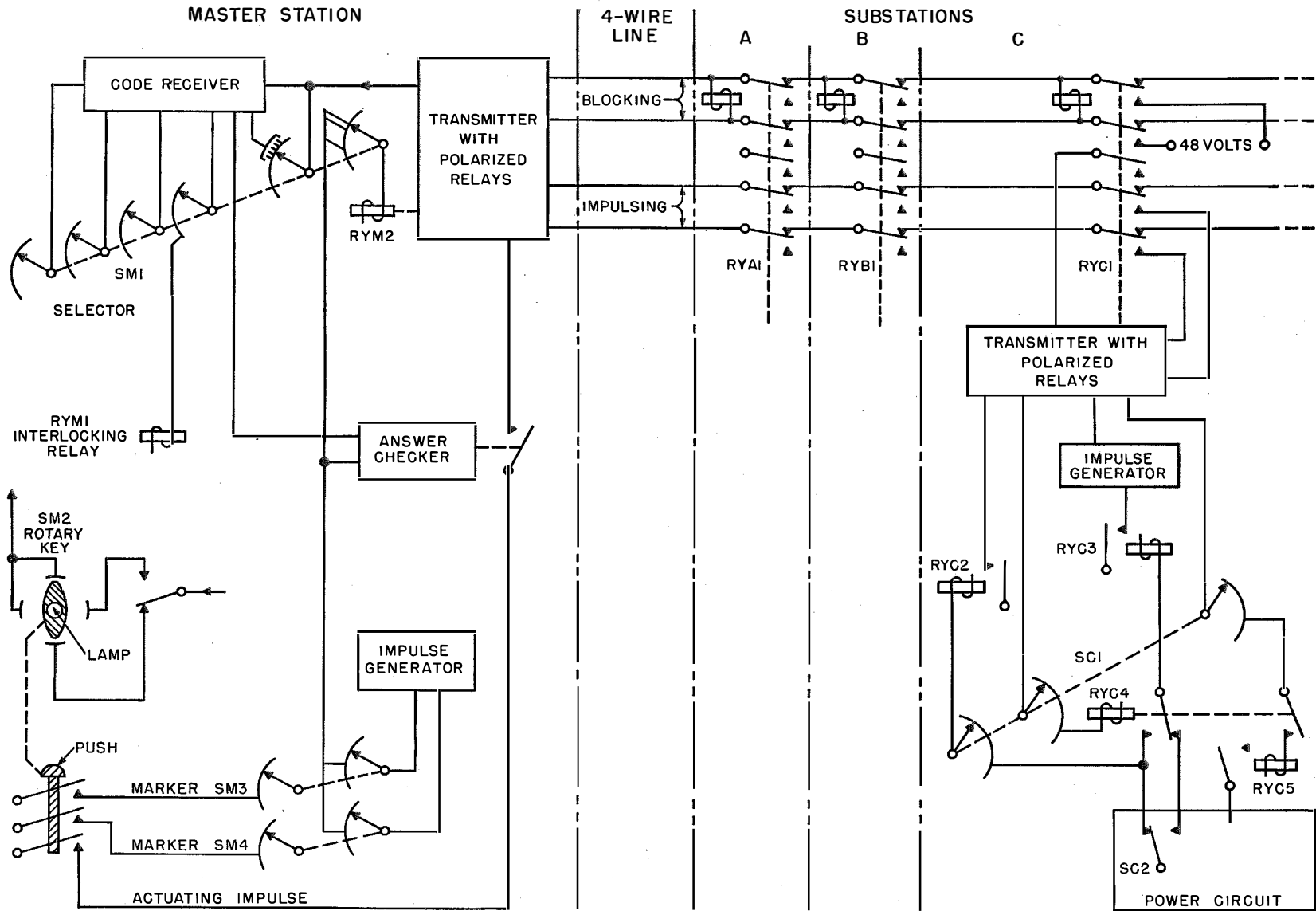


Figure 4—Block diagram of the operation of the signaling and remote-control facilities.

in synchronism during signaling, the substation transmits impulses of constant length and intensity that provide for step-by-step movement at both the local selector and that in the control room.

The state of the apparatus being controlled is indicated for transmission purposes by a change-over contact that is connected to the 48-volt battery and is mounted on the apparatus itself or on an auxiliary relay.

As an example of the operation of the circuit, a power switch in substation *C* is represented in the lower right corner of Figure 4. Signaling contact *SC2*, associated with this power switch, has two positions corresponding to the closed and opened positions of the power switch. The contacts of *SC2* and of *RYC4* are connected in such a manner that the common signal-starting relay *RYC3* is energized whenever the contacts of *RYC4* and *SC2* are in discordant positions, i.e., when one is operated and the other is released.

Therefore, at the moment the position of the power switch is changed, *RYC3* operates and causes signals indicating the new position of the power switch to be transmitted to the master station. During this cycle, *RYC4* comes in accordance with the new position of *SC2*.

To explain the above in a more-detailed manner, once *RYC3* is energized, the circuit first verifies if the line is free (whether the blocking relay *RYC1* is unenergized). In the next step, the blocking line is opened and 48 volts are applied to the blocking pair in the direction of the master station. On reception of this potential, the master station sends one starting pulse, the arrival of which at the substation will permit the start of transmission.

On receipt of this impulse, *RYC3* starts an impulse sender. These impulses at approximately 12.5 per second cause the local selector *SC1* at the substation and the selector *SM1* at the master station to rotate in synchronism

As can be seen, this manner of engaging the line and the use of the starting impulse completely avoids any interference between the emissions of the various substations.

During its rotation, *SC1* connects a relay *RYC2* to its various contacts in succession. The first six of these terminals are reserved for the identification code of the sending substation (which code is generated through the permanent

connection to the positive pole of the battery of a combination of two of these six terminals). Each of the following terminals of *SC1* is connected to positive 48-volt battery through the make contact of the switches associated with the various pieces of apparatus. (In the case of the power switch of Figure 4 this would be *SC2*). Relay *RYC2* controls the polarity of the impulse thus sent to the master station.

The first six of the impulses thereby indicate the identity of the transmitting substation; each of the following impulses being positive or negative according to the ON or OFF position of the corresponding substation apparatus.

It should be noted that during this rotation of *SC1*, each relay *RYC4* is at the same time set by *RYC2* in accordance with the position of the corresponding apparatus.

At the master station, two polarized relays receive the incoming impulses and either one causes the master-station selector *SM1* to rotate. According to the code received during the first six impulses, these polarized relays direct the following impulses via one of the several wipers of *SM1* to the various individual interlocking relays *RYM1*. These relays *RYM1* correspond to the various pieces of apparatus in the substations and cause signals to appear on the master control board according to the positions of the power apparatus in the substations.

At the conclusion of the impulsing cycle, both *SC1* and *SM1* will have returned to normal where they will remain until the changeover of another piece of apparatus again causes *RYC3* to operate. In case of faulty synchronization, the master-station selector *SM1* will stop at the conclusion of signaling in an off-normal position. An alarm will then be given, after which the operator can cause an entirely new series of impulses to be transmitted from the substation.

At the master station, each piece of apparatus is represented by a rotary key *SM2*. The lamps of the keys corresponding to the substation power apparatus that has changed position will be lit and at the same time an audible signal calls the operator's attention to these lamps, which may be put out by changing the position of the keys in which the lamps are contained. When the key is rotated, the lamp will go out and its new position will correspond to the new position of the power apparatus.

This signaling panel is of the extinguishing type and is both economical and comprehensive, but other signaling methods may be used.

10.2 REMOTE CONTROL

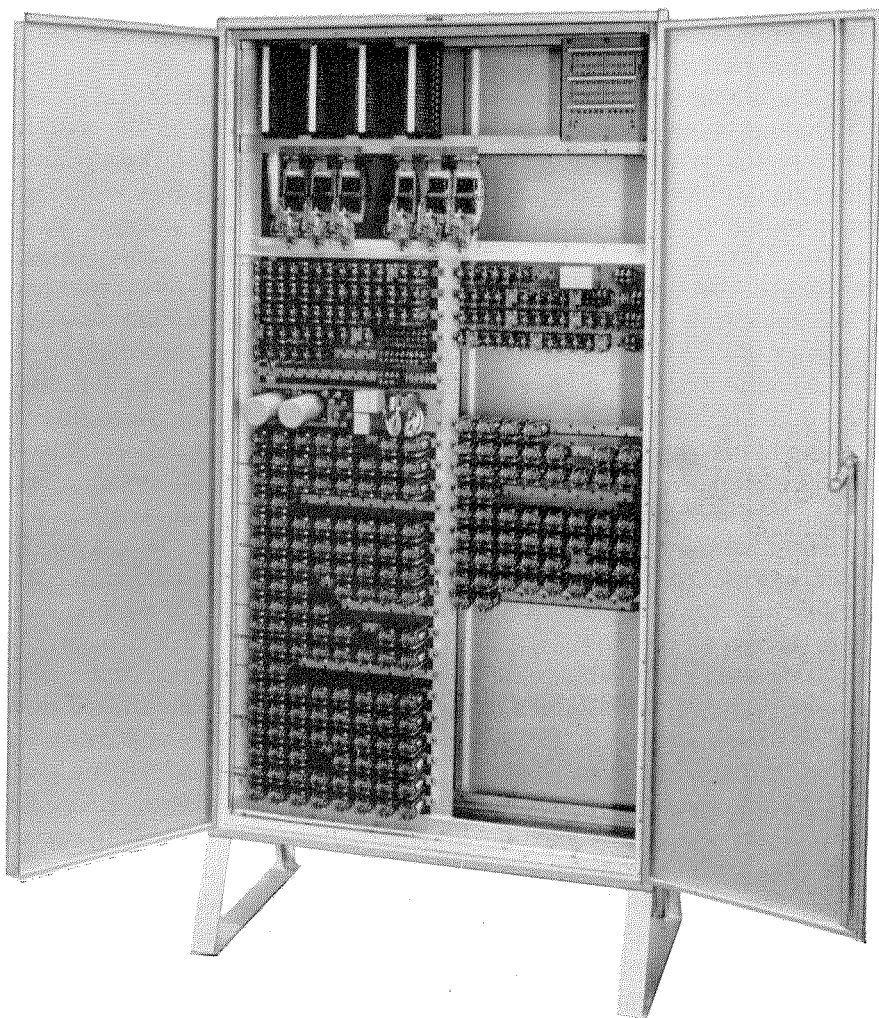
Let us now presume that the operator at the master control board wishes in the particular substation shown in Figure 4 to change the position of the power switch.

He will first turn the key of *SM2* to the new position desired. On depressing the same key, potentials corresponding to the desired position are placed on the contact banks of two step-by-step marker switches *SM3* and *SM4*. The wipers of *SM3* will move across the contacts and stop on the one corresponding to the number of the substation where the apparatus to be operated is located. The wipers in the second switch stop on the terminals corresponding to the power switch. The impulse generator of the master station then advances synchronously selector *SM1* at the master station and the selectors *SC1* at all of the substations.

Three of these impulses are polarized by a relay *RYM2* at the master station; this relay is operated twice in accordance with the code registered in the contacts of *SM3* and then once more in accordance with the power-apparatus number registered on *SM4*. As soon as the desired substation has recognized its code, it blocks the other substations by placing a potential on the blocking pair

toward the control station and cutting the other side of both pairs. By this action, all selectors *SC1* at the other substations automatically return to normal position whereas *SC1* at the desired substation continues to rotate under control of the transmitted impulses. During this rotation, it energizes *RYC4*, associated with the desired power switch, and stops in the normal position at the end of the impulse train.

Then in return, *SC1* sends a sequence of impulses back to the master station where *SM1* continues to revolve in synchronism. The first six impulses signal the code of the connected substation. The following impulses will be positive until the one corresponding to the power switch



One of the master transmitter cabinets at Zwolle is shown above.

that is to be operated. This impulse will be negative and its effect will be to stop both *SC1* and *SM1* on the proper terminal corresponding to the desired power switch *RYC5*.

Some additional impulses having a polarity

commence a complete new cycle by means of which the position of all apparatus in this substation is retransmitted to the master station for checking purposes.

The complete control cycle described above requires approximately 12 seconds.

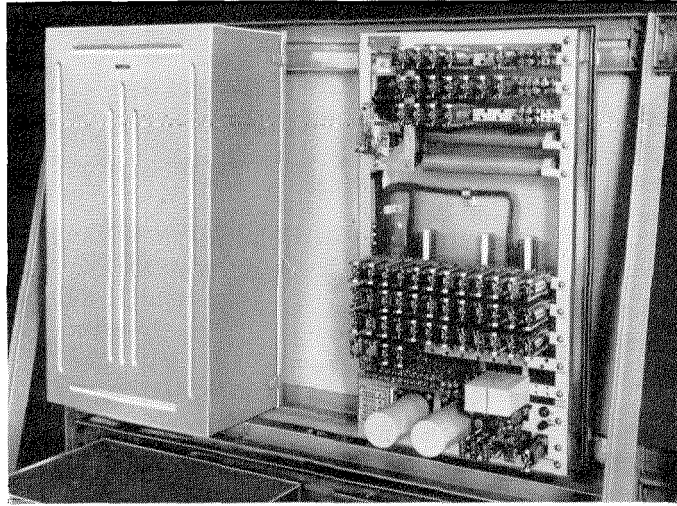
If the operator should change his mind before sending the actuating impulse to the station by the second depression of *SM2*, he can cancel his previous orders by depressing a special common key.

10.3 CHECKS AND ALARMS

Operations such as checking for proper signaling performance of one or all substations, testing of lamps, automatic signaling of voltage loss of the control battery for each substation, and the disabling of any substation are additional features that have been incorporated in the system.

It should be noted that the system is immune to any disturbance through breaking of signaling lines, false pulsing, or blocking of impulses that

occur either during signaling or control, because all signals to substations must be properly answered. Unless the answer is correct, the signaling system is blocked and an alarm is given until corrective action is taken.



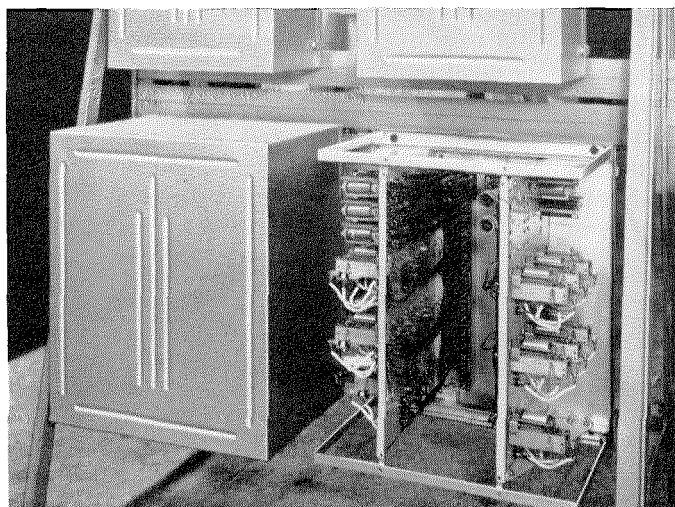
The transmitter at a substation.

determined by the actual position of the power switch will be sent from the substation to the master station. These will not move either *SC1* or *SM1* but in the master station will cause a red or a green lamp to flash.

If the chain of impulses from the substation corresponds exactly with the indications of substation apparatus as marked in the beginning on the terminals of *SM3* and *SM4*, a second depression of *SM2* will complete the operation by sending a single actuating impulse to the substation.

At the substation, this impulse is directed through contacts of *SC1* to the coil circuit of contacting mercury relay *RYC5*. Operation of *RYC5* will close the control circuit of the power switch, which will thereupon move to the desired position.

As soon as this power switch has been operated, *SC1* and *SM1* return to normal position and from there



Mercury-type contacting relays for control of substation switches.

Electrical and Physical Properties of IN-420: A New Chlorinated Liquid Dielectric*

By A. J. WARNER

Federal Telecommunication Laboratories, Incorporated; Nutley, New Jersey

A FAMILY of new chlorinated liquid dielectrics has been developed. One member of this series, dichloro-1,3,3-trimethyl-1-phenylindan (designated as *IN-420*), appears particularly suitable for use as a capacitor impregnant. Values of dissipation factor and direct-current resistivity are comparable to or somewhat better than existing commercial chlorinated biphenyls. Its dielectric constant and dielectric strength are somewhat superior to those of the chlorinated biphenyls.

In life-test studies in which capacitors impregnated with *IN-420* were compared with capacitors containing stabilized and unstabilized chlorinated biphenyls, a marked superiority was shown in life-test characteristics and particularly at temperatures as high as 125 degrees centigrade.

. . .

The use of chlorinated hydrocarbons in electric apparatus and components has increased steadily in the past few years, particularly in applications such as capacitors where the use of high-dielectric-constant materials is advantageous.¹⁻³ Continued research and development has produced materials useful over a wide temperature range and possessing good performance characteristics under prolonged electrical stress. Typical of such materials are the chlorinated biphenyls (Aroclors) and the chlorinated naphthalenes (Halowaxes). It is the purpose of this paper to

* Reprinted from *Communication and Electronics*, number 3, pages 330-335; November, 1952. Presented before the American Institute of Electrical Engineers Summer General Meeting, Minneapolis, Minnesota; June 23-27, 1952.

¹ F. M. Clark, "Nonflammable Dielectric Organic Compounds," *Industrial and Engineering Chemistry*, volume 29, pages 698-702; June, 1937.

² L. J. Berberich, C. V. Fields, and R. E. Marbury, "Characteristics of Chlorinated Impregnants in Direct-Current Paper Capacitors," *Proceedings of the IRE*, volume 33, pages 389-397; June, 1945.

³ F. M. Clark, "Electrical Insulation," *Chemical and Engineering News*, volume 25, pages 2976-2978; October 13, 1947.

introduce a new family of chlorinated hydrocarbons, although details will be given for just one member of the family at this time.

1. Chlorinated Indans

For many years the Federal Telecommunication Laboratories has been interested in the substituted phenylindan derivatives, and particularly in the compound having the structural formula shown in Figure 1.

This material can be obtained in good yields, and economically, from available raw materials by relatively simple processes. It is a crystalline material having a melting point of 52 degrees centigrade, a boiling point of 145 degrees centigrade at a mercury pressure of 4 millimeters, and a refractive index at 20 degrees centigrade of

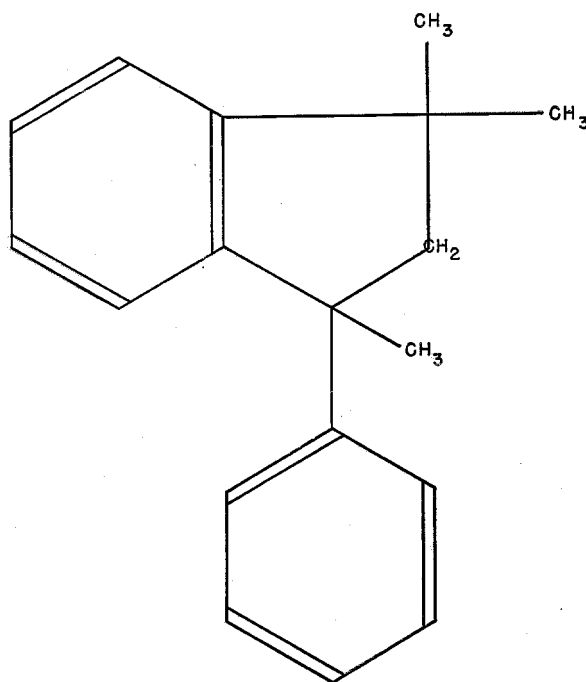


Figure 1—Structural formula of 1,3,3-trimethyl-1-phenylindan.

1.5660. At its melting point, it has a dielectric constant of 2.55 and a dissipation factor of 0.001₄. Despite the fact that it is not possible to construct a model of this compound using conventional Fisher-Hirschfelder building blocks,

pentachlorobiphenyl (Aroclor 1254), are shown in Table 1. The data for *IN-420* and Aroclor 1254 were determined in our laboratories; those obtained for the latter impregnant are in general accord with the information contained in the trade literature.⁴

The viscosity of *IN-420* as a function of temperature is given in Figure 2.

The electrical properties of this material have been extensively investigated using a rhodium-plated guarded test cell. The 60-cycle-per-second dielectric constant and dissipation factor measurements were made on a modified 60-cycle Schering bridge operating at 3000 root-mean-square volts, and with a dielectric voltage stress of 37.5 volts per mil. Direct-current volume-resistivity measurements were made with a General Radio type 544-B megohm bridge. Measurements of dissipation factor and dielectric constant at frequencies from 400 to 100,000 cycles per second were made on a special audio-frequency test set. The temperature of the test

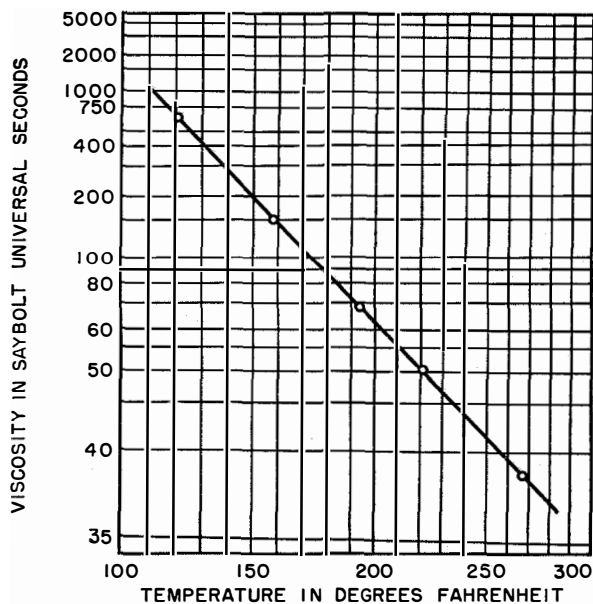


Figure 2—Saybolt viscosity of dichloro-1,3,3-trimethyl-1-phenylindan as a function of temperature. Plotted on American Society for Testing Materials standard viscosity-temperature chart B.

which is normally taken as indicating that such a structure, if possible, would be highly unstable, the substituted indan has been found to possess a high order of stability.

This high stability encouraged the preparation of the chlorinated derivatives, and it has been found possible to prepare the full range of products up to and including the nonachloro derivative, ranging from a mobile light-colored liquid to brittle high-melting-point resins. Although data have been accumulated on the whole range of products obtained, the particular properties of the dichloro derivative were such as to offer immediate application possibilities, and these properties have been studied most extensively.

Dichloro-1,3,3-trimethyl-1-phenylindan, to which the trivial name *IN-420* has been given, is a clear, lightly yellow-colored, medium-viscosity material having a bluish fluorescence. Representative physical data, in comparison with

TABLE 1

PHYSICAL PROPERTIES OF *IN-420* AND AROCLOR 1254

Property	<i>IN-420</i>	Aroclor 1254
Refractive Index at 25 Degrees Centigrade	1.5838	1.6380
Specific Gravity at 65 Degrees per 15.5 Degrees	1.141	1.502
Pour Point in Degrees Centigrade	8	8
Acidity in Milligrams NaOH per Gram	0.001	0.001
Free Inorganic Chlorides in Parts per Million	0.1	0.05
Distillation Range in Degrees Centigrade		
First Drop	340	—
10 Percent	343	370
40 Percent	347	376
90 Percent	356.6	387
Flash Point in Degrees Centigrade	185	—
Fire Point in Degrees Centigrade	250	—

cell was maintained within 0.2 degree centigrade for a 45-minute period previous to each measurement.

The curves of dielectric constant and dissipation factor at 60 cycles versus temperature are plotted in Figures 3 and 4. The dissipation factor above 30 degrees centigrade is purely ionic, increasing logarithmically with increasing

⁴ "The Aroclors," Monsanto Chemical Company Technical Bulletin P-115, St. Louis, Missouri; June, 1950.

temperature. Below 30 degrees centigrade, the dissipation factor increases, going through a maximum at -6 degrees, then decreasing. The 60-cycle dielectric constant decreases as the temperature is increased from 5 to 100 degrees centigrade with an average relative change of 0.012 per degree centigrade due primarily to

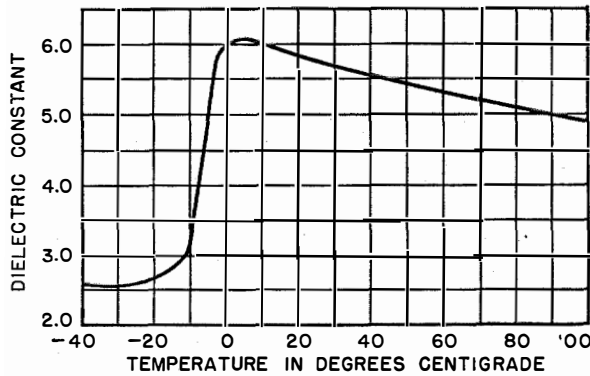


Figure 3—Dielectric constant at 60 cycles of dichloro-1,3,3-trimethyl-1-phenylindan as a function of temperature.

decreasing density. Below 5 degrees centigrade, the dielectric constant decreases rapidly, becoming asymptotic to a value of approximately 2.58. The inflection point of this curve occurs at approximately -6 degrees centigrade. The phenomenon centering about the -6 -degree point is the dipolar anomalous dispersion, the molecule dipole being in resonance with the applied 60-cycle voltage at this temperature.

Individual samples may show slight differences in dissipation factor at temperatures above 30 degrees centigrade due to the presence of small amounts of adventitious material such as water, but the values shown may be taken as representative of clean, dried material.

A curve of dissipation factor at 24.0 degrees centigrade versus frequency from 60 cycles to 100 kilocycles per second is plotted in Figure 5. Measurements were made on two specimens over the 400-

cycle to 100-kilocycle range. The 60-cycle point is taken from Figure 4. The change in dielectric constant over the frequency range is less than 1 percent, the mean value being 5.71.

A curve of direct-current volume resistivity versus temperature from 40 to 100 degrees centigrade is plotted in Figure 6. The points plotted are the averages of measurements made on four specimens. These measurements were made after an electrification period of 3 minutes. Although a 1-minute electrification is the more common, it was found that use of a 3-minute period resulted in the obtaining of more stable values and hence in an improved reproducibility of measurements.

The corresponding data for Aroclor 1254 indicate a general similarity, and for comparison we may take data at 50 and 100 degrees centigrade as shown in Table 2.

TABLE 2

ELECTRICAL PROPERTIES OF *IN-420* AND AROCLOR 1254

Material	Degrees Centigrade	Tan δ	ϵ'
<i>IN-420</i>	50	0.00085	5.31
	100	0.0400	4.90
Aroclor 1254	50	0.0011	4.80
	100	0.0427	4.25

The values of dissipation factor for *IN-420* are slightly better than for Aroclor 1254 and the direct-current resistivity values for the two

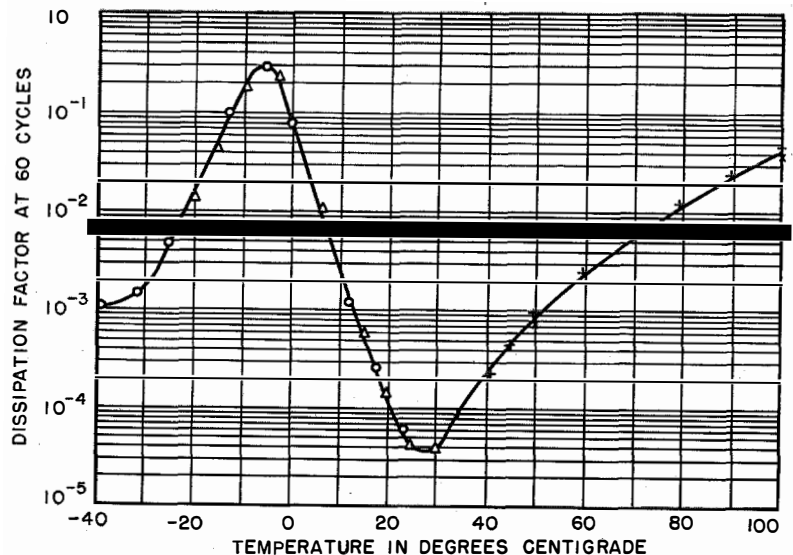


Figure 4—Dissipation factor at 60 cycles of dichloro-1,3,3-trimethyl-1-phenylindan as a function of temperature.

materials are comparable. *IN-420* however, has a somewhat higher dielectric constant of 4.90 at 100 degrees centigrade as compared to 4.25 for *Aroclor 1254* at the same temperature.

The dielectric-strength properties of impregnants are obviously of great importance to the user of such materials for electric apparatus and components, and comparative tests in our laboratory made on *IN-420* and *Aroclor 1254* gave values of greater than 45 kilovolts and greater than 35 kilovolts, respectively, for an electrode spacing of 100 mils. Also of interest is the maintenance of high breakdown values on repeated testing of the same sample of *IN-420*.

2. Life-Test Studies

On the basis of the physical and electrical results obtained on this new material, it was felt that some practical data on its use potentialities would be in order. Therefore, capacitors were

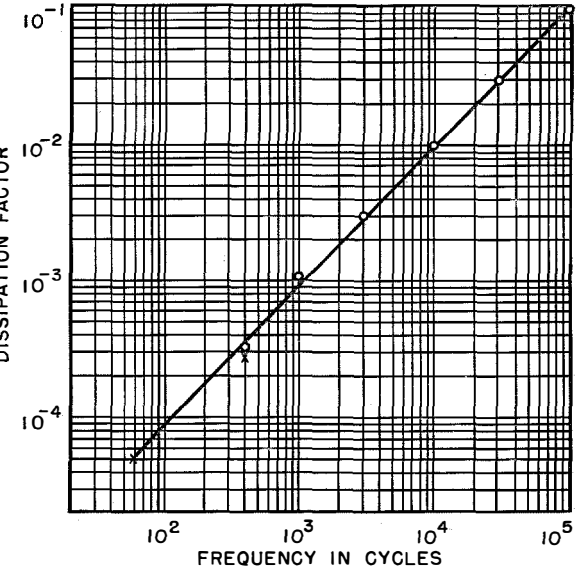


Figure 5—Dissipation factor at 24 degrees centigrade of dichloro-1,3,3-trimethyl-1-phenylindan as a function of frequency.

assembled, comprising 0.0005-inch-thick aluminum foil separated by two thicknesses of 0.0004-inch unbleached kraft capacitor tissue (Peter J. Schweitzer, Inc.), having an approximate capacitance of 0.06 microfarad when impregnated. Kraft tissue was used in assembling these capacitors in view of the reported superiority of

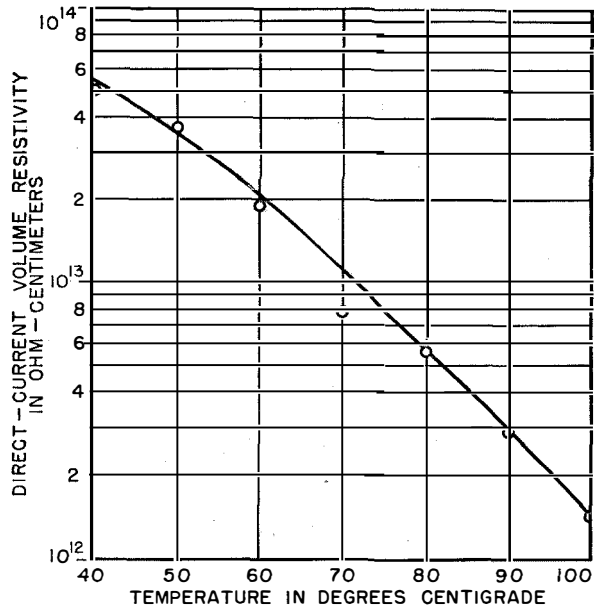


Figure 6—Direct-current volume resistivity of dichloro-1,3,3-trimethyl-1-phenylindan as a function of temperature.

this material compared with linen paper.^{5,6} For comparison purposes, *Aroclor 1254* was used as an impregnant in half of the units assembled, and the greatest care was exercised during assembly and impregnation to ensure minimum contamination. In some experiments stabilizers^{7,8} were added to the chlorinated impregnant.

Some of the units were put on continuous life test at 120 and others at 125 degrees centigrade, while the voltages used were 450 and 600 volts direct current. The results obtained have been plotted in a conventional manner on logarithmic probability paper, from which the life value for 50-percent failure can be obtained. A direct comparison of these data enables some measure of the usefulness of the new impregnant to be

⁵ D. A. McLean, "Paper Problems in Telephone Apparatus," *Paper Trade Journal*, volume 118, pages 31-34; January 27, 1944.

⁶ D. A. McLean, L. Egerton, and C. C. Houtz, "Paper Capacitors Containing Chlorinated Impregnants," *Industrial and Engineering Chemistry*, volume 38, pages 1110-1116; November, 1946.

⁷ D. A. McLean and L. Egerton, "Paper Capacitors Containing Chlorinated Impregnant—Stabilization by Anthraquinone," *Industrial and Engineering Chemistry*, volume 37, pages 73-79; January, 1945.

⁸ L. J. Berberich and R. Friedman, "Stabilization of Chlorinated Biphenyl in Paper Capacitors," *Industrial and Engineering Chemistry*, volume 40, pages 117-123; January, 1948.

determined. Figure 7 gives the data for 120 degrees centigrade and 450 volts, Figure 8 that for 120 degrees centigrade and 600 volts, and Figure 9 that for 125 degrees centigrade and 450 volts.

From Figures 7 and 8, it will be seen that the *IN-420* is superior in life characteristics under the stated conditions to Aroclor *1254*, even when the Aroclor is improved in a known manner by the addition of 0.5-percent anthraquinone. Thus, as is seen in Figure 7, the 50-percent-failure point for plain Aroclor *1254* was 85 hours; for Aroclor *1254* plus 0.5-percent anthraquinone, it was 300 hours; whereas for plain *IN-420* the value was 375 hours. Should 0.5-percent anthraquinone be added to the *IN-420*, then the same stabilizing influence of the additive is evidenced, the 50-percent-failure point for this mixture being in excess of 2000 hours. Similarly, as shown in Figure 8, the 50-percent-failure point for capacitors impregnated with stabilized *IN-420* at 600 volts direct current was 250 hours as compared with 122 hours for the stabilized Aroclor *1254*.

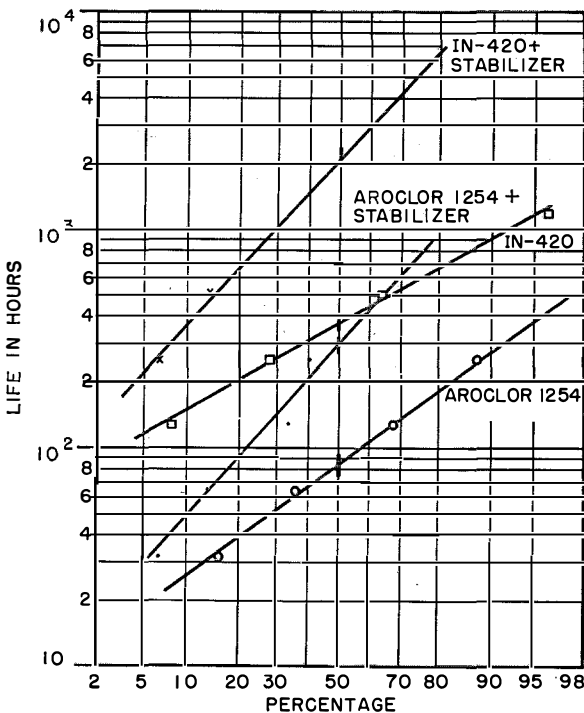


Figure 7—Continuous-life-test data at 120 degrees centigrade and 450 volts direct current of capacitors impregnated with stabilized and unstabilized *IN-420* and Aroclor *1254*.

At the somewhat higher temperature of 125 degrees centigrade, as shown in Figure 9, a corresponding superiority was maintained, the 50-percent-failure points being 35 hours and 85 hours.

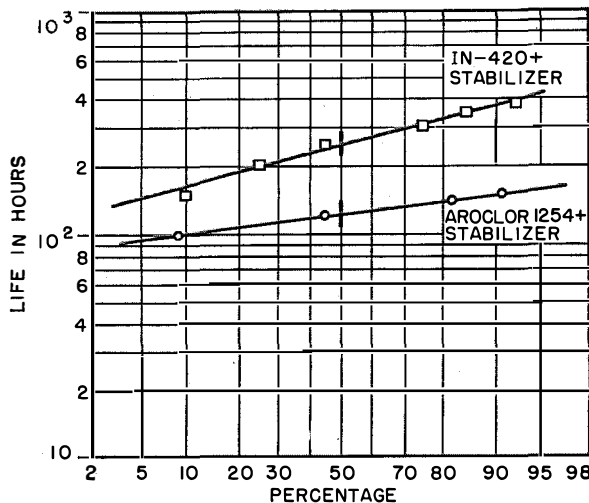


Figure 8—Continuous-life-test data at 120 degrees centigrade and 600 volts direct current of capacitors impregnated with stabilized *IN-420* and Aroclor *1254*.

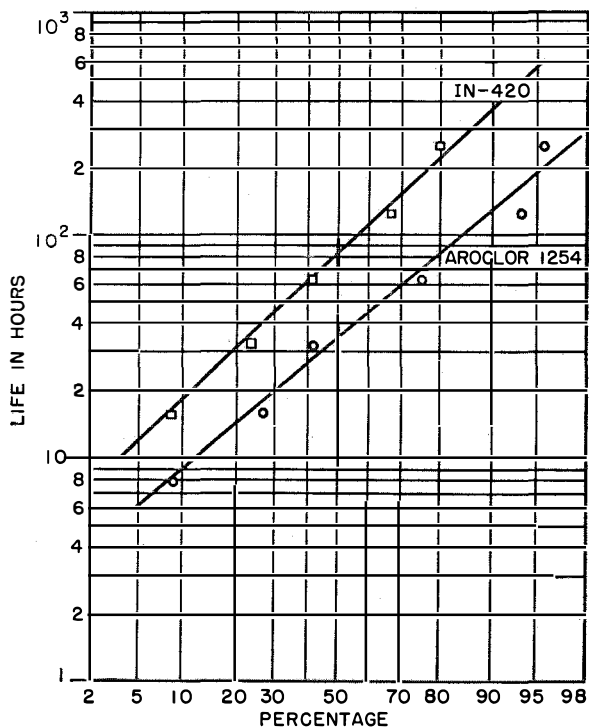


Figure 9—Continuous-life-test data at 125 degrees centigrade and 450 volts direct current of capacitors impregnated with unstabilized *IN-420* and Aroclor *1254*.

hours for the unstabilized Aroclor 1254 and *IN-420*, respectively.

The life-test studies reported herein were performed under direct-current-test conditions because of the severer and more rapid breakdown of impregnated capacitors under such a stress.^{9,10} Preliminary results reported by an outside laboratory on capacitors impregnated with *IN-*

420 and evaluated under alternating-current test conditions are very promising. Further evaluation of alternating-current applications is continuing, and these results will be reported at another time.

3. Conclusion

It will be seen, therefore, on the basis of the foregoing, that *IN-420*, a new chlorinated liquid dielectric, possesses physical and electrical characteristics indicating its usefulness particularly in capacitor applications and for use at elevated temperatures where its remarkable stability under electrical stress can be exploited.

⁹ D. A. McLean, L. Egerton, G. T. Kohman, and M. Brotherton, "Paper Dielectrics Containing Chlorinated Impregnants; Deterioration in Direct-Current Fields," *Industrial and Engineering Chemistry*, volume 34, pages 101-109; January, 1942.

¹⁰ M. Brotherton, "Capacitors—Their Use in Electronic Circuits," First Edition, D. Van Nostrand Company, New York, New York; 1946.

Microwave Technique for Studying Discharges in Gases*

By M. A. LAMPERT† and A. D. WHITE

Federal Telecommunication Laboratories, Incorporated; Nutley, New Jersey

MICROWAVE measurement techniques have been applied in recent years with notable success to the study of discharges in gases. Outstanding contributions in this field have been made by the group associated with Professors Allis and Brown at Massachusetts Institute of Technology. The efforts of this group have been concentrated largely on the study of discharges initiated and maintained by radio-frequency energy. The authors' group, until recently under the guidance of Ladislas Goldstein‡, has also used microwave techniques to study both continuous and pulsed radio-frequency and direct-current discharges. Most of the previous studies have been concerned with problems of gas breakdown and with measurements of electron density, electron temperature, and with electron-molecule collisional frequencies. It is the purpose of the present paper to describe a new technique for the exploration of a gaseous discharge, namely a technique in which a microwave signal functions as a type of localized probe. Though the technique in its present form does not admit of very great precision, nevertheless, the results obtained thus far are sufficiently interesting and suggestive to merit publication at this time.

1. Glow-Discharge Field Distribution

A few remarks are in order as to some of the considerations underlying this work. Figure 1 shows various characteristics of a cold-cathode glow discharge, as taken from the Druyvesteyn-Penning article.¹ Of particular interest is the

* Presented at the Conference on Gaseous Electronics at Princeton, New Jersey, on September 5, 1952. This work was sponsored by the United States Army Signal Corps Engineering Laboratories; Fort Monmouth, New Jersey.

† Now with RCA Laboratories Division; Princeton, New Jersey.

‡ Now on the faculty of the University of Illinois; Urbana, Illinois.

¹ M. J. Druyvesteyn and F. M. Penning, "Mechanism of Electrical Discharges in Gases of Low Pressure," *Reviews of Modern Physics*, volume 12, pages 87-174; April, 1940.

electric-field-distribution curve E , which is seen to cover a wide range of values, even reversing in a narrow region near the cathode. In view of such a distribution, it might be expected that if in some fashion one could subject successive localized regions of the direct-current discharge to radio-frequency fields, then the resulting effects on the discharge would depend markedly on the region exposed.

2. Apparatus

A way of making such a study is illustrated in Figure 2. A small-bore cold-cathode discharge tube is inserted through a section of specially fabricated pancake waveguide, as shown on the right. This pancake waveguide has an inside height of only 0.040 inch (1 millimeter). The discharge is maintained continuously by a battery, and the current is limited by a series resistor. When microwave energy is fed into the waveguide transmission system, a radio-frequency field is impressed across that narrow part of the discharge inside the pancake waveguide. The presence of the microwave electric field

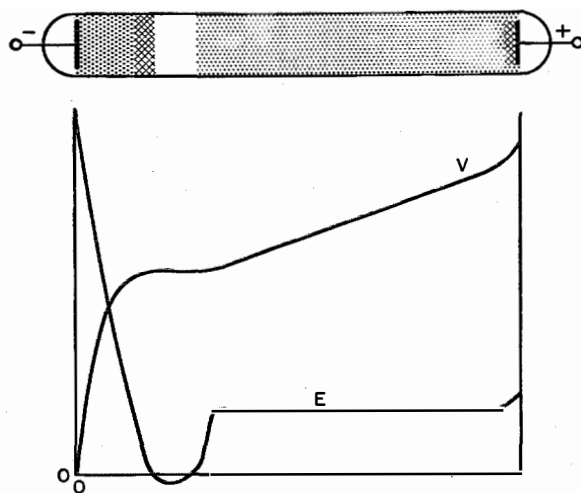


Figure 1—Light emission (at top), potential distribution V , and field strength E of a direct-current glow discharge in a long tube.

across part of the discharge causes a change in the discharge direct current. This current change is the quantity studied in these experiments.

The waveguide system seen to the left in Figure 2 consists of standard measuring and

limit this spreading, metallic collars have been placed around the discharge tube. The diameter of the collars is such that rapid attenuation of the signal takes place in the collar. However, to the extent that signal leakage into the collar

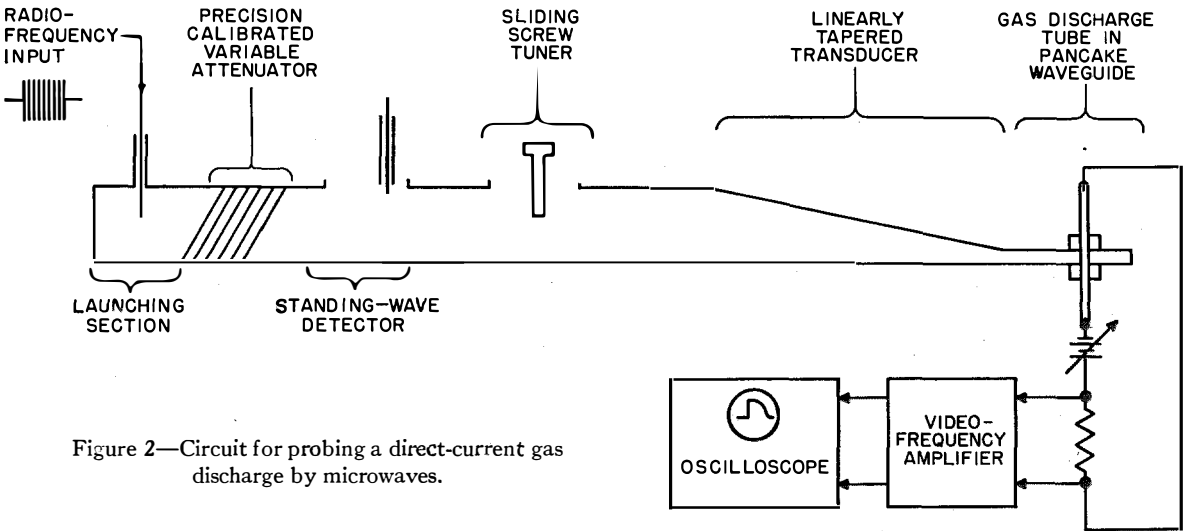


Figure 2—Circuit for probing a direct-current gas discharge by microwaves.

matching components. A linearly tapered transducer matches the standard 2-by-1-inch (5-by-2.5-centimeter) waveguide to the pancake waveguide. The signal frequency used in the experiments was approximately 5000 megacycles, and the radio-frequency power level was in all cases less than 100 milliwatts. By using a microwave pulse, rather than a continuous signal, it was possible to display visually the effects of the microwave energy on the discharge current by connecting a video-frequency amplifier and cathode-ray oscilloscope to the series resistor.

The microwave pulse envelope was rectangular and between 10 and 40 microseconds long.

Actually, signal is applied only to the region of the discharge within the pancake guide, but the fields also spread through the holes in the guide to adjacent regions of the discharge. To

regions takes place, the microwave "probe" is correspondingly not sharply defined.

Figure 3 shows a magnified version of the test end of the experimental setup. The section of pancake waveguide is shorted at a point three-quarters of a guide wavelength from the gas tube to subject the part of the discharge inside the guide to a region of maximum signal field.

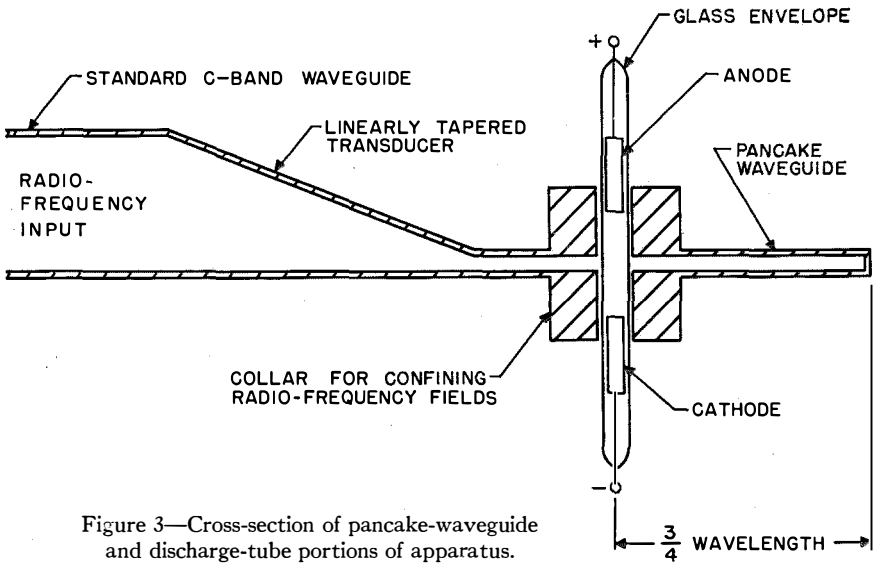


Figure 3—Cross-section of pancake-waveguide and discharge-tube portions of apparatus.

3. Experimental Results

Some qualitative forms of the data obtained with a neon discharge are shown in Figure 4. The visual appearance of the discharge is indicated on the left, the outlines of the luminous regions being shown. On the right are displayed various discharge-current waveforms as viewed on the oscilloscope. The waveform at *E* is the envelope of the applied signal pulse. The others show the rectified-current pulses that appear across the limiting resistor with various regions of the discharge exposed to the signal field. Of particular interest is the fact that the current pulse *A* obtained at the cathode end of the discharge shows a prolonged decay following the termination of the signal. This is obviously not the case with the pulse *D* obtained at the anode end. It should be pointed out that for the amplitudes of the various pulses in Figure 4 to appear about equal, substantial changes in the microwave signal power level were necessary.

This point is made evident by Figure 5, in which are plotted quantitative data obtained in the same experiment. It was observed that a linear relationship exists between the signal power level and the resultant change in dis-

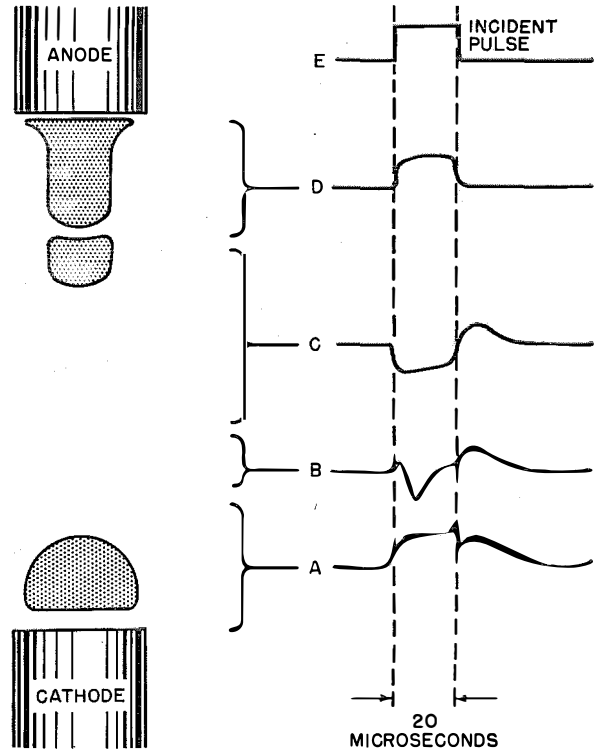


Figure 4—Variation of current through the discharge tube when the microwave pulse is applied to the indicated regions of the discharge. The form of the microwave pulse is shown at *E*. The discharge tube was filled with neon at a pressure of 5 millimeters of mercury. The electrodes were of aluminum. The steady-state discharge current was 0.30 milli-ampere.

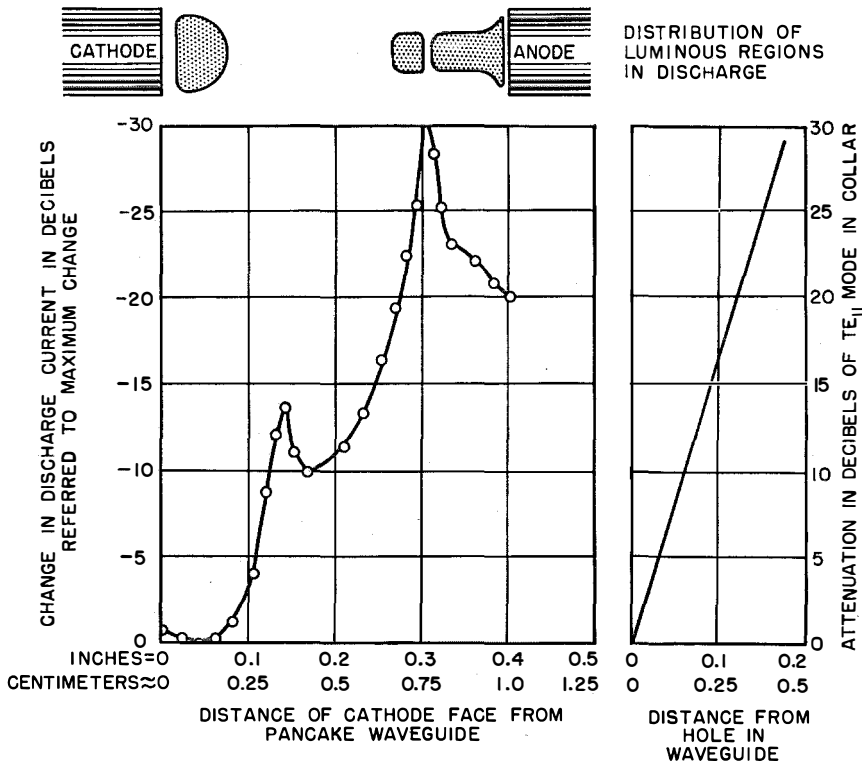


Figure 5—At left, change in discharge current during radio-frequency pulse as a function of the position of the gas tube in the waveguide. The sketch above the chart shows the corresponding luminous regions in the discharge. The tube was filled with neon to a pressure of 5 millimeters of mercury and had aluminum electrodes. Steady-state discharge current was 0.50 milli-ampere. The attenuation curve has a slope of 6.6 decibels per millimeter (168 decibels per inch).

charge current. Thus, even though the experiments were done by varying the power level in the waveguide to hold the change in the discharge current constant, it is permissible to plot the results as though the signal power had been

computed attenuation of the microwave signal (in the TE_{11} mode) inside the collar region measured from the point where the signal is impressed. This attenuation amounts to 6.6 decibels per millimeter (168 decibels per inch).

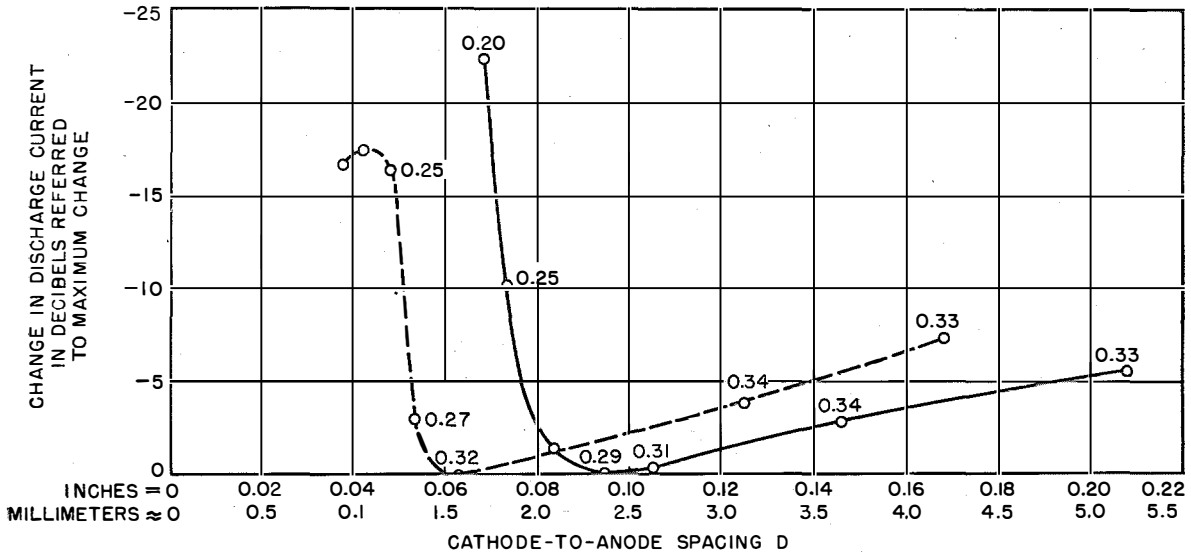
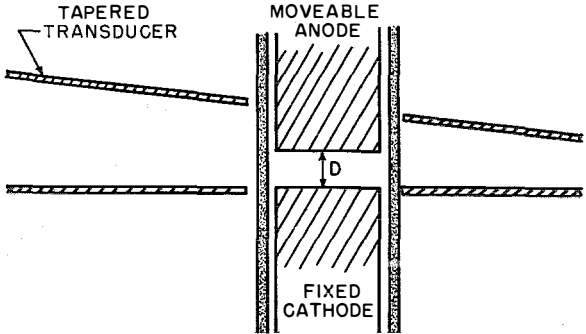


Figure 6—Change in discharge current during radio-frequency pulse as a function of cathode-to-anode spacing. The sketch at the right indicates the placement of the movable-electrode discharge tube in the tapered transducer. The tube had aluminum electrodes and was filled with neon plus one-percent argon to pressures of 6 millimeters of mercury (solid line) and 12 millimeters (dashed line). The numbers indicate the steady-state discharge currents in milliamperes for the various spacings.



held constant and the discharge-current changes were measured directly. The results are plotted in this fashion as the ordinate of the graph on the left in Figure 5, the abscissa being the position of the discharge tube with respect to the pancake waveguide. Directly above the chart is shown the corresponding region of the discharge that is exposed to the radio-frequency field. The ordinates are plotted in decibels below the maximum change in current. Thus, the minima in the curve indicate regions in the discharge that are particularly sensitive to signal influence. It is seen that there are three such regions, the most sensitive being near the cathode, the other two being near the anode and in a middle region, respectively. The graph on the right shows the

The general parallelism of the sensitivity characteristic on the left and the attenuation curve on the right indicates that the sensitive regions are really very narrow. The sensitivity characteristic would, no doubt, rise much more steeply away from the minima if it were not for the spreading of the microwave signal into the collar region.

These results may be related to the characteristics of the glow discharge, particularly to the electric-field distribution. Thus, it is a reasonable hypothesis that the region of the discharge near the cathode that is sensitive to radio-frequency fields is the narrow region of reversed electric field near the cathode seen in Figure 1. Supporting this hypothesis are the data illustrated in

Figure 6. In this experiment, the gas tube was mounted in a fixed position through two holes in the transducer, as shown, and the over-all sensitivity of the discharge to the signal was measured as the cathode-to-anode spacing was varied. The ordinate is the same as in Figure 5, and again a minimum in the curve indicates high sensitivity. Results are plotted for a glow discharge in a gas mixture of neon plus 1-percent argon at two pressures. The battery voltage is fixed, the single variable in the experiment being the cathode-to-anode spacing, plotted as the abscissa. The discharge currents for various electrode spacings are indicated for various points on the curves. The most conspicuous feature of the sensitivity characteristic is the sharp decrease in sensitivity when the spacing is below that corresponding to maximum sensitivity. The slowly changing discharge current in this region indicates that this decrease in sensitivity is not due to a fundamental change in the over-all discharge but simply to removal of the localized region sensitive to the microwave field. The pressure dependence is as expected, the lower the pressure, the farther the sensitive region is from the cathode.

4. Conclusions

One may speculate, using plausible physical arguments, as to why the region of reversed electric field near the cathode in the glow discharge should be very sensitive to microwave

fields. Insofar as the initial nonequilibrium disturbance of the discharge by the signal field is concerned, one may reason as follows. This region of reversed electric field is a barrier region that slow electrons cannot cross on their way to the anode. The presence of such slow electrons in this region is assured by the substantial number of ionizing and other inelastic collisions occurring in the region. The slow electrons that cannot pass the barrier are temporarily trapped. The presence of even a very weak signal field in this region changes the number of trapped slow electrons. (There may be an increase or decrease depending on many factors, such as the direct-current and radio-frequency electric-field distributions in this region.) This change could account for the onset of the disturbance. For the disturbance to reach equilibrium, it must reach the cathode where either the electron or ion current must change.

The major purpose of the present paper has been to illustrate the use of a new technique for the exploration of gaseous discharges, namely a technique in which a microwave signal is employed as a localized probe. In addition, it is felt by the authors that these experiments lend substantial weight to the hypothesis that sensitivity of a direct-current cold-cathode glow discharge to radio-frequency fields is related to the existence of one or more regions of reversed electric field in the discharge.

Telephone Statistics of the World*

APPROXIMATELY 79.4 million telephones were in service throughout the world on January 1, 1952, reflecting an increase during the year of 4.6 million.

Nine countries reported more than one million telephones in service on January 1, 1952: United States, United Kingdom, Canada, Western Germany, France, Japan, Sweden, Italy, and Australia. Of the world's principal countries, six had more than 15 telephones per 100 of the population: United States (29.3), Sweden (25.2), Canada (22.1), Switzerland (19.9), New Zealand (19.9), and Denmark (17.5).

The entire telephone industry in the United States is operated under private ownership. The American Telephone and Telegraph Company and its subsidiaries operated more than 80 percent of this country's 45,636,437 telephones;

there were nearly 5,500 other privately owned telephone companies at the beginning of 1952.

Physical facilities exist for the potential connection of a telephone user in the United States with about 96 percent of the world's telephones, although political restrictions prohibit certain international connections at present.

Only those telephones that are available to the general public are taken into consideration. Thus private intercommunicating sets and private-line telephones used exclusively by railroads and other agencies not having connection with a commercial system are excluded. Statistics reported as of other dates have been adjusted to January 1, 1952. Where current official data could not be obtained, estimates have been based on the latest figures available.

TELEPHONES IN CONTINENTAL AREAS

Partly estimated; statistics reported as of other dates have been adjusted to January 1, 1952

Continental Area	Total Telephones			Privately Owned		Automatic (Dial)	
	Number	Percent of Total World	Per 100 Population	Number	Percent of Total	Number	Percent of Total
North America	48,796,300	61.5	28.7	48,353,000	99.1	34,909,100	71.5
Middle America	593,700	0.7	1.1	540,500	91.0	422,700	71.2
South America	1,931,000	2.4	1.7	966,200	50.0	1,468,400	76.0
Europe	22,362,000	28.2	3.6	3,453,400	15.4	15,903,500	71.1
Africa	986,000	1.2	0.5	18,200	1.8	648,800	65.8
Asia	2,944,000	3.7	0.2	213,100	7.2	1,393,000	47.3
Oceania	1,787,000	2.3	12.2	125,400	7.0	1,156,400	64.7
World	79,400,000	100.0	3.3	53,669,800	67.6	55,901,900	70.4
United States	45,636,437	57.5	29.3	45,636,437	100.0	32,900,000	72.1

* Abridgement from a booklet issued by The American Telephone and Telegraph Company; New York, New York.

TELEPHONES IN COUNTRIES OF THE WORLD

January 1, 1952

Country	Total Telephones	Per 100 Population	Percent Automatic (Dial)	Ownership	
				Private	Government
NORTH AMERICA					
Alaska	19,669	15.0	61.5	19,605	64
Canada (1)	3,140,000	22.1	63.6	2,697,000	443,000
Greenland	0	—	—	—	—
St. Pierre and Miquelon	160	3.5	0	0	160
United States	45,636,437	29.3	72.1	45,636,437	0
MIDDLE AMERICA					
Bahamas	4,891	6.0	98.8	0	4,891
Barbados	4,787	2.2	97.6	4,787	0
Bermuda (2)	6,912	18.5	100	6,912	0
British Honduras	746	1.1	0	0	746
Canal Zone (3) (4)	6,184	7.7	100	0	6,184
Costa Rica	9,938	1.2	0	9,700	238
Cuba	131,405	2.4	84.5	130,905	500
Dominican Republic	7,360	0.3	69.5	7,211	149
El Salvador	8,100	0.4	71.0	0	8,100
Guadeloupe	926	0.3	0	0	926
Guatemala	5,575	0.2	80.5	0	5,575
Haiti	3,809	0.1	88.1	0	3,809
Honduras	2,451	0.2	55.3	0	2,451
Jamaica	14,704	1.0	96.3	14,704	0
Leeward Islands	880	0.8	0	0	880
Martinique	2,746	1.0	0	0	2,746
Mexico	299,327	1.2	67.8	298,494	833
Netherlands Antilles	6,292	3.8	97.1	0	6,292
Nicaragua	3,522	0.3	0	0	3,522
Panama	13,107	1.6	81.6	13,107	0
Puerto Rico	41,291	1.8	52.3	38,788	2,503
Trinidad and Tobago	16,170	2.5	86.0	16,170	0
Virgin Islands (United States)	1,055	2.9	0	0	1,055
Windward Islands					
Dominica	299	0.5	0	0	299
Grenada	800	1.1	0	0	800
St. Lucia	366	0.4	0	0	366
St. Vincent	400	0.6	0	0	400
Total	1,865	0.7	0	0	1,865
SOUTH AMERICA					
Argentina	852,327	4.8	77.8	81,587	770,740
Bolivia	10,535	0.3	94.9	10,535	0
Brazil	591,700	1.1	78.6	590,200	1,500
British-Guiana	3,481	0.8	7.8	0	3,481
Chile	137,700	2.3	66.8	137,700	0
Colombia	97,864	0.8	51.1	17,999	79,865
Ecuador (1)	9,000	0.3	11.1	1,200	7,800
Falkland Islands	307	13.3	0	0	307
French Guiana	276	1.0	0	0	276
Paraguay	5,316	0.4	86.5	0	5,316
Peru	51,407	0.6	81.2	51,407	0
Surinam	1,961	0.9	36.3	0	1,961
Uruguay	95,080	4.0	74.0	1,085	93,995
Venezuela	74,494	1.5	93.6	74,494	0
EUROPE					
Albania (1)	1,300	0.1	0	0	1,300
Andorra	100	2.0	0	0	100
Austria	426,934	6.2	76.0	0	426,934
Belgium	715,228	8.2	75.5	0	715,228
Bulgaria (1)	60,000	0.8	43.3	0	60,000
Czechoslovakia (5)	350,708	2.9	59.4	0	350,708
Denmark	760,244	17.5	40.6	722,090	38,154
Finland	359,201	8.8	57.6	312,282	46,919
France	2,520,762	5.9	62.4	0	2,520,762
Germany, Eastern, and Berlin (1)	359,000	1.7	55.7	0	359,000
Germany, Western (1)	2,700,104	5.6	87.3	0	2,700,104
Gibraltar (1)	1,400	6.4	89.3	0	1,400
Greece (1)	88,439	1.2	93.8	88,439	0
Hungary (1)	117,000	1.3	73.3	0	117,000

(1) Data partly estimated.

(2) June 30, 1952.

(3) Excluding telephone systems of the United States military forces.

(4) June 30, 1951.

(5) January 1, 1948 (latest official statistics).

(6) March 31, 1952.

(7) January 1, 1936 (latest official statistics).

+ Less than 0.1.

TELEPHONES IN COUNTRIES OF THE WORLD—Continued

Country	Total Telephones	Per 100 Population	Percent Automatic (Dial)	Ownership	
				Private	Government
EUROPE—Continued					
Iceland	21,368	14.6	65.3	0	21,368
Ireland	90,307	3.1	65.3	0	90,307
Italy	1,382,438	3.0	92.9	1,382,438	0
Liechtenstein	1,967	14.1	100	0	1,967
Luxemburg	24,679	8.5	71.5	0	24,679
Malta and Gozo	(6) 7,366	2.4	0	0	7,366
Monaco	2,532	13.3	79.0	0	2,532
Netherlands	821,036	8.0	90.8	0	821,036
Norway	(4) 476,706	14.5	59.2	80,050	396,656
Poland	(1) 230,000	0.9	67.4	0	230,000
Portugal	168,161	2.0	49.1	108,566	59,595
Romania	(1) 137,000	0.9	74.5	0	137,000
San Marino	(1) 100	0.7	0	0	100
Spain	742,473	2.6	77.3	728,843	13,630
Sweden	1,788,874	25.2	66.2	1,881	1,786,993
Switzerland	952,450	19.9	97.3	0	952,450
Trieste	27,191	7.3	98.2	26,691	500
Russia	(7) 861,181	0.5	19.9	0	861,181
United Kingdom	(6) 5,724,440	11.4	72.8	0	5,724,440
Yugoslavia	(1) 85,000	0.5	65.0	0	85,000
AFRICA					
Algeria	102,858	1.1	65.3	0	102,858
Anglo-Egyptian Sudan	9,824	0.1	73.5	0	9,824
Basutoland	401	+	0	0	401
Bechuanaland Protectorate	123	+	0	0	123
Belgian Congo	6,993	+	59.0	0	6,993
British East Africa	24,031	0.1	67.7	0	24,031
British South Africa					
Nyasaland Protectorate	1,234	+	27.1	0	1,234
Northern Rhodesia	4,738	0.2	89.7	0	4,738
Southern Rhodesia	26,729	1.2	76.1	0	26,729
Total	32,701	0.5	76.2	0	32,701
British South-West Africa	(1) 5,000	1.6	50.0	0	5,000
British West Africa					
Gambia	290	0.1	0	0	290
Gold Coast	7,498	0.2	1.8	0	7,498
Nigeria	12,032	+	3.2	0	12,032
Sierra Leone	1,250	+	72.0	0	1,250
Total	21,070	+	6.7	0	21,070
Comoro Archipelago	0	—	—	—	—
Egypt	125,308	0.6	66.9	0	125,308
Eritrea	2,796	0.3	73.4	0	2,796
Ethiopia	2,050	+	78.0	0	2,050
French Cameroon	1,182	+	0	0	1,182
French Equatorial Africa	1,332	+	0	0	1,332
French Somaliland	499	1.0	0	0	499
French Togo	560	+	0	0	560
French West Africa	13,920	+	41.2	0	13,920
Libya	4,912	0.4	71.6	0	4,912
Liberia	0	—	—	—	—
Madagascar	5,900	0.1	0	0	5,900
Mauritius	5,142	1.0	5.6	0	5,142
Morocco					
French Zone	61,762	0.7	77.7	0	61,762
Spanish Zone	10,332	1.0	59.0	10,332	0
Tangier Zone	7,661	7.7	96.5	7,398	263
Total	79,755	0.8	77.1	17,730	62,025
Portuguese Africa					
Angola	2,120	+	73.3	0	2,120
Cape Verde Islands	130	+	0	0	130
Mozambique	4,963	+	73.1	0	4,963
Portuguese Guinea	170	+	79.4	0	170
South Tome and Principe	246	0.4	0	0	246
Total	7,629	+	69.7	0	7,629
Reunion	(1) 2,050	0.8	0	0	2,050
St. Helena	87	1.7	0	0	87
Seychelles and Dependencies	66	0.2	0	0	66
Somalia	765	+	0	0	765
Somaliland Protectorate	170	+	0	0	170
Spanish Guinea	432	0.2	66.7	432	0

TELEPHONES IN COUNTRIES OF THE WORLD—Continued

Country	Total Telephones	Per 100 Population	Percent Automatic (Dial)	Ownership	
				Private	Government
AFRICA—Continued					
Spanish West Africa					
Ivory	100	0.3	0	0	100
Spanish Sahara	52	0.1	0	0	52
Total	152	0.2	0	0	152
Swaziland	393	0.2	0.8	0	393
Tunisia	27,227	0.8	57.2	0	27,227
Union of South Africa	(6) 514,675	4.1	69.0	0	514,675
Zanzibar and Pemba	420	0.2	0	0	420
ASIA					
Aden, Colony of	1,460	1.5	100	0	1,460
Afghanistan	(1) 4,500	+	6.7	0	4,500
Bahrain	718	0.7	100	718	0
Brunei	86	0.2	0	0	86
Burma	5,200	+	20.0	0	5,200
Cambodia	1,833	+	0	0	1,833
Ceylon	18,362	0.2	91.9	0	18,362
China	(1) 255,000	+	70.6	95,000	160,000
Cyprus	5,347	1.1	40.6	5,347	0
French India	76	+	100	0	76
Hong Kong	(4) 31,947	1.5	100	31,947	0
India	(6) 183,935	+	47.1	1,966	181,969
Indonesia	58,707	+	2.1	0	58,707
Iran	(1) 30,000	0.2	36.7	26,800	3,200
Iraq	24,165	0.4	64.6	0	24,165
Israel	35,972	2.3	89.2	0	35,972
Japan	(6) 2,013,439	2.4	42.4	0	2,013,439
Jordan	4,714	0.3	75.7	0	4,714
Kuwait	600	0.3	80.0	0	600
Laos	187	+	0	0	187
Lebanon	19,649	1.5	0	0	19,649
Macao	1,536	0.5	99.3	0	1,536
Malaya	28,086	0.5	40.7	0	28,086
Muscat and Oman	102	+	100	0	102
North Borneo	675	0.2	16.3	0	675
Pakistan	20,662	+	49.5	0	20,662
Philippine Republic	30,345	0.1	59.8	28,026	2,319
Portuguese India	220	+	0	0	220
Sarawak	720	0.1	0	0	720
Saudi Arabia	6,080	+	0	0	6,080
Singapore	21,625	2.0	100	21,625	0
Syria	20,449	0.6	66.0	0	20,449
Thailand	(1) 6,100	+	100	0	6,100
Turkey	72,730	0.3	88.1	0	72,730
Viet-Nam	11,120	+	44.6	0	11,120
Other Places	(1) 82,000	0.2	30.0	0	82,000
OCEANIA					
American Samoa	297	1.6	100	0	297
Australia	1,259,212	14.7	64.0	0	1,259,212
Fiji	2,667	0.9	0	0	2,667
French Oceania					
French Settlements	642	1.2	0	0	642
New Caledonia	1,719	2.8	0	0	1,719
Total	2,361	2.0	0	0	2,361
Hawaii	125,353	24.6	94.1	125,353	0
Netherlands New Guinea	566	+	0	0	566
New Zealand	(6) 394,566	19.9	59.1	0	394,566
Pacific Islands (British)					
Gilbert and Ellice Islands	64	0.2	0	0	64
New Hebrides Condominium	87	0.2	0	0	87
Pitcairn Islands	0	—	—	—	—
Solomon Islands Protectorate	0	—	—	—	—
Tonga (Friendly) Islands	241	0.5	0	0	241
Total	392	0.2	0	0	392
Papua-New Guinea	1,851	0.1	0	0	1,851
Portuguese Timor	306	+	0	0	306
South Seas Mandate (United States)					
Caroline Islands	105	0.3	0	0	105
Guam	4,407	5.2	61.4	0	4,407
Marianne Islands (less Guam)	770	7.7	0	0	770
Marshall Islands	150	1.5	0	0	150
Total	5,432	3.9	49.8	0	5,432
Western Samoa	381	0.5	0	0	381

TELEPHONE CONVERSATIONS FOR THE YEAR 1951

Conversation data were not available for all countries

Country	Number of Conversations in Thousands			Conversations Per Capita
	Local	Toll	Total	
Algeria	47,400	18,900*	66,300	7.4
Argentina	2,921,800	37,000	2,958,800	167.7
Australia	957,100	70,600	1,027,700	121.9
Belgium	433,200	62,300	495,500	57.1
Brazil	1,841,900	32,800	1,874,700	35.1
Canada	5,170,000	127,700	5,297,700	378.2
Ceylon	37,700	2,800	40,500	5.2
Chile	359,000	19,500	378,500	64.0
Colombia	346,300	5,300	351,600	31.2
Cuba	715,000	5,500	720,500	131.7
Denmark	946,400	159,900	1,106,300	257.1
Egypt	456,500	10,400	466,900	22.5
Finland	483,400	75,800	559,200	138.0
France	1,275,200	454,500	1,729,700	41.0
Germany, Western	1,828,500	364,400	2,192,900	45.6
Greece	264,400	3,800	268,200	35.3
Iceland	51,700	1,200	52,900	364.8
Ireland	75,300	11,000	86,300	29.2
Israel	70,700	3,300	74,000	55.0
Italy	2,182,000	131,600*	2,313,600	49.7
Jamaica	43,000	500	43,500	30.5
Japan (1)	7,162,000	402,500	7,564,500	89.3
Luxemburg	9,600	7,800	17,400	59.8
Malaya	68,800	9,900	78,700	14.8
Mexico	692,000	8,700	700,700	26.6
Netherlands	587,500	173,800	761,300	74.2
Norway (2)	466,800	49,800	516,600	157.5
Paraguay	17,200	200	17,400	12.3
Peru	136,000	2,200	138,200	16.1
Philippine Republic	231,100	400	231,500	11.7
Portugal	157,700	30,300	188,000	22.0
Puerto Rico	87,900	2,600	90,500	40.7
Spain	1,619,300	66,000	1,685,300	59.5
Sweden (3)	2,080,100	117,900	2,198,000	309.6
Switzerland	408,400	315,100*	723,500	152.3
Tunisia	15,600	6,500	22,100	6.8
Turkey	91,600	11,000	102,600	4.9
Union of South Africa (1)	569,700	42,500	612,200	49.2
United Kingdom (1)	3,273,100	263,400	3,536,500	70.3
United States	56,025,000	2,080,000	58,105,000	376.3
Uruguay	296,000	4,300	300,300	125.5
Venezuela	304,800	1,200	306,000	60.5

* Three-minute units.

(1) Year ended March 31, 1952.

(2) Year ended June 30, 1951.

(3) Year ended June 30, 1952.

Propagation of Space-Charge Waves in Infinite and Finite Electron Beams*

By PHILIP PARZEN

Federal Telecommunication Laboratories, Incorporated; Nutley, New Jersey

A THEORY of the propagation of space-charge waves in infinite and finite electron beams is given. It is shown that for infinite beams in diodes, the theory agrees with that of Llewellyn and Peterson. In the case of a diode with a finite beam, the current modulation propagates as a growing wave. The reduction in the noise figure of a traveling-wave amplifier due to a voltage jump is smaller for a finite beam than for an infinite beam.

. . .

1. Introduction

The alternating-current properties of diodes¹ with arbitrary direct-current space-charge conditions have already been discussed^{2,3} by Llewellyn, but his analysis is restricted to electron beams of infinite lateral extension and cannot readily be extended to finite beams. In this particular paper, Llewellyn's treatment has been dispensed with and it becomes necessary to start anew with a small-signal-theory analysis of the propagation of space-charge waves in an infinite beam. The analysis is then extended to finite beams.

2. Propagation of Space-Charge Waves in an Infinite Beam

The small-signal-theory Maxwell equations for a one-dimensional propagating process in an infinite electron beam are

$$\left(j\omega + \frac{\partial v_0}{\partial Z}\right)v + v_0 \frac{\partial v_0}{\partial Z} = \frac{e}{m}E, \quad (1)$$

$$\frac{\partial J}{\partial Z} + j\omega\rho = 0, \quad (2)$$

$$J + j\omega\epsilon_0 E = 0, \quad (3)$$

$$J = \rho_0 v + \rho v_0. \quad (4)$$

* This work was sponsored by the Signal Corps Engineering Laboratories, Fort Monmouth, New Jersey.

¹ A diode is a region between two plane electrodes.

² F. B. Llewellyn, "Electron-Inertia Effects," First Edition, Cambridge University Press, London, England; 1941.

³ F. B. Llewellyn and L. C. Peterson, "Vacuum-Tube Networks," *Proceedings of the IRE*, volume 32, pages 144-146; March, 1944.

All field quantities vary exponentially ($e^{j\omega t}$) and the alternating-current quantity is assumed to be small with respect to the corresponding direct-current quantity. Furthermore, E , J , v , and ρ are the alternating-current electric field, current density, velocity, and charge density, respectively; E_0 , J_0 , v_0 , and ρ_0 are the corresponding direct-current quantities. The charge e on the electron is negative, and m is the mass of the electron.

Solving for all field quantities in terms of J , the following differential equations⁴ are obtained for J , where the exponential factor $j\omega t$ has been deleted:

$$v_0^3 - \frac{\partial^2 J}{\partial Z^2} + \left(3v_0^2 \frac{\partial v_0}{\partial Z} + j2\omega v_0^2\right) \frac{\partial J}{\partial Z} + \left(\frac{eJ_0}{m\epsilon_0} + j2\omega v_0 \frac{\partial v_0}{\partial Z} - \omega^2 v_0\right) J = 0, \quad (5)$$

$$v = \frac{v_0}{J_0} \left(J + \frac{v_0}{j\omega} \frac{\partial J}{\partial Z}\right). \quad (6)$$

Equation (5) can be simplified by replacing distance Z by the transit time τ . Let

$$J = \frac{Y}{v_0} \exp(-j\omega\tau), \quad (7)$$

then

$$\tau = \int_0^Z \frac{\partial Z}{v_0}. \quad (8)$$

Substituting (7) and (8) into (5), we find

$$\frac{\partial^2 Y}{\partial \tau^2} - K^2 Y = 0, \quad (9)$$

where

$$K^2 = \frac{1}{v_0} \left(\frac{\partial^2 v_0}{\partial \tau^2} - \frac{eJ}{m\epsilon_0}\right) \quad (10)$$

and

$$v = \frac{1}{j\omega J_0} \left(\frac{\partial Y}{\partial \tau} - \frac{Y}{v_0} \frac{\partial v_0}{\partial \tau}\right) \exp(-j\omega\tau). \quad (11)$$

⁴ This equation is also derived by J. Bernier in "Essai de Théorie du Tube Electronique à Propagation d'Ondes," *L'Onde Electrique*, volume 27, pages 231-243; June, 1947; see page 232. Also by L. D. Smullin in "Propagation of Disturbances in One-Dimensional Accelerated Electron Streams," *Journal of Applied Physics*, volume 22, pages 1496-1498; December, 1949.

Thus, given v_0 as a function of τ , one may solve from (9) for Y , and find J and v from (7) and (8).

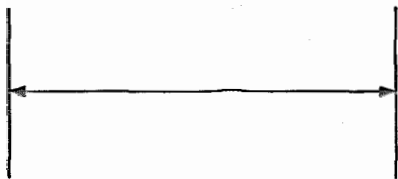


Figure 1—Diode with an infinite electron beam.

The theory will now be applied to a diode (Figure 1) with an infinite electron beam. In this case,

$$\frac{\partial^2 v_0}{\partial \tau^2} = \frac{eJ_0}{m\epsilon_0} \quad (12)$$

Hence,

$$v_0 = \frac{1}{2} \frac{eJ_0}{m\epsilon_0} \tau^2 + a_{01}\tau + v_{01}, \quad (13)$$

where a_{01} and v_{01} are the direct-current acceleration and velocity at electrode 1. Also from (1) and (12) we see that $K=0$. Hence the solution of (9) is

$$J = \frac{C_1\tau + C_2}{v_0} \exp(-j\omega\tau), \quad (14)$$

and (14) substituted into (11) gives

$$v = \frac{1}{j\omega J_0} \left(C_1 - \frac{C_1\tau + C_2}{v_0} \frac{\partial v_0}{\partial \tau} \right) \exp(-j\omega\tau). \quad (15)$$

C_1 and C_2 are arbitrary constants to be determined by the initial conditions at electrode 1. Let the subscripts 1 and 2 denote the values of the field quantities at the corresponding electrodes. Then, at $\tau \neq 0$, from (14) and (15),

$$C_2 = J_1 v_{01}, \quad (16)$$

$$v_1 = \frac{1}{j\omega J_0} \left(C_1 - \frac{C_2}{v_{01}} a_{01} \right). \quad (17)$$

If we solve for C_1 and C_2 and substitute in (14) and (15), J and v are given by

$$J = J_1 \left(\frac{a_{01}\tau + v_{01}}{v_0} \right) + v_1 \frac{j\omega J_0}{v_0} \tau, \quad (18)$$

$$v = \frac{J_1}{j\omega J_0} \left[a_{01} \left(1 - \frac{\tau}{v_0} \frac{\partial v_0}{\partial \tau} \right) - \frac{v_{01}}{v_0} \frac{\partial v_0}{\partial \tau} \right] + v_1 \left(1 - \frac{\tau}{v_0} \frac{\partial v_0}{\partial \tau} \right). \quad (19)$$

The expressions for J and v in an infinite electron beam are the same as those given² by Llewellyn. Their agreement with the results³ of Llewellyn and Peterson can be shown by obtaining an expression for a_{01} in terms of the space-charge parameter \mathcal{E} . Thus,

$$\frac{eJ_0}{m\epsilon_0} = (v_{01} + v_{02}) \frac{2\mathcal{E}}{\tau_2^2} = (v_{01} - a_{01}\tau_2 - v_{01}) \frac{2}{\tau_2^2}. \quad (20)$$

Hence,

$$a_{01} = \frac{-(v_{01} + v_{02})\mathcal{E} + v_{02} - v_{01}}{\tau_2}. \quad (21)$$

By this method, it is possible to obtain solutions for regions other than diodes. Let us consider an electrostatic lens in which the direct-current velocity varies linearly with time or,

$$v_0 = a_0\tau + v_{01}. \quad (22)$$

Then, from (10),

$$K^2 = -\frac{eJ_0}{m\epsilon_0} \frac{1}{v_0},$$

and

$$Y = \phi^{1/2} [C_1 J_1(2A^{1/2}\phi^{1/2}) + C_2 Y_1(2A^{1/2}\phi^{1/2})].$$

Hence,

$$\phi = v_0/v_{02}, \quad (23)$$

and

$$A = \frac{v_{02}}{a_{01}^2} \frac{eJ_0}{m\epsilon_0}.$$

In (23), J_1 and Y_1 are Bessel functions of the first and second kind of order 1, and C_1 and C_2 are arbitrary constants to be determined by the initial conditions. Thus, one advantage of this method is that its application is not restricted to diodes. A second advantage is that it may be extended to include the effects of thermal velocities⁵ and of the finite lateral extent of the electron beam.⁶

3. Application to Finite Electron Beam

It has been shown⁵ that the effect of the electron-beam geometry may be obtained by modifying K^2 in (10) as follows:

⁵ Philip Parzen, "Effect of Thermal-Velocity Spread on the Noise Figure in Traveling-Wave Tubes," *Electrical Communication*, volume 30, pages 139-154; June, 1953; also, *Journal of Applied Physics*, volume 23, pages 394-406; April, 1952.

⁶ Philip Parzen, "Space-Charge-Wave Propagation in a Cylindrical Electron Beam of Finite Lateral Extent," *Electrical Communication*, volume 29, pages 238-242; September, 1952; also *Journal of Applied Physics*, volume 23, pages 215-219; February, 1952.

$$K^2 = \frac{1}{v_0} \left(\frac{\partial^2 v_0}{\partial \tau^2} - \frac{eJ_0}{m\epsilon_0} \frac{1}{1 + T^2/\gamma_0^2} \right). \quad (24)$$

Here, $\gamma_0 = \omega/v_0$, and T/γ_0 is a function of $\gamma_0 b$. The ratio of the beam radius b to the radius of the surrounding tube is shown in Figure 2. The case of the complete-space-charge diode, in which $a_{01} = v_{01} = 0$, has already been discussed.⁶ The case now to be discussed is that in which the beam current is injected into a diode region (Figure 3), and the direct-current velocity is an almost linear function of the transit time. This corresponds to the case of the voltage-jump gun that is used as a noise-reducing device in a traveling-wave amplifier. Here, the direct-current velocity v_0 is given by

$$v_0 = \frac{1}{2} \frac{eJ_0}{m\epsilon_0} \tau^2 + a_{01}\tau + v_{01}. \quad (13)$$

It is assumed that for most of the time

$$\frac{1}{2} \frac{eJ_0}{m} \tau^2 \ll a_{01}\tau + v_{01}. \quad (25)$$

This will be true for small space-charge factors. Thus,

$$K^2 = \frac{eJ_0}{m\epsilon_0} \frac{T^2/\gamma_0^2}{1 + T^2/\gamma_0^2} \frac{1}{v_0}, \quad (26)$$

and v_0 may be approximated by $a_{01}\tau + v_{01}$.

Since K^2 is always positive, it is seen from (9) that the current modulation will propagate as a growing wave in a diode. The resultant differential equation may be solved approximately by the W.K.B.⁷ method, giving

⁷ L. Schiff, "Quantum Mechanics," First Edition, McGraw-Hill Book Company, New York, New York, 1949; page 181.

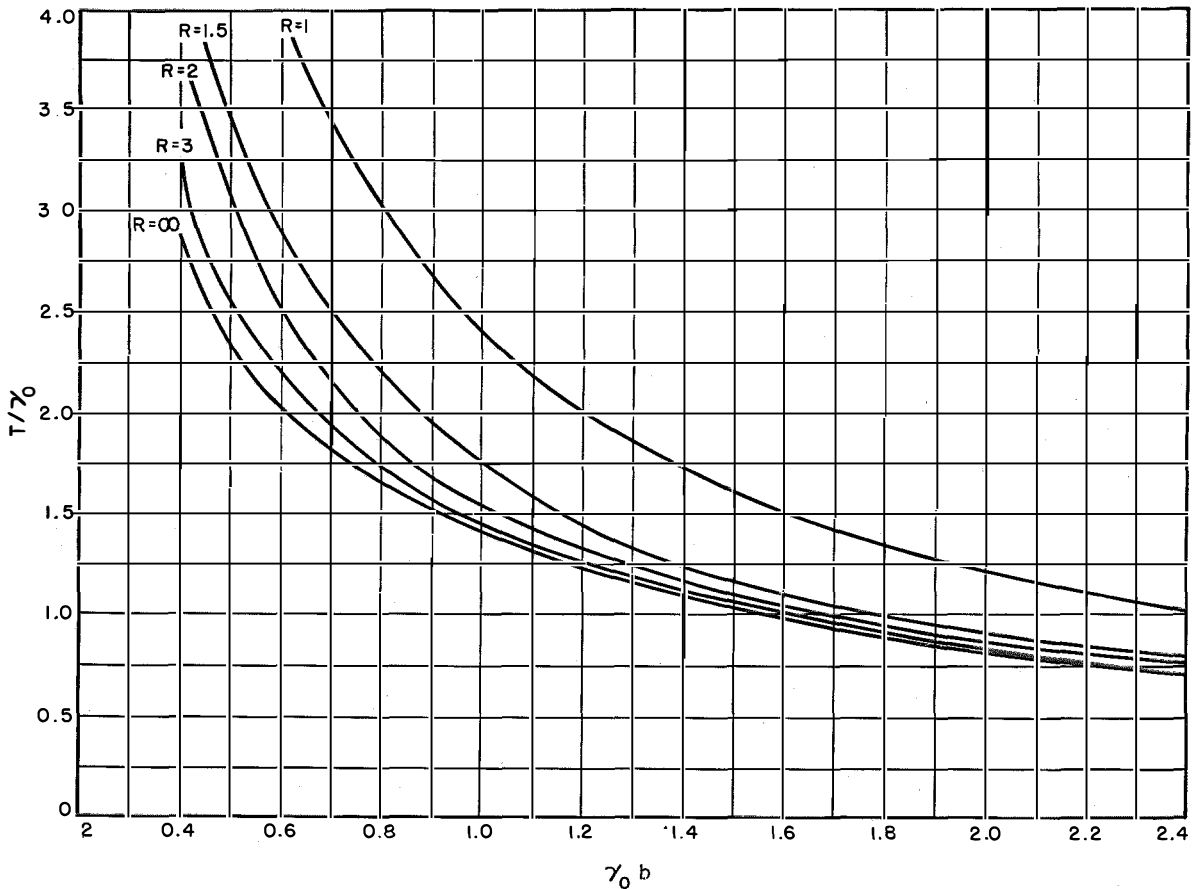


Figure 2—Effect of drift-tube geometry on the plasma frequency in the drift tube. Here, R = drift-tube radius/beam radius, $\gamma_0 = \omega/v_0 = 2\pi f$ /beam velocity, b = beam radius, ω_d = plasma frequency in drift tube, and ω'_d = plasma frequency corrected for beam and drift-tube geometry. Then, $\omega'_d/\omega_d = 1/[1 + (T/\gamma_0)^2]^{1/2}$.

$$Y = \frac{C_1 \exp(\psi) + C_2 \exp(-\psi)}{K^{1/2}}, \quad (27)$$

$$\psi = \int_0^\tau K d\tau.$$

Hence, deleting the transit-time factor and substituting (27) in (7) and (11),

$$J = \frac{1}{v_0 K^{1/2}} [C_1 \exp(\psi) + C_2 \exp(-\psi)], \quad (28)$$

and

$$v = \frac{1}{j\omega J_0} \left[C_1 \exp(\psi) \left(K^{1/2} - \frac{1}{2K^{3/2}} \frac{\partial K}{\partial \tau} - \frac{1}{v_0 K^{1/2}} \frac{\partial v_0}{\partial \tau} \right) + C_2 \exp(-\psi) \left(-K^{1/2} - \frac{1}{2K^{3/2}} \frac{\partial K}{\partial \tau} - \frac{1}{v_0 K^{1/2}} \frac{\partial v_0}{\partial \tau} \right) \right]. \quad (29)$$

C_1 and C_2 are to be determined by the initial conditions at electrode 1. Only the case of $J_1 = 0$ will be considered here. Thus, in this case,

$$\left. \begin{aligned} C_1 &= -C_2, \\ C_1 &= j\omega J_0 v_0 / 2K^{1/2}, \end{aligned} \right\} (30)$$

and

$$J = \frac{j\omega J_0}{v_0} \frac{\sinh \psi}{K_1^{1/2} K^{1/2}} v_1. \quad (31)$$

$$\frac{v}{v_1} = \frac{1}{K_1^{1/2}} \left(K^{1/2} \cosh \psi - \frac{1}{2K^{3/2}} \frac{\partial K}{\partial \tau} \sinh \psi - \frac{1}{v_0} \frac{\partial v_0}{\partial \tau} \frac{\sinh \psi}{K^{1/2}} \right). \quad (32)$$

Letting

$$\phi = gv_0/v_{02} \text{ and } g = tb/\gamma_{02}b, \quad (33)$$

$$\psi = \frac{A}{g^{1/2}} \int_{\phi_1}^{\phi} G d\phi,$$

$$K = \left(\frac{eJ_0 g}{m\epsilon_0 v_{02}} \right)^{1/2} G, \quad (34)$$

$$A^2 = \frac{eJ_0 v_{02}}{m\epsilon_0 a_{01}^2} = 2\mathcal{E}v_{02} \frac{v_{01} + v_{02}}{(v_{02} - v_{01})^2},$$

where \mathcal{E} is the space-charge parameter and

$$G = \left(\frac{\phi}{1 + \phi^2} \right)^{1/2}.$$

Hence,

$$J_2 = \frac{j\omega J_0}{\omega_{p2}} g^{1/2} \frac{\sinh \psi_2}{\phi_2 G_1^{1/2} G_2^{1/2}} \frac{v_1}{v_{02}}, \quad (35)$$

$$\frac{v_2}{v_1} = \frac{1}{G_1^{1/2}} \left[G_2^{1/2} \cosh \psi_2 - \frac{g^{1/2}}{A} \frac{\sinh \psi_2}{G_2^{1/2}} \left(\frac{5}{4} \frac{1}{\phi_2} - \frac{G_2^2}{2} \right) \right], \quad (36)$$

where ω_{p2} is the plasma frequency at electrode 2. A plot of G and $\int_0^\phi G d\phi$ versus ϕ is given in Figure 4.

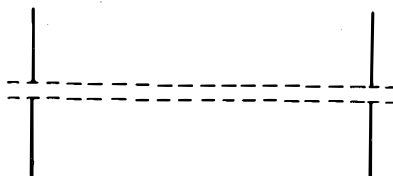


Figure 3—Voltage-jump diode.

The corresponding formulas for an infinite beam are, from (18) and (19),

$$J_2 = j\omega\tau_2 J_0 v_1/v_{02}, \quad (37)$$

$$v_2/v_1 = v_{01}/v_{02}. \quad (38)$$

The effectiveness of the voltage-jump gun as a noise-reducing device depends on the degree of

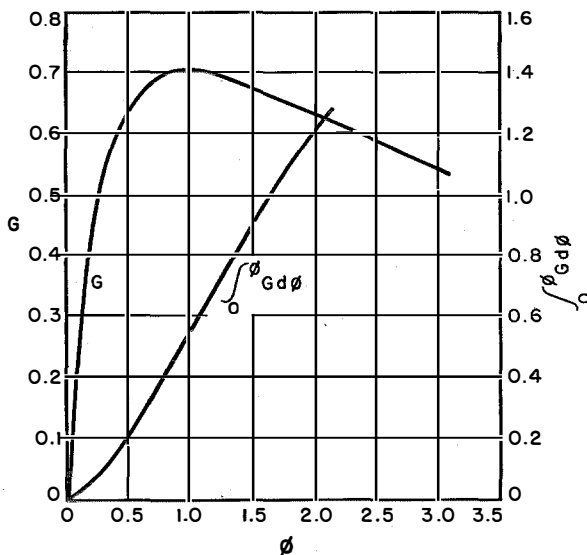


Figure 4—Plot of G and $\int_0^\phi G d\phi$ against ϕ .

validity of (38). As a result, it is important to determine the effect of the finite-beam geometry on the noise reduction. This is best illustrated by the following numerical example. Let, $v_{02} = 2v_{01}$, $\mathcal{E} = 0.2$, and $g = 1$. Then,

$$\begin{aligned} \phi_1 &= 0.5, & G_2 &= 0.70, \\ \phi_2 &= 1.0, & \psi_2 &= 0.34, \\ G_1 &= 0.63, & A &= 1.55. \end{aligned}$$

For an infinite beam, therefore,

$$v_2/v_1 = 0.5, \tag{39}$$

and for the finite beam,

$$v_2/v_1 = 0.76.$$

This means that the reduction in noise figure is 3.5 decibels greater for the infinite beam than for the finite beam considered here.

4. Conclusions

A theory of the propagation of space-charge waves in infinite and finite beams has been given. The Llewellyn-Peterson theory of diodes with infinite beams is a special case of this theory, which may be applied to configurations other than diodes.

The current modulation in a diode with a finite beam propagates as a growing wave. The reduction in the noise figure of a traveling-wave amplifier due to a voltage jump is smaller for a finite beam than for an infinite beam.

Effect of Thermal-Velocity Spread on the Noise Figure in Traveling-Wave Tubes*

By PHILIP PARZEN

Federal Telecommunication Laboratories, Incorporated; Nutley, New Jersey

EFFECTS of thermal-velocity spread on the noise figure of a traveling-wave tube have been computed by extending a method of Hahn. To accomplish this, it has been necessary to work out a new theory for the diode-drift tube and traveling-wave tube that includes the effect of the thermal-velocity spread at very high frequencies. Some computations are given for conditions met in practice.

• • •

Calculation of the noise figure of a traveling-wave-tube amplifier may be reduced to the computation of the current- and velocity-modulation fluctuations in three distinct regions (Figure 1). Region I is a diode with a heated cathode, region II is a field-free drift region, and region III is the traveling-wave-tube amplifier.

A detailed analysis will be given of the fluctuations in each region, which includes the effect of the thermal-velocity spread. Inasmuch as this theory applies rigorously only to an infinite rectilinear electron beam, it will be necessary to apply certain correction factors to account for the finite beam and the surrounding conductors. Approximations for these correction factors may be obtained from the simpler computation for a monovelocity beam.

Of the three regions, the diode region is the most difficult to handle since it is in a direct-current accelerating field. As is well known, the direct-current theory of the diode by Langmuir¹

is at best a numerical theory, and certainly not much more can be expected for an alternating-current theory. To attempt to work out an alternating-current theory by Langmuir's method does not seem fruitful for microwave frequencies. However, such theories have been worked out for low frequencies by Thompson et al.² and Rack.³

Rack has extended his theory to higher frequencies by using Llewellyn's⁴ theory of diodes in an approximate manner. On the basis of the Rack theory, Peterson⁵ has computed the fluctuations in the drift tube. This was utilized by Pierce⁶ to compute the fluctuations in the traveling-wave amplifier. Subsequently, this theory

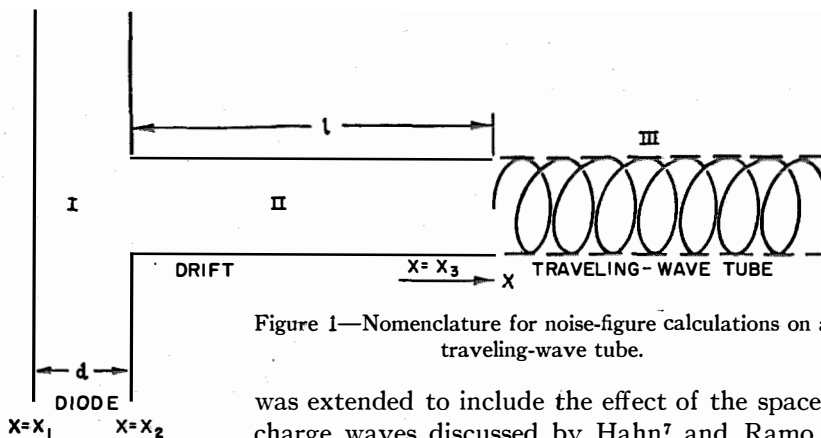


Figure 1—Nomenclature for noise-figure calculations on a traveling-wave tube.

was extended to include the effect of the space-charge waves discussed by Hahn⁷ and Ramo.⁸

² B. J. Thompson, D. O. North, and W. A. Harris, "Fluctuations in Space-Charge-Limited Currents at Moderately High Frequencies—Part II," *RCA Review*, volume 5, pages 106–124; July, 1940.

³ A. J. Rack, "Effect of Space Charge and Transit Time on the Shot Noise in Diodes," *Bell System Technical Journal*, volume 17, pages 592–619; October, 1938.

⁴ F. B. Llewellyn, "Electron Inertia Effects," First Edition, Cambridge University Press, London, England; 1941.

⁵ L. C. Peterson, "Space Charge and Transit-Time Effects on Signal and Noise in Microwave Tetrodes," *Proceedings of the IRE*, volume 35, pages 1264–1272; November, 1947.

⁶ J. R. Pierce, "Traveling-Wave Tubes," First Edition, D. Van Nostrand Company, New York, New York; 1950; see page 109.

⁷ W. C. Hahn, "Small Signal Theory of Velocity-Modulated Electron Beams," *General Electric Review*, volume 42, pages 258–270; June, 1939.

⁸ Simon Ramo, "The Electronic-Wave Theory of Velocity-Modulation Tubes," *Proceedings of the IRE*, volume 27, pages 757–763; December, 1939.

* Reprinted from *Journal of Applied Physics*, volume 23, pages 394–406; April, 1952. This work was sponsored by the Signal Corps Engineering Laboratories; Fort Monmouth, New Jersey.

¹ Irving Langmuir, "The Structure of the Helium Atom," *Physical Review*, volume 17, pages 339–353; March, 1921; see page 341.

This method of calculation of the fluctuations in the traveling-wave amplifier will hereafter be designated as the RPHP (Rack-Peterson-Hahn-Pierce) method. In view of the many approximations made, it is not possible to assess the accuracy of this theory except by comparison with experiment. The agreement is very good for large noise figures.

For noise figures of the order of 10 decibels or less, however, one cannot expect experimental agreement within 1 decibel with this theory, unless it be fortuitous. It is expected that the weakest link of the RPHP theory is the diode region. Thus a high-frequency theory of diode impedance and fluctuations including the effect of a multivelocity beam would be quite useful.

Another method of attack is to base the alternating-current theory on the direct-current theory of Hahn.⁹ Hahn has shown that it is possible to discuss the effect of the thermal velocities on the direct-current behavior of diodes in terms of a monovelocity electron beam whose acceleration is determined not only by the applied electric field but also by a hydrostatic-pressure term, which accounts for the multivelocity beam. The alternating-current theory will be worked out as a perturbation of the direct-current properties determined by the Hahn theory.

1. Alternating-Current Theory of Diode Impedance and Fluctuations

1.1 GENERAL

The diode consists of two infinite parallel planes; the space between is traversed by an infinite rectilinear beam. The diode is connected either to an alternating-current generator or a load Z_L (Figures 2 and 3).

Then, following Hahn, the basic equations are

$$\bar{v}_t + \bar{v}\bar{v}_x = \frac{e}{m} \bar{E} - \frac{k\bar{T}}{mn} \bar{n}_x, \quad (1)$$

$$\bar{J}_x + en_t = 0, \quad (2)$$

$$\bar{E}_x = e\bar{n}/\epsilon_0 \quad \text{or} \quad \bar{J} + \epsilon_0 \bar{E}_t = I, \quad (3)$$

$$\bar{J} = e\bar{n}\bar{v}. \quad (4)$$

⁹ W. C. Hahn, "Effects of Hydrostatic Pressure on Electron Flow in Diodes," *Proceedings of the IRE*, volume 36, pages 1115-1121; September, 1948.

The subscripts t and x denote the partial derivatives with respect to t and x . A bar over the letter denotes total unnormalized quantities, i.e. direct current + alternating current. e and m are the charge and mass of an electron. n , v , J , and E are particle density, mean velocity, convection-current density, and electric field, respectively. ϵ_0 is the dielectric constant of free space. I is the total current density, i.e. convection plus displacement. T is the temperature

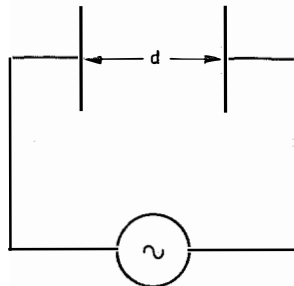


Figure 2—Diode connected to an alternating-current generator.

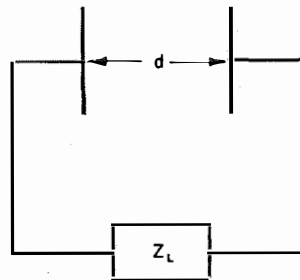


Figure 3—Diode connected to a load Z_L .

of the electron gas¹⁰ that constitutes the electron beam. k is Boltzmann's constant. Meter-kilogram-second units are used.

All field quantities are functions of x and t except \bar{I} , which is a function of t only, and \bar{T} , which is assumed to be constant. Thus $\bar{T} = T_0$, which is assumed to equal the cathode temperature. The major justification for this assumption is that the direct-current potential distribution is approximately the same as derived by Langmuir, who assumes an adiabatic process. So far as the alternating-current potential distribution is concerned, it remains an assumption. It is seen that the equation of motion (1) has been augmented with a hydrostatic-pressure term.

1.2 SMALL-SIGNAL APPROXIMATIONS

According to the small-signal approximations, one puts

$$\bar{J} = J_0 + J \exp j\omega t; \quad J \ll J_0 \quad (5)$$

and similarly for all other field quantities. The

¹⁰ Philip Parzen and Ladislav Goldstein, "Effect of Hydrostatic Pressure in an Electron Beam on the Operation of Traveling-Wave Devices," *Electrical Communication*, volume 28, pages 228-232; September, 1951; also *Journal of Applied Physics*, volume 22, pages 398-401; April, 1951.

subscript zero indicates direct-current quantities and ω is the applied frequency. It is also assumed that the alternating-current temperature is zero. The alternating-current and direct-current equations separate out.

Alternating-current equations are

$$(j\omega + v_{0x})v + v_0v_x = \frac{e}{m} E - \frac{kT_0}{mn_0} n_x + \frac{kT_0}{mn_0^2} n_{0x}n, \quad (1A)$$

$$J_x + j\omega en = 0, \quad (2A)$$

$$J + j\omega \epsilon_0 E = I, \quad (3A)$$

$$J = e(n_0v + nv_0). \quad (4A)$$

Direct-current equations are

$$v_0v_{0x} = \frac{e}{m} E_0 + \frac{kT_0}{m} \frac{1}{v_0} v_x, \quad (1B)$$

$$E_{0x} = J_0/\epsilon_0v_0, \quad (3B)$$

$$J_0 = en_0v_0. \quad (4B)$$

The alternating-current quantities are all functions of x except I , which is a constant. The direct-current quantities are all functions of x except J_0 and T_0 , which are constants. It is now possible to solve for all the alternating-current quantities in terms of J and J_x . Thus,

$$v = \frac{1}{J_0} \left(v_0J + \frac{v_0^2}{j\omega} J_x \right), \quad (6)$$

$$n = -\frac{1}{j\omega \epsilon_0} J_x, \quad (7)$$

$$E = \frac{I}{j\omega \epsilon_0} - \frac{J}{j\omega \epsilon_0}, \quad (8)$$

$$\frac{v_0}{j\omega J_0} \left(\frac{kT_0}{m} - v_0^2 \right) J_{xx} + \frac{1}{J_0} \left(\frac{1}{j\omega} \frac{kT_0}{m} v_{0x} - \frac{3}{j\omega} v_0^2 v_{0x} - 2v_0^2 \right) J_x + \left(-\frac{e}{m} \frac{1}{j\omega \epsilon_0} - \frac{2v_0}{J_0} v_{0x} - j\omega \frac{v_0}{J_0} \right) J = -\frac{e}{m} \frac{1}{j\omega \epsilon_0} I. \quad (9)$$

These equations can be somewhat simplified by normalizing the units of distance, velocity, and current density. Let

$$y = (x - x_c)/D, \quad (10)$$

where x_c is the position of the virtual cathode, and let the unit of velocity α be such that

$$\frac{e}{m} \frac{1}{\epsilon_0} \frac{D^2 J_0}{\alpha^3} = \frac{2}{9}, \quad (11)$$

where D is the unit of distance for normalization and J_0 is the unit of current density. Then, in terms of these normalized units

$$v = v_0J + \frac{v_0^2}{j\theta} J_y, \quad (12)$$

$$v_0(\mu^2 - v_0^2)J_{yy} + (\mu^2v_{0y} - 3v_0^2v_{0y} - j2\theta v_0^2)J_y + [- (2/9) - 2j\theta v_0v_{0y} + \theta^2v_0]J = - (2/9)I, \quad (13)$$

where

$$\theta = \omega D/\alpha \quad \text{and} \quad \mu^2 = kT_0/m\alpha^2. \quad (14)$$

For different regions, one may choose different values of D and α subject to (11). Hereafter, only normalized quantities will be used unless otherwise specified.

1.3 SOLUTION OF THE DIRECT-CURRENT EQUATIONS

It follows immediately from (1B) that at the virtual cathode, at which $y = 0$, $E_0 = 0$, $v_0 = \mu$. In general, v_0 satisfies the following integral equation

$$v_0^2 = \mu^2 \left(1 + \log \frac{v_0^2}{\mu^2} \right) + \frac{4}{9} \int_0^y dy \int_0^y \frac{dy}{v_0}. \quad (15)$$

This equation cannot be solved without lengthy numerical computations, except for the two following special cases: For $|y| \ll 1$,

$$v_0 = \mu + \frac{1}{3\mu^{3/2}} y + \frac{1}{648\mu^{3/2}} y^3 + \dots, \quad (16)$$

which is obtained by assuming for v_0 a power-series expansion around $y = 0$. For those values of y for which $(v_0/\mu)^2 \gg 1 + \log (v_0/\mu)^2$,

$$v_0 = y^{2/3}. \quad (17)$$

This will occur for sufficiently large positive values of y , and it corresponds to the region in which Child's law is valid. Inasmuch as there is no simple expression for the region in between, it has been decided to fill in this region by matching (16) to (17). It is seen from Figure 4 that they intersect at $y = y_m = 2.4\mu^{3/2}$ at which $v_0 = 1.76\mu$. Thus the direct-current solution, of which the

alternating-current solution is a perturbation, will be taken as follows:

$$\left. \begin{array}{l} \text{for } y < 2.4\mu^{3/2}, v_0 \text{ is given by (16),} \\ \text{for } y > 2.4\mu^{3/2}, v_0 \text{ is given by (17).} \end{array} \right\} (18)$$

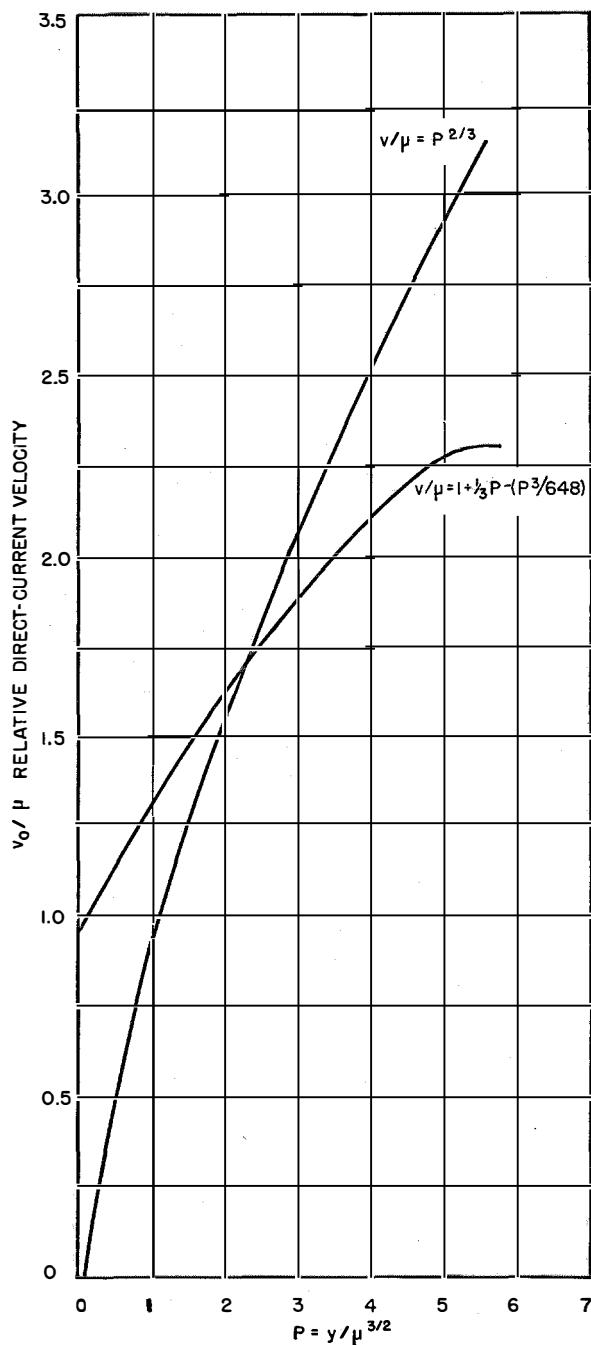


Figure 4—Merging of Child's law region in the cathode region.

All these assumptions will be approximately satisfied if the ratio of current density to saturation current density is not too small. The voltage V relative to the virtual cathode in the region $y < 0$ is

$$\left. \begin{array}{l} V = \frac{4}{9} \frac{V_0}{\mu} \left(\frac{y^2}{2} - \frac{1}{18\mu^{3/2}} y^3 \right. \\ \left. + \frac{1}{108\mu^3} y^4 + \dots \right), \end{array} \right\} (19)$$

$$V_0 = m\alpha^2/2|e|.$$

Let subscripts 1 and 2 denote conditions at the cathode and anode, respectively.

$$eV_1/kT = \log J_0/J_s, \quad (20)$$

J_s being the saturation current density.

Choosing α such that $4eV_0/9kT = -1$, it follows from (20) that

$$y_1 = - \left(2 \log \frac{J_s}{J_0} \right)^{1/2} \left[1 - 0.12 \left(2 \log \frac{J_s}{J_0} \right)^{1/2} \right]^{1/2}, \quad (21)$$

$$\left. \begin{array}{l} \alpha = \left(\frac{9}{2} \right)^{1/2} \left(\frac{kT_0}{m} \right)^{1/2}, \\ D = \left[\frac{\epsilon_0}{eJ_0} \left(\frac{kT_0}{m} \right)^{1/2} kT_0 \right]^{1/2}. \end{array} \right\} (22)$$

With this choice of D and α , y is the same as Hahn's s and Langmuir's $\zeta = 1.583y$. Also, $\mu = 0.61$. Thus given T_0 , J_0 , and d , one may compute y_1 from (21), D from (22), and hence x_c . Then knowing y_2 , one computes V_2 from (16) and (17), and V_1 from (20). Thus $V_2 - V_1$ is the required voltage. Hahn has already shown that for $y > 0$, V computed from his theory agrees fairly well with that obtained by Langmuir. The agreement in the region $y < 0$ between this theory and that of Langmuir is shown in Figure 5 in which y_1 is plotted against J_s/J_0 . It is seen that for $J_s/J_0 < 3$, the agreement is fairly good. An exact solution of the direct-current equation is given in the appendix. It will not be used here.

1.4 SOLUTION OF THE ALTERNATING-CURRENT EQUATION

The alternating-current equation is

$$\begin{aligned} v_0(\mu^2 - v_0^2)J_{yy} + (\mu^2v_{0y} - 3v_0^2v_{0y} - j2\theta v_0^2)J_y \\ + [- (2/9) - [2j\theta v_0v_{0y} + \theta^2v_0]]J = - (2/9)I. \end{aligned} \quad (13)$$

It should be noted that this differential equation has a singularity at $y = 0$. In view of this, the homogeneous differential equation ($I = 0$) possesses only one regular solution at $y = 0$. Thus there are only two constants to be determined, I and the arbitrary constant of the regular solution. The required initial conditions will be given later.

An approximate solution of (13) is obtained as follows. Let us rewrite (13) in the form

$$y^2 \sum_0 A_i y^i J_{yy} + y \sum_0 B_i y^i J_y + y \sum_0 C_i y^i J = - (2/9) I y. \quad (23)$$

From (16),

$$\left. \begin{aligned} A_0 &= -\frac{2}{3} \mu^{3/2}, \\ A_1 &= -\frac{1}{3}, \\ B_0 &= \mu^{3/2} (-\frac{2}{3} - j2\epsilon), \\ B_1 &= -\frac{2}{3} (1 + j2\epsilon), \\ C_0 &= -2/9 [1 - (9/2)\epsilon^2 + j3\epsilon], \\ C_1 &= -\frac{2}{9} \frac{1}{\mu^{3/2}} \epsilon (-\frac{3}{2}\epsilon + j), \\ \epsilon &= \theta \mu^{1/2} = 0.47 \omega / \omega_p, \\ &= 2 \times 10^{-12} \omega \frac{T_0^{3/4}}{|J_0|^{1/2}}, \end{aligned} \right\} (24)$$

where $|J_0|^{1/2}$ is in amperes per square centimeter and ω_p is the plasma frequency at the virtual cathode. One assumes a power-series solution.

$$J = \sum_0 a_n y^n \quad (25)$$

in the region $y_1 < y < 2.4\mu^{3/2}$. Equating coefficients of powers of y , one has

$$\left. \begin{aligned} a_1 &= -\frac{C_0}{B_0} a_0 - \frac{2I}{9B_0}, \\ a_2 &= \frac{a_0}{2(A_0 + B_0)} \\ &\quad \times \left[-C_1 + (B_1 + C_0) \frac{C_0}{B_0} \right] \\ &\quad + \frac{B_1 + C_0}{2(A_0 + B_0)} \frac{2I}{9B_0}. \end{aligned} \right\} (26)$$

This expansion will not be carried out further here.

It will be assumed that in view of the smallness of y the first three terms of the series suffice to approximate J in this region. In the region $y > 2.4\mu^{3/2}$, a solution is obtained in the following

manner. In this region, v_0 is given by (17), which implies physically that the effects of the initial thermal-velocity spread may be neglected. It will be assumed that this is still true for the

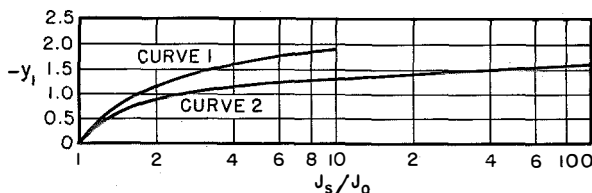


Figure 5—Variation of position of virtual cathode with anode current. Curve 1 is computed from equations in this paper and curve 2 from Langmuir's curves. y_1 is the normalized coordinate of the cathode, J_0 is the anode direct-current density, and J_s is the saturation-current density.

alternating-current process, since it is a perturbation of the direct-current process. This is equivalent to putting $\mu = 0$ in (13). The solution of (13) is now

$$J = \left(\frac{c_1}{Z} + \frac{c_2}{Z^2} \right) \exp(-j3\theta Z) - \frac{2I}{9\theta^2 Z^2}, \quad (27)$$

$$Z^3 = y, \quad (28)$$

$$v = - \left(\frac{c_1}{j3\theta} + \frac{2c_2}{j3\theta Z} \right) \exp(-j3\theta Z) - \frac{2I}{9\theta^2 Z^2} \left(Z^2 - \frac{2Z}{j3\theta} \right). \quad (29)$$

c_1 and c_2 are computed by matching the value of J_m and J_{my} at $y = y_m = 2.4\mu^{3/2}$ of this solution to that derived from (25). Thus

$$\left. \begin{aligned} J_m &= a_0 + a_1 y_m + a_2 y_m^2, \\ J_{my} &= a_1 + 2a_2 y_m, \end{aligned} \right\} (30)$$

and

$$\left. \begin{aligned} c_1 &= (2Z_m J_m + j3\theta v_m) \exp(j3\theta Z_m) \\ &\quad - \frac{2I}{j3\theta} \exp(j3\theta Z_m), \\ c_2 &= (-Z_m^2 J_m - j3\theta Z_m v_m) \exp(j3\theta Z_m) \\ &\quad + 2I \left(\frac{Z_m}{j3\theta} + \frac{1}{9\theta^2} \right) \exp(j3\theta Z_m), \end{aligned} \right\} (31)$$

$$v_m = Z_m^2 \left(J_m + \frac{J_{m2}}{j3\theta} \right). \quad (32)$$

The transit angle B_{m2} from matching point to anode is equal to

$$3\theta(Z_2 - Z_m) = 3.9\epsilon(Z_2 - Z_m). \quad (33)$$

Thus the solution of the alternating-current

problem has been reduced to the determination of a_0 and I . It is here that the problems of alternating-current impedance (Figure 2) and fluctuations (Figure 3) diverge. It is to be noted from (24) that the frequency appears only in the quantity ϵ . For a given set of direct-current conditions, the alternating-current behavior of a diode¹¹ is determined solely by the ratio of the applied frequency to the plasma frequency at the virtual cathode. Thus ϵ plays an important role and determines whether the process is to be classified as high or low frequency. For electron guns as used in microwave tubes, the process is definitely one of high frequency, as will be shown later. The initial conditions that J must satisfy will now be given.

1.5 INITIAL CONDITIONS FOR CURRENT DENSITY J

As mentioned previously, the initial conditions are different for the cases of alternating-current impedance (Figure 2) and fluctuations (Figure 3). They will be treated separately.

1.5.1 Case 1: Alternating-Current Impedance

At $y = y_1$ the initial conditions are

$$J = J_1, \quad (34A)$$

$$J_y = 0. \quad (34B)$$

The second initial condition corresponds to the statement that the alternating-current density is zero at the cathode. This will be so, since the density at the cathode, which is the source of electrons, is determined solely by conditions inside the metal and the image forces. These correspond to forces that are much greater than those applied by external means.

From (25)

$$\left. \begin{aligned} a_0 + a_1 y_1 + a_2 y_1^2 &= J_1, \\ a_1 + 2a_2 y_1 &= 0. \end{aligned} \right\} (35)$$

Equations (35), (26), and (27) may now be solved for the coefficients and I . The alternating-voltage drop V may be computed as follows:

$$V = - \int_0^d E dx = \frac{J_0 D}{j\omega\epsilon_0} \int_{v_1}^{v_2} (J - I) dy. \quad (36)$$

¹¹ This is not an approximate relation and may be shown to be always true by replacing v_0 by $Y = v_0^2/\mu^2$ in (13).

The alternating-current impedance

$$Z_{ac} = - V/I. \quad (37)$$

While the problem of the calculation of alternating-current impedance has been solved in principle, it is not possible to obtain results for a particular case without lengthy numerical computations. Only the case of $y_1 = 0$ will be considered here.

It is of interest to digress for a moment to observe how (27) may be used to solve the complete-space-charge diode of Llewellyn.¹² Here, the direct-current relation (17) holds up to $y = 0$ at the cathode. The values of c_1 , c_2 , and I are determined solely by the initial condition $J = J_1$ at $y = 0$ and J_1 is finite. Thus, for J to be finite at $Z = 0$, it follows immediately that

$$\left. \begin{aligned} c_1 &= - \frac{2I}{jB_{12}}, \\ c_2 &= - \frac{2I}{j^2 B_{12}^2}. \end{aligned} \right\} (38)$$

Hence,

$$J = \frac{2I}{j^2 B_{12}^2} \times \left[\frac{1 - jB_{12}Z \exp(-jB_{12}Z) - \exp(-jB_{12}Z)}{Z^2} \right]. \quad (39)$$

Using the initial condition in (39),

$$I = J_1. \quad (40)$$

It will also follow automatically that at $Z = 0$, v and E are both zero. It should be noted that Llewellyn was forced to assume that $v = 0$ or $E = 0$ at the cathode, but actually this follows automatically from Maxwell's equations for a complete-space-charge region.

1.5.2 Case 1A: Calculation of Alternating-Current Impedance for $y_1 = 0$

Here

$$\left. \begin{aligned} a_0 &= J_1, \\ a_1 &= 0, \\ I &= [1 - (9/2)\epsilon^2 + j3\epsilon]J_1, \\ a_2 &= \frac{-j\theta}{12\mu^{3/2}} J_1. \end{aligned} \right\} (41)$$

It is to be noted that I is not equal to J_1 as in Llewellyn's case.

¹² See reference 4, page 45. Here the thermal-velocity spread is entirely neglected, giving for this case $Z_m = 0$.

The value of the other constants are

$$\left. \begin{aligned} c_1 &= -\frac{2J_1}{j3\theta} [1 - (9/2)\epsilon^2 \\ &\quad + j3\epsilon](1 + p) \exp j4.13\epsilon, \\ c_2 &= \frac{2J_1}{9\theta^2} [1 - (9/2)\epsilon^2 \\ &\quad + j3\epsilon](1 + q) \exp j4.13\epsilon, \end{aligned} \right\} (42)$$

$$p = -j\epsilon \frac{(4.13 + 4.25\epsilon^2)}{1 - (9/2)\epsilon^2 + j3\epsilon}, \quad (43)$$

$$q = \frac{\epsilon}{1 + j3\epsilon - (9/2)\epsilon^2} \times [4.35\epsilon - 17.2\epsilon^3 + j(15\epsilon^2 - 4.13)]. \quad (44)$$

The modulation at the anode and alternating-current impedance is given by

$$\left. \begin{aligned} J_2 &= -\frac{2}{9} \mu J_1 \frac{1 - (9/2)\epsilon^2 + j3\epsilon}{\epsilon^2} \{1 - [jB_{m2}(1 + p) + 1 + q] \exp j(4.13\epsilon - B_{m2})\}, \\ v_2 &= -\frac{2}{9} \mu J_1 \frac{1 - (9/2)\epsilon^2 + j3\epsilon}{\epsilon^2} \left\{ 1 - \frac{2}{jB_{m2}} + \frac{1}{jB_{m2}} [jB_{m2}(1 + p) + 2 + 2q] \right. \\ &\quad \left. \times \exp j(4.13\epsilon - B_{m2}) \right\}, \end{aligned} \right\} (45)$$

where $B_{m2} = 3\theta(Z_2 - Z_m)$, the transit time in the Child's law region.

$$Z_{ac} = Z_{ac}^{(1)} + Z_{ac}^{(2)},$$

$$\left. \begin{aligned} Z_{ac}^{(1)} &= \frac{d}{j\omega\epsilon_0} \left\{ 1 + \frac{6}{j^3 B_{m2}^3} \{ - (jB_{m2} + 2) \exp [j(4.13\epsilon - B_{m2})] + 2 - jB_{m2} \} \right\}, \\ Z_{ac}^{(2)} &= - \left(\frac{kT_0}{m} \right)^{1/2} \frac{G\epsilon}{j\epsilon_0\omega^2} + \frac{6d}{j\omega\epsilon_0 B_{m2}^3} \{ (-jB_{m2}p - p - q) \exp [j(4.13\epsilon - B_{m2})] \\ &\quad + p(j4.13\epsilon + 1) + 4.13\epsilon + q + j1.35B_{m2}\mu^{1/2} \}, \end{aligned} \right\} (46)$$

$$\left. \begin{aligned} G &= \frac{2.5 - j0.435\epsilon}{1 - (9/2)\epsilon^2 + j3\epsilon} \\ &= \frac{2.5 - 12.5\epsilon^2 + j\epsilon(-8 + 2\epsilon^2)}{1 + (81/4)\epsilon^4}. \end{aligned} \right\} (47)$$

For small ϵ , $Z_{ac}^{(1)}$ reduces to Llewellyn's formula. For large B_{m2} , these formulas may be simplified somewhat. It may be noted that for large B_{m2} there will always be a resistive component, while the Llewellyn formula predicts a purely capacitive component. Physically, this is to be expected in view of the velocity spread. The value of the impedance at high frequencies, Z_∞ , is

$$Z_\infty = \left[- \left(\frac{kT_0}{m} \right)^{1/2} \frac{G\epsilon}{\omega} + d \right] \frac{1}{j\omega\epsilon_0}. \quad (48)$$

It is seen that for $\epsilon^2 > 0.2$ there is always a positive resistive component of the impedance. Also, it is possible to conceive values of ϵ , ω , T_0 , and d for which Z_∞ has a considerable resistive component. This could possibly be checked experimentally by methods similar to those employed by Robertson.¹³

1.5.3 Case 2: Fluctuations in Diodes

At $y = y_1$ the initial conditions are

$$J = J_1, \quad (49)$$

and the circuit equation is

$$V = IZ_L, \quad (50)$$

in which V is given by (36).

Sufficient conditions are now known to determine the constants in (26) and (27). Unfortunately, the work required to compute the fluctuations for all values of Z_L is very great. Thus, only the case of the open circuit, $Z_L = \infty$ and $I = 0$, will be discussed here. This is the case of interest for the diode region in the electron gun of the traveling-wave tube. Furthermore, it is seen from (27) and (29) that for large transit angles, J_2 and v_2 will not depend on I . Hence, for large transit angles the open-circuit case will be a good approximation for all diode terminations.

¹³ S. D. Robertson, "Electronic Admittances of Parallel-Plane Electron Tubes at 4000 Megacycles," *Bell System Technical Journal*, volume 28, pages 619-646; October, 1949.

For the open-circuit case, $I = 0$, the constants are given as follows:

$$\left. \begin{aligned} \frac{a_0}{J_1} &= \frac{1}{1 + y_1(a_1/a_0) + y_1^2(a_2/a_0)}, \\ \frac{a_1}{a_0} &= \frac{1 - 4.5\epsilon^2 + j3\epsilon}{1.41(1 + j3\epsilon)}, \\ \frac{a_2}{a_0} &= -\frac{1}{5.65} \left[2.12j\epsilon + (4 + j3\epsilon) \frac{a_1}{a_0} \right]. \end{aligned} \right\} (51)$$

From these, the current modulation J_2 and velocity modulation v_2 at the anode can be computed as follows:

$$\frac{J_2}{J_1} = \left(\frac{1}{Z_2} \frac{c_1}{J_1} + \frac{1}{Z_2^2} \frac{c_2}{J_1} \right) \exp - jB_{m2}, \quad (52)$$

$$\frac{v_2}{J_1} = - \left(\frac{Z_2}{jB_{m2}} \frac{c_1}{J_1} + \frac{2}{jB_{m2}^2} \frac{c_2}{J_1} \right) \exp - jB_{m2}, \quad (53)$$

and

$$\left. \begin{aligned} \frac{c_1}{J_1} &= \left(2.12 \frac{J_m}{J_1} + j3.9\epsilon \frac{v_m}{J_1} \right) \exp j4.13\epsilon, \\ \frac{c_2}{J_1} &= \left(-1.12 \frac{J_m}{J_1} - j4.13\epsilon \frac{v_m}{J_1} \right) \\ &\quad \times \exp j4.13\epsilon, \end{aligned} \right\} (54)$$

$$\frac{J_m}{J_1} = \left(1 + 1.13 \frac{a_1}{a_0} + 1.28 \frac{a_2}{a_0} \right) \frac{a_0}{J_1},$$

$$\frac{v_m}{J_1} = 1.11 \left(\frac{J_m}{J_1} + \frac{1}{j3.9\epsilon} \frac{J_{mz}}{J_1} \right),$$

$$\frac{J_{mz}}{J_1} = 3.35 \left(\frac{a_1}{a_0} + 2.26 \frac{a_2}{a_0} \right) \frac{a_0}{J_1}.$$

Also at the virtual cathode

$$\left. \begin{aligned} J_c &= a_0, \\ v_c &= \frac{0.61 + 2.75\epsilon^2 a_0}{9\epsilon^2 - j3\epsilon} \frac{a_0}{J_1}. \end{aligned} \right\} (55)$$

To convert to unnormalized units (denoted by a subscript u) one uses the following:

$$\left. \begin{aligned} J_u &= (J/J_1)J_{1u}, \\ v_u &= \left(\frac{v}{J_1} \right) \frac{J_{1u}}{J_0} \left(\frac{kT_0}{m} \right)^{1/2} 1.65, \end{aligned} \right\} (56)$$

and

$$(J_{1u}S)^2 = 2eJ_0Sdf, \quad (57)$$

where S is the cross-sectional area of the beam under consideration.

Thus, with the use of (52) through (57), one

may compute the value of all fluctuating-field quantities. The corresponding equations derived from the RPHP theory are: At the virtual cathode

$$v_u = 0.655(kT_0/m)^{1/2}J_{1u}/J_0, \quad (55A)$$

and at the anode⁶

$$v_{2u} = -0.655 \left(\frac{kT_0}{m} \right)^{1/2} \frac{J_{1u}}{J_0} \exp - j3.9\epsilon Z_2, \quad (53A)$$

$$J_{2u} = j \frac{2.36\epsilon}{Z_2} (0.655)J_{1u} \exp - 3.9\epsilon Z_2. \quad (52A)$$

To convert from Pierce's notation to the one used here, one uses the fact that B_{m2} (transit angle from virtual cathode to anode) = $3.9\epsilon Z_2$.

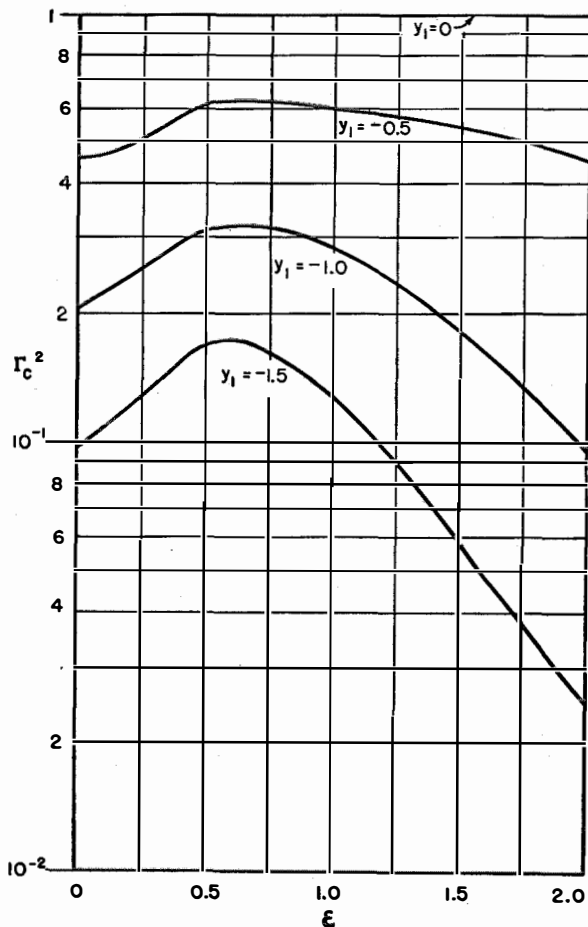


Figure 6—Current fluctuation at the virtual cathode as a function of frequency, $\epsilon = 0.47 \omega/\omega_p$, $(J_c S^2)_{AV} = \Gamma_c^2 \times 2eI_0df$.

An important deduction from the RPHP theory is that J_{2u} and v_{2u} are 90 degrees out of phase and that

$$J_{2u}/v_{2u} = -j2.36\epsilon J_0/Z_2(kT_0/m)^{1/2}. \quad (58)$$

This ratio is still true for large Z_2 in our theory, as can be seen from (52) and (53). Thus for large Z_2 it is necessary only to compute v_2 .

Let the following noise factors be defined: At the virtual cathode let

$$\begin{aligned} \langle (J_{cu}S)^2 \rangle_{Av} &= \Gamma_e^2 2eI_0 df, \\ \langle v_{cu}^2 \rangle_{Av} &= q_c^2 \frac{e}{m} \frac{kT_0}{I_0} df, \end{aligned}$$

and let I_0 be the total beam current, and Γ_2^2 and q_2^2 be the corresponding factors at the anode. These noise factors have the following values in the RPHP theory:

$$\begin{aligned} q_c^2 &= q_2^2 = 0.86 \\ \Gamma_2^2 &= 2.2(\epsilon/Z_2)^2. \end{aligned}$$

These noise factors have been plotted versus ϵ in Figures 6 through 9. It is seen that the noise factors decrease as y becomes more negative and that they vary with y , ϵ , and Z_2 . Furthermore, there is no question as to the coherence of the various fluctuations, since they are all derived from the shot-noise fluctuations at the cathode. The phase angle between the current and velocity fluctuations at the anode θ_2 and virtual cathode θ_c is plotted against ϵ in Figure 10. It is seen that θ_2 is almost 90 degrees for large Z_2 . However, it is not exactly 90 degrees and does deviate about 3 degrees.

1.6 CONCLUSIONS

It is possible to work out a theory of alternating-current impedance and fluctuations in diodes by accounting for the thermal-velocity spread by the hydrostatic-pressure method of Hahn.

The equations are difficult to solve, and it becomes necessary to make certain approximations. Comparisons of these theories and those of Llewellyn for diode impedance, and those of Rack-Peterson (RP) for fluctuations are made. It is shown that the high-frequency impedance always has a resistive component, which may be large in some cases, especially in diodes of small spacing and low anode currents. In general, the fluctuations depend on more parameters and may be greater than predicted by the RP theory.

For a given direct-current condition everything is determined by ϵ , which is proportional to the ratio of the applied frequency to the plasma frequency at the virtual cathode ($\epsilon = 0.47\omega/\omega_p$).

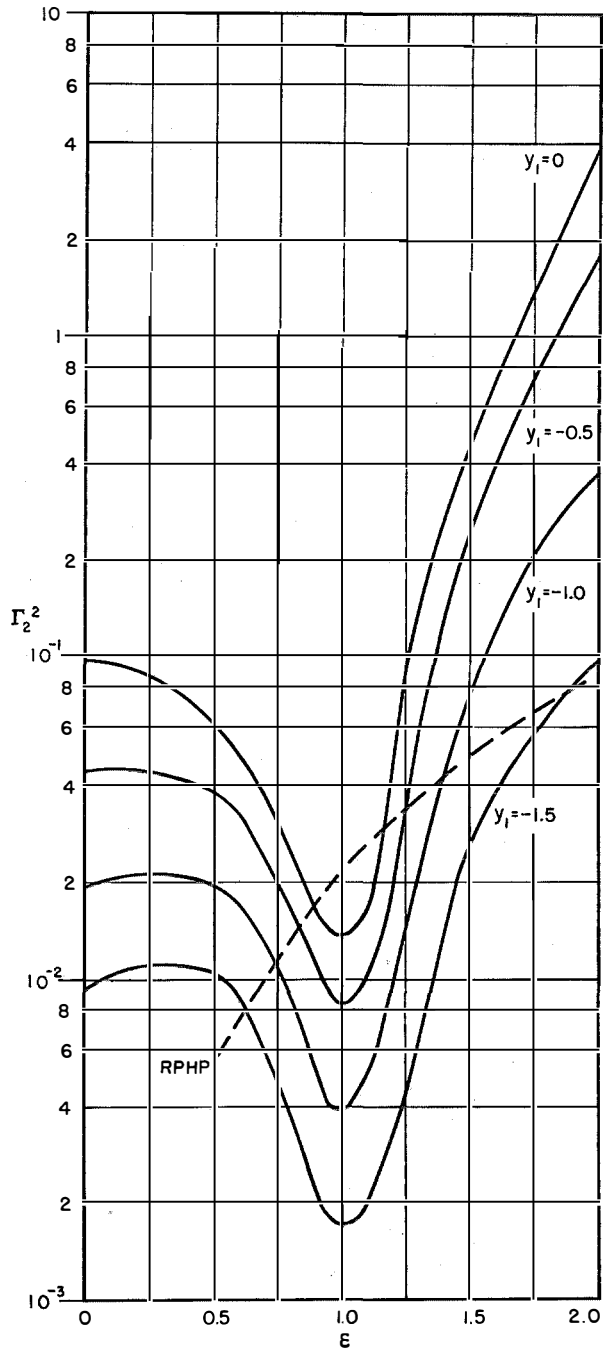


Figure 7—Current fluctuation at anode plotted against frequency $\epsilon = 0.47 \omega/\omega_p$, $\langle J_2 S^2 \rangle_{Av} = \Gamma_2^2 2eI_0 df$, and $Z_2 = 10$. The dashed line is for the RPHP theory.

2. Alternating-Current Properties of Drift Tube

2.1 GENERAL

The propagation of space-charge waves in an electron beam, neglecting the effect of the thermal-velocity spread, has been discussed by Hahn⁷ and Ramo.⁸ The effect of the thermal-velocity spread will be discussed here.

In this case the beam velocity v_0 is a constant $= v_{0d}$. The subscript d will denote the value of quantities in the drift region. In this region let the normalizing parameter $\alpha = v_{0d}$. Hence,

$$\left. \begin{aligned} D &= (2/9)^{1/2} v_{0d} / \omega_d, \\ \theta &= (2/9)^{1/2} \omega / \omega_d, \end{aligned} \right\} (59)$$

where ω_d is the plasma frequency in the drift region.

The differential equation for J now reduces to

$$(1 - \mu_d^2) J_{yy} + j2\theta J_y + (2/9 - \theta^2) J = (2/9) I, \quad (60)$$

of which the solution is

$$J = \frac{I}{1 - (\omega/\omega_d)^2} + a_1 \exp(-\Gamma_1 x) + a_2 \exp(-\Gamma_2 x), \quad (61)$$

$$\Gamma_1 = \frac{j\gamma_0}{1 - \mu_d^2} \left\{ 1 + \left[\left(\frac{\omega_d}{\omega} \right)^2 (1 - \mu_d^2) + \mu_d^2 \right]^{1/2} \right\}, \quad (62)$$

$$\Gamma_2 = \frac{j\gamma_0}{1 - \mu_d^2} \left\{ 1 - \left[\left(\frac{\omega_d}{\omega} \right)^2 (1 - \mu_d^2) + \mu_d^2 \right]^{1/2} \right\}, \quad (63)$$

$$\gamma_0 = \omega / v_{0d}, \quad (64)$$

$$\mu_d^2 = kT_0 / mv_{0d}^2. \quad (65)$$

2.2 MODES IN AN INFINITE BEAM

a_1 and a_2 are arbitrary constants to be determined by the initial conditions. There are two possible modes in an infinite beam.

2.2.1 a_1 and $a_2 = 0$, $I \neq 0$; No Propagation of Space-Charge Waves

This is a mode where there is no propagation. The density modulation is zero, while the alternating-current field and convection-current density are constant along the x direction.

2.2.2 $I = 0$; a_1 and $a_2 \neq 0$; Propagation of Space-Charge Waves

This is the mode where there is propagation. The case of interest is that for which I vanishes and $\mu_d \ll 1$. Hence,

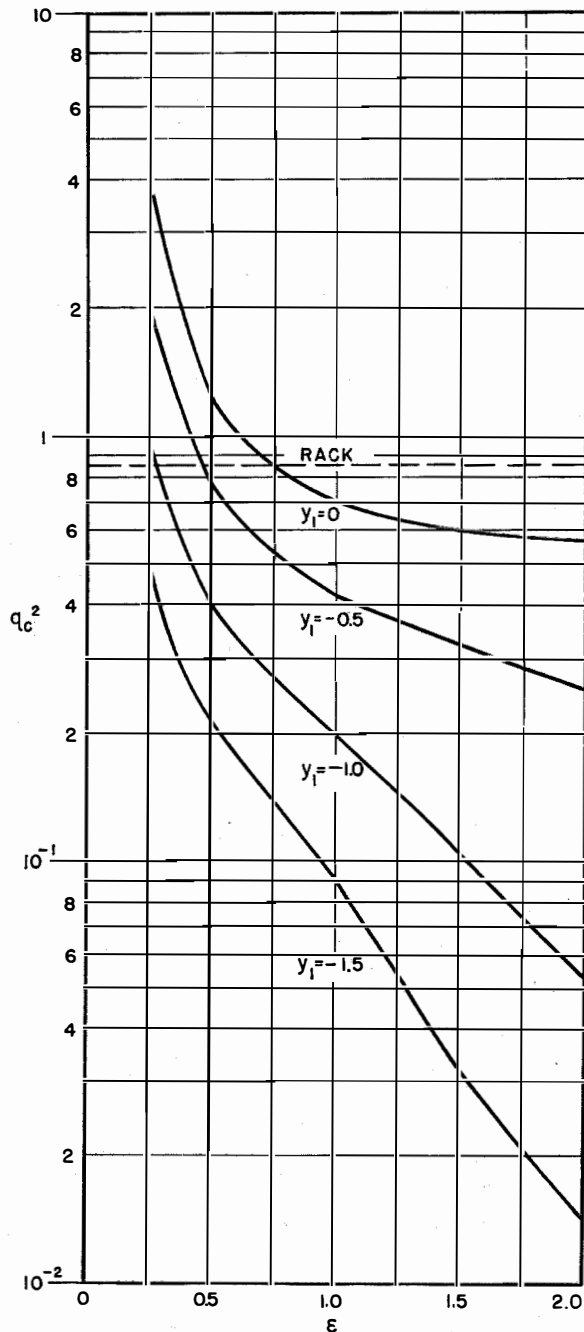


Figure 8—Velocity fluctuation at virtual cathode versus frequency. $\epsilon = 0.47 \omega / \omega_p$ and $\langle v_c^2 \rangle_{AV} = q^2 e k T \alpha f / m I_0$.

$$\Gamma_1 = j\gamma_0(1 + \delta_d), \quad (66)$$

$$\Gamma_2 = j\gamma_0(1 - \delta_d), \quad (67)$$

and the correction for the space-charge-wave number is

$$\delta_d = \frac{\omega_d}{\omega} \left(1 + \frac{kT_0}{mv_{0d}^2} \frac{\omega^2}{\omega_d'^2} \right)^{1/2}. \quad (68)$$

Solving for a_1 and a_2 in terms of the current and velocity fluctuations at the beginning of the drift region, the current modulation $J_{3\mu}$ and velocity modulation $v_{3\mu}$ along the drift region is

$$J_{3\mu} = - \exp[-j\gamma_0(x - x_2)] \times jv_{2\mu} \frac{\rho_{0d}}{\delta_d} \sec \phi_0 \sin(\phi_0 - \phi), \quad (69)$$

$$v_{3\mu} = \exp[-j\gamma_0(x - x_2)] v_{2\mu} \times \sec \phi_0 \cos(\phi_0 - \phi), \quad (70)$$

$$\rho_{0d} = \text{direct-current density in drift region,} \quad (71)$$

$$\tan \phi_0 = - \frac{J_{2u} \delta_d}{jv_{2u} \rho_{0d}} = 1.4 \frac{\omega_d'}{\omega_d} \left(1 + \frac{kT_0}{mv_{0d}^2} \frac{\omega^2}{\omega_d'^2} \right)^{1/2}, \quad (72)$$

which follows from (58) and (74).

$$\phi = \gamma_0 \delta_d (x - x_2). \quad (73)$$

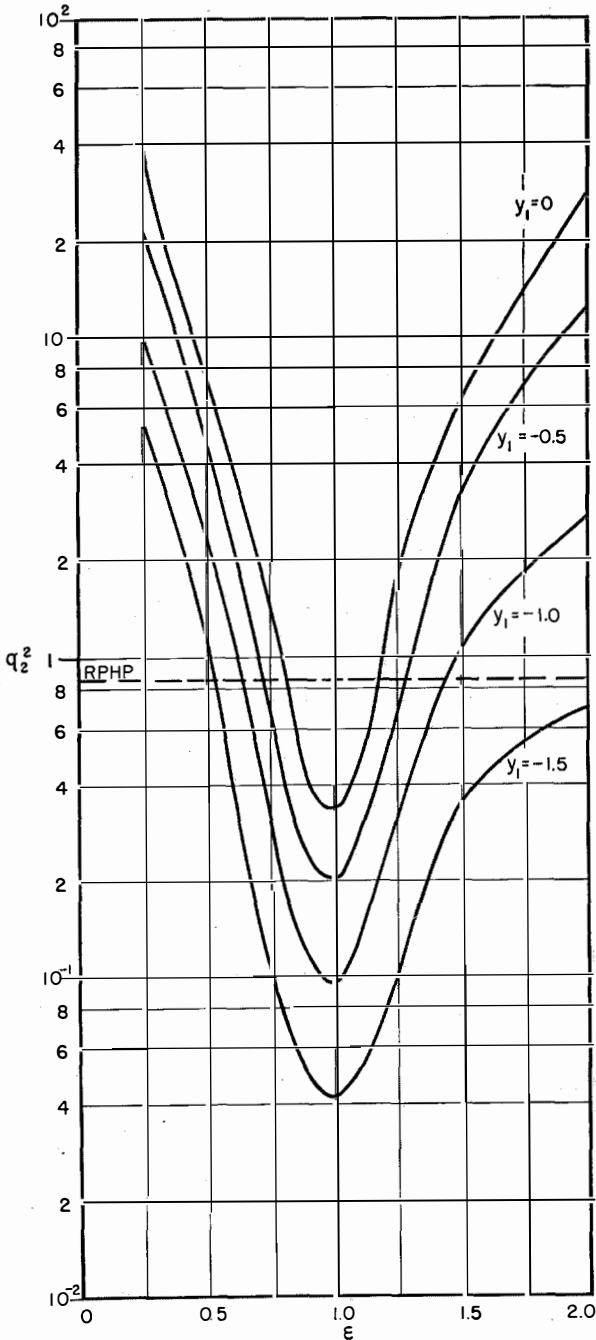


Figure 9—Velocity fluctuation at anode as a function of frequency. $\epsilon = 0.47 \omega/\omega_p$, $(v_{2\mu}^2)_{Av} = q_2^2 e k T_0 d f / m I_0$, and $Z_2 = 10$.

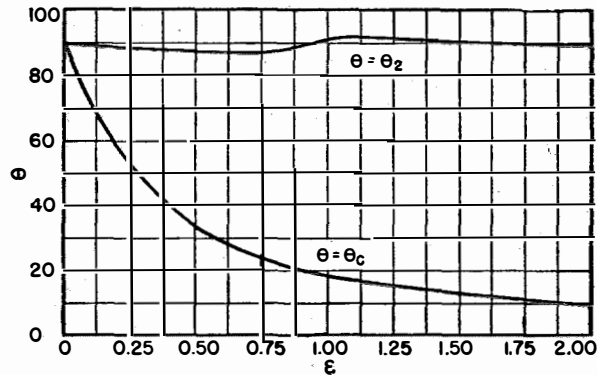


Figure 10—Phase angle between current and velocity fluctuations at the virtual cathode and anode plotted against frequency. $\epsilon = 0.47 \omega/\omega_p$, $\theta_2 =$ angle at anode, $\theta_c =$ angle at virtual cathode, and $Z_2 = 10$.

These expressions are valid for an infinite electron beam. For the practical case of a circular electron beam of radius b in a circular drift tube of radius a , one may account for the finite geometry by applying the correction used in the case of no thermal-velocity spread. This⁸ is accomplished by reducing the plasma frequency ω_d by a factor given by

$$\omega_d' = \omega_d / [1 + (\tau/\gamma_0)^2]^{1/2}. \quad (74)$$

τ/γ_0 is a function of $\gamma_0 b$ and a/b only for small densities. A plot of τ/γ_0 versus $\gamma_0 b$ is given in Figure 11.

According to (69) and (70), J_{3u} and v_{3u} are periodic functions of distance of period $2\pi/\gamma_0\delta_d$. The periodicity of J_{3u} has been observed experimentally by several investigators. The effect of temperature is to decrease this period.

3. Traveling-Wave-Tube Amplifier Region

3.1 GENERAL

The usual theory of the traveling-wave-tube amplifier, such as that of Pierce,⁶ depends on a knowledge of the circuit and ballistic equations. According to Pierce and using his notation, the circuit equation for a filamentary electron beam is in unnormalized units

$$V = \left[\frac{\Gamma\Gamma_1(E^2/B^2P)}{2(\Gamma^2 - \Gamma_1^2)} - \frac{j\Gamma}{\omega c_1} \right] i, \quad (75)$$

where $i = JS$, $E = \Gamma V$, and V is voltage.

The ballistic equation, which includes the effect of thermal-velocity spread, is⁹

$$i = \frac{I_0}{2V_0} \frac{jB_e\Gamma V}{(jB_e - \Gamma)^2 - \mu_d^2\Gamma^2}, \quad (76)$$

where I_0 is the total beam current, which equals $-J_0S$, and B_e is the electron-beam wave number.

$$v = -\frac{v_{0d}}{2V_0} \frac{(jB_e - \Gamma)\Gamma V}{(jB_e - \Gamma)^2 - \mu_d^2\Gamma^2}$$

Comparing (75) and (76), one has the following equation for Γ :

$$(jB_e - \Gamma)^2 = \frac{j2B_e\Gamma^2\Gamma_1C^3}{(\Gamma_1^2 - \Gamma^2)} + \Gamma^2 \left(4QC + \frac{\mu_d^2}{C^2} \right), \quad (77)$$

where C is the Pierce coupling parameter and QC is the Pierce space-charge parameter.

$$\left. \begin{aligned} C^3 &= E^2I_0/B^2P8V_0, \\ Q &= B_e/\omega c_1(E^2/B^2P). \end{aligned} \right\} (78)$$

Only the case of synchronism and no loss will be considered here. Following Pierce,⁶ page 113, let

$$\Gamma = jB_e - j\delta B_e C; \quad \delta \ll 1,$$

$\Gamma_1 = jB_e$ for synchronism. Hence,

$$\delta^3 - [4QC + (\mu_d^2/C^2)]\delta - 1 = 0. \quad (79)$$

For small space charge, QC may be approximately computed by associating the second term of (75) with the propagation of space-charge waves in the electron beam independently of the external circuit. Thus,

$$-\frac{\omega C_1}{j\Gamma} = \frac{I_0}{2V_0} \frac{jB_e\Gamma}{(jB_e - \Gamma)^2 - \mu_d\Gamma^2}, \quad (80)$$

and the value of Γ is given by (66). Thus, approximately

$$\omega C_1/B_e = I_0/2V_0(\omega/\omega_h)^2, \quad (81)$$

where ω_h is the plasma frequency in this region. Hence,

$$4QC = (\omega_h/\omega)^2 1/C^2. \quad (82)$$

A more-rigorous solution would be obtained by utilizing the expression of (76) in the various field theories of the traveling-wave tube. This will not be carried out here.

It is of interest to digress for a moment to observe that the space-charge parameter of Pierce for small QC may be obtained by modifying the ballistic equation to include a polarization term. Neglecting thermal-velocity spread, the equation of motion is

$$m dv/dt = e(E - P/\epsilon_0); \quad (83)$$

P , which is the polarization, equals $n_0 e \zeta$. ζ is the alternating-current displacement of an electron.

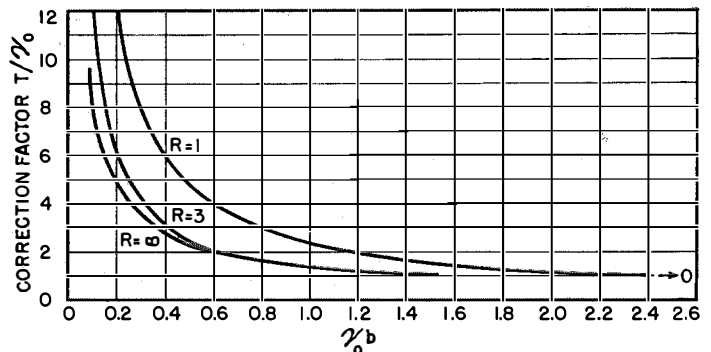


Figure 11—Correction factor to the plasma frequency in the drift tube for beam and drift-tube geometries. R is the ratio of the radius of the drift tube to the radius of the beam. $\gamma_0 = \omega/v_{0d} = 2\pi f/\text{beam velocity}$. $\omega_d'/\omega_d = 1/[1 + (\tau/\gamma_0)^2]^{1/2}$, where ω_d is the plasma frequency in the drift tube and ω_d' is the plasma frequency corrected for beam and drift-tube geometries.

The reason for this is as follows: The acceleration of an electron is proportional to the force F acting on the electron under consideration. E , however, includes the force resulting from the electron under consideration. Thus, in order to obtain F , one must subtract the force resulting from the electron, which is approximated on the average by the electric field in a small slice bounded by infinite parallel planes around the electric field.

This force equals P/ϵ_0 . Hence $F = E - P/\epsilon_0$. The alternating current

$$i = \frac{\partial P}{\partial t} = \frac{I_0}{2V_0} \frac{jB_e \Gamma V}{(jB_e - \Gamma)^2 + (\omega_h/\omega)^2 B_e^2}. \quad (84)$$

Combining this with the circuit equation (75) and with $C_1 = \infty$, one has

$$(jB_e - \Gamma)^2 = \frac{j2B_e \Gamma^2 \Gamma_1 C^3}{(\Gamma_1^2 - \Gamma^2)} - \left(\frac{\omega_h}{\omega}\right)^2 B_e^2. \quad (85)$$

Now since Γ can be approximated by jB_e for small space charge at synchronism and using (82), it is seen that (85) is equivalent to (76) for $\mu_d = 0$. Thus, in this case the Pierce space-charge correction may be accounted for on purely ballistic grounds.

three modes is determined by the initial conditions, which are

$$\sum E_m = E_i - \frac{j}{\omega C_1} \sum \Gamma_m^2 i_m, \quad (87)$$

$$\sum \frac{jB_e - \Gamma_m}{(jB_e - \Gamma_m)^2 - \mu_d \Gamma_m^2} E_m = -\frac{2V_0}{v_0} v_{3u}, \quad (88)$$

$$\sum \frac{E_m}{(jB_e - \Gamma_m)^2 - \mu_d \Gamma_m^2} = \frac{2V_0}{jB_e I_0} J_{3u} S. \quad (89)$$

Only the case of $\mu_d \ll 1$ will be treated here. With this condition, these equations reduce to

$$\sum_1^3 e_m \left(1 - \frac{2\Omega_t C}{\delta_m} - \frac{\Omega}{\delta_m^2}\right) = E_i, \quad (90)$$

$$\sum \frac{e_m}{\delta_m} = -j \frac{2V_0 B_e C}{v_{0d}} v_{3u}, \quad (91)$$

$$\sum \frac{e_m}{\delta_m^2} = -\frac{2V_0}{jB_e I_0} B_e^2 C^2 J_{3u} S, \quad (92)$$

$$e_m = E_m/1 - \frac{2\Omega_t C}{\delta_m} - \frac{\Omega}{\delta_m^2}. \quad (93)$$

Thus, the gaining wave E_1 (δ_1 is complex) is given by

$$E_1 = \left(1 - \frac{2\Omega_t C}{\delta_1} - \frac{\Omega}{\delta_1^2}\right) \frac{E_i + j \frac{2V_0 B_e C}{v_{0d}} (-\delta_1 - 2\Omega_t C) v_{3u} - \frac{2V_0 B_e^2 C^2}{jB_e I_0} \left(\frac{1}{\delta_1} + \Omega\right) J_{3u} S}{\left(1 - \frac{\delta_2}{\delta_1}\right) \left(1 - \frac{\delta_3}{\delta_1}\right)}. \quad (94)$$

The noise figure F is given by

$$F - 1 = \frac{\left| j \frac{2V_0 B_e C}{v_{0d}} (-\delta_1 - 2\Omega_t C) v_{3u} - \frac{2V_0 B_e^2 C^2}{jB_e I_0} \left(\frac{1}{\delta_1} + \Omega\right) J_{3u} S \right|}{|E_i|^2}. \quad (95)$$

3.2 COMPUTATION OF GAIN AND NOISE FIGURE

Let

$$\left. \begin{aligned} \Omega_s &= 4QC = \left(\frac{\omega_h}{\omega}\right)^2 \frac{1}{C^2}, \\ \Omega_t &= \frac{\mu_d^2}{C^2} = \frac{kT_0}{mv_{0d}^2} \frac{1}{C^2}, \\ \Omega &= \Omega_s + \Omega_t, \end{aligned} \right\} (86)$$

then

$$\delta^3 - \Omega\delta - 1 = 0. \quad (79A)$$

The three solutions of this cubic correspond to three propagating modes of voltage amplitudes V_m , $m = 1, 2, 3$. The distribution among the

Now from (70) and Figure 9

$$\left. \begin{aligned} |v_{3u}|^2 &= q_2^2 \frac{e}{m} \frac{kT_0}{J_0 S} df \sec^2 \phi_0 \cos^2(\phi_0 - \phi), \\ J_{3u} &= -j \frac{\rho_{0d}}{\delta_d} \tan(\phi_0 - \phi) v_{3u}. \end{aligned} \right\} (96)$$

Also in root-mean-square values

$$|E_i|^2 = B_e^2 \frac{4V_0}{I_0} C^3 kT_0 df, \quad (97)$$

where T_a is the ambient temperature. Hence,

$$F - 1 = \frac{q_2^2 T_0}{2C T_a} \frac{\sec^2 \phi_0}{1 + (\delta_d/C)^2 Y^2} \times \left| j(-\delta_1 - 2\Omega_i C) - Y \left(\frac{1}{\delta_1} + \Omega \right) \right|^2, \quad (98)$$

$$Y = C/\delta_d \tan(\phi_0 - \phi),$$

in which T_0 is the cathode temperature. This may be further reduced by noting that

$$\tan \phi_0 = 1.4 \frac{\omega_d'}{\omega_d} \left(1 + \frac{kT_0}{mv_{0d}^2} \frac{\omega^2}{\omega_d'^2} \right)^{1/2}, \quad (72)$$

$$(\delta_d/C)^2 = \Omega,$$

according to (68). Hence,

$$F - 1 = \frac{q_2^2 T_0}{2C T_a} \frac{\sec^2 \phi_0}{1 + \Omega Y^2} \times \left| j(-\delta_1 - 2\Omega_i C) - Y \left(\frac{1}{\delta_1} + \Omega \right) \right|^2, \quad (99)$$

$$Y = -\frac{1}{\Omega^{1/2}} \tan [B_e C \Omega^{1/2} (x_3 - x_2) - \phi_0], \quad (100)$$

$$\sec^2 \phi_0 = 1 + 1.96 \left(\frac{\omega_d'}{\omega_d} \right)^2 \left(1 + \frac{kT_0}{mv_{0d}^2} \frac{\omega^2}{\omega_d'^2} \right).$$

In Figure 12, δ_1 has been plotted against Ω .

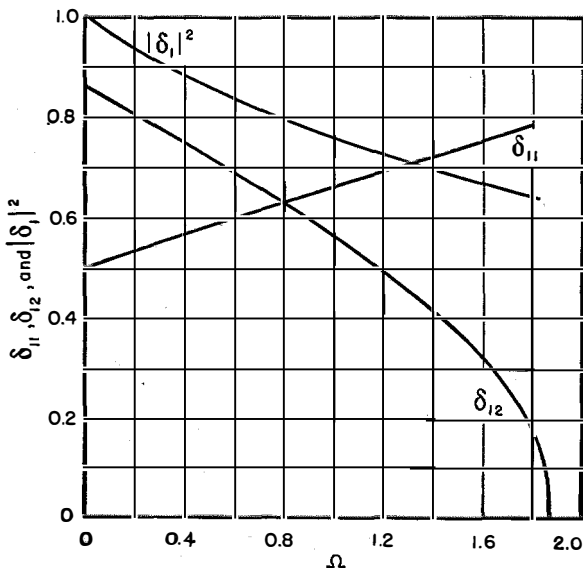


Figure 12—Relative phase shift δ_{11} , logarithmic gain δ_{12} , and $|\delta_1|^2$, $\delta_1 = -\delta_{11} - j\delta_{12}$ are plotted against $\Omega = 4QC + kT_0/mv_{0d}^2 \times 1/C^2$.

Thus one has all the necessary formulas to compute F .

It is seen that the noise figure is a periodic function of the length of the drift tube of period $\pi/B_e C \Omega^{1/2}$. Thus it is possible to vary Y from 0 to ∞ by varying the length of the drift tube. These correspond to the cases where the beam emerges from the drift tube with only velocity modulation or only current modulation, respectively. In general, $\Omega_i C$ is quite small. Hence, (98) may be rewritten as

$$F - 1 = \frac{q_2^2 T_0}{2C T_a} \sec^2 \phi_0 f_1, \quad (101)$$

where

$$f_1 = \frac{\left| j\delta_1 + Y \left(\frac{1}{\delta_1} + \Omega \right) \right|^2}{1 + \Omega Y^2}. \quad (102)$$

Thus, f_1 measures the effect of the drift tube and the traveling-wave tube while the other factor measures the effect of the diode. In those cases where Ω_s is much larger than Ω_i , the effect of the thermal spread will appear only in the factor q^2 . This is probably the case in practice since $\mu_d^2 \sim 1 \times 10^{-4}$ for a 500-volt beam, and $(\omega_d'/\omega)^2$ will be greater than 10^{-4} . In the case where Ω_s is much less than Ω_i , there will be a reduction in the noise factor because of the thermal-velocity spread, which can be estimated by considering the cases $Y = 0$ and $Y = \infty$. For $Y = 0$,

$$f_1 = |\delta_1|^2, \quad (103)$$

which is plotted in Figure 12. For $Y = \infty$,

$$f_1 = \frac{\left| \frac{1}{\delta_1} + \Omega \right|^2}{\Omega^2}. \quad (104)$$

A plot of $|(1/\delta) + \Omega|^2$ against Ω is given in Figure 13. Thus, it is seen that there is a reduction in noise factor because of the thermal-velocity spread.

It should be remarked that in actual practice C and Q are not too easy to evaluate. Thus a rigorous theory of the effect of thermal-velocity spread can exist only in a field theory.

The case of $\Omega_i = 0$ and $q^2 = 0.86$ has already been discussed in great detail by others, such as the Stanford group. This will not be discussed here.

A numerical example is as follows:

Diode spacing	= 0.635 centimeter
Beam radius	= 0.064 centimeter
Drift-tube radius	= 0.192 centimeter
T_0	= 1000 degrees Kelvin
Direct-current diode voltage	= 500 volts
Direct-current density	= 63×10^{-3} ampere per square centimeter
ω	= 3×10^{10} /cycle
$\gamma_0 b$	= 1.5
T/γ_0	= 1
$\omega d'$	= 0.7×10^9
C	= 0.075 ⁽¹⁴⁾
ϵ	= 1.34
Z_2	= 10
q_2^2	= 0.6
Γ_2^2	= 0.04
Ω_s	= 0.08
Ω_t	= 0.02
y_1	= -1 ⁽¹⁵⁾

In this case, as seen from (101), the effect of the thermal-velocity spread will be felt only in the factor q^2 . Thus, the RPHP theory in practice will be qualitatively correct. One cannot, however, expect a quantitative agreement between theory and experiment as seen from Figure 9. For less-dense electron beams, the RPHP theory will not be qualitatively correct, since the effect resulting from Ω_t will predominate.

4. Conclusions

It is possible to find the effect of the thermal velocity on noise figure by extending a method of Hahn. This effect can be characterized by the calculation of two quantities, q_2^2 and Ω_t . For a given set of direct-current conditions in the diode region, q_2^2 is a function only of ϵ , which is proportional to the ratio of applied frequency to the plasma frequency at the virtual cathode. It is this quantity ϵ that determines whether the process is to be characterized as that of low or high frequency. Computations are given for q_2^2 as a function of ϵ . These results agree with those computed from the Rack-Peterson theory only under certain conditions.

For those cases where $\Omega_t \ll 4QC$, the effect of the thermal-velocity spread will be determined

¹⁴ This was computed from Figure A6.5 in Pierce's book and is probably too high.

¹⁵ This assumes a saturation-current density of 120 milliamperes per square centimeter.

solely by q_2^2 . Thus, the RPHP theory will still give qualitatively correct results. Experimental agreement with the RPHP theory within a few decibels, however, is not to be expected.

The noise figure F at synchronism is given by

$$F - 1 = \frac{q_2^2 T_0 \sec^2 \phi_0}{2CT_a} \left| \frac{1}{\delta_1} + \Omega \right|^2, \quad (99A)$$

where q_2^2 is a function of ϵ and is given in Figure 9,

$$\Omega = 4QC + \frac{kT_0}{mv_{0d}^2} \frac{1}{C^2},$$

$$Y = -\frac{1}{\Omega^{3/2}} \tan(B_s C \Omega^{1/2} l_d - \phi_0), \quad (100)$$

$l_d = x_3 - x_2$ = length of drift tube, and δ_1 is given in Figure 12.

In the course of this work the general theory of the diode, including the effect of the thermal-

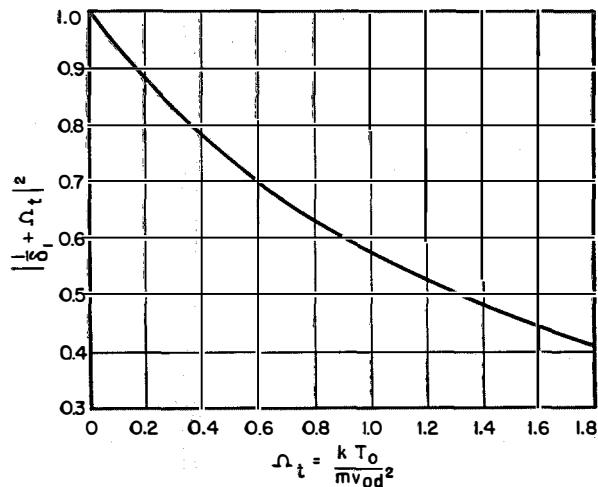


Figure 13—Reduction in noise figure by thermal-velocity spread in a current-modulated electron beam.

velocity spread, has also been derived. An experimental check of this theory would be to measure the diode resistance at very high frequencies.

5. Acknowledgment

The aid of Mrs. Betsy White in performing the computations is gratefully acknowledged.

6. Appendix

For the exact solution of the direct-current equation, we may start with (15)

$$v_0^2 = \mu^2 \left(1 + \log \frac{v_0^2}{\mu^2} \right) + \frac{4}{9} \int_0^y dy \int_0^y \frac{dy}{v_0}. \quad (15)$$

Introducing the new independent variable

$$\rho = \int_0^y \frac{dy}{v_0}, \quad (15A)$$

one obtains

$$\frac{v_0^2}{\mu^2} = 1 + \log \frac{v_0^2}{\mu^2} + \frac{4}{9} \int_0^\rho \rho v_0 d\rho, \quad (15B)$$

and, differentiating this with ρ , it follows that

$$2v_0 v_{0\rho} = 2 \frac{\mu^2}{v_0} v_{0\rho} + \frac{4}{9} \rho v_0, \quad (15C)$$

of which the solution is

$$v_0 + \frac{\mu^2}{v_0} - 2\mu = \frac{1}{9} \rho^2, \quad (15D)$$

and

$$v_0 = \mu + \frac{1}{3} \mu^{3/2} \rho \left(1 + \frac{1}{36} \frac{\rho^2}{\mu^{3/2}} \right)^{1/2} + \frac{1}{18} \rho^2. \quad (15E)$$

The expressions for y and the potential distribution follow from (15E). Thus,

$$\frac{y}{\mu^{3/2}} = P + 4 \left[\left(1 + \frac{P^2}{36} \right)^{3/2} - 1 \right] + \frac{P^3}{54}, \quad (15F)$$

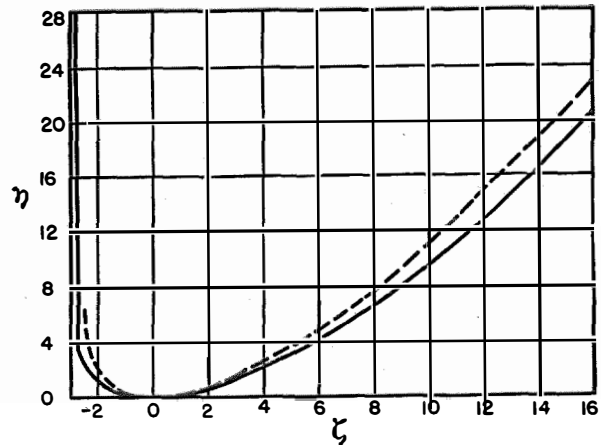


Figure 14—Potential distribution in diode with thermal velocities according to Langmuir (dashed) and Hahn (solid) curves. $\eta = eV/kT_0$ and $\zeta = 1.58y$.

$$\eta = \frac{eV}{kT_0} = \frac{2}{9} \left[\frac{P^2}{2} + \frac{P^4}{72} + \frac{1}{3} \int_0^P P^2 \left(1 + \frac{P^2}{36} \right)^{1/2} dP \right], \quad (15G)$$

$$P = \rho/\mu^{1/2}. \quad (15H)$$

ρ and P vary from $-\infty$ to $+\infty$. As ρ approaches $-\infty$, y approaches the asymptotic value $-4\mu^{3/2} = -1.9$. A curve of η versus $\zeta = 1.58y$ is shown in Figure 14, which is compared to the corresponding curve of Langmuir.

Composite-Dielectric Coaxial Line*

By J. A. KOSTRIZA

Federal Telecommunication Laboratories, Incorporated; Nutley, New Jersey

PROPGATION of electromagnetic waves is investigated in a uniform composite-dielectric coaxial line of fixed ratio between conductor and dielectric radii and of specific dielectric-constant ratio.

The following modes exist: A, a dominant TM_{00} mode; B, a simple TM_{0r} mode; C, a simple TE_{0r} mode; D, a linear combination of E_z and H_z waves, labeled the $(E_z + H_z)_{nr(c, h)}$ mode. Complete fields are specified for A, B, and C; while in D only the $n=1$ type is presented, although a general fundamental equation is derived. General cutoff-frequency equations are derived and values of these are given for TM_{01} , TM_{02} , TE_{01} , $(E_z + H_z)_{1r(c=1, 2; h=1)}$ modes, so that the frequency range of realizability of the TM_{00} mode only is defined. A comparison is made with a homogeneous-dielectric coaxial line as regards the ratios of the cutoff frequencies of the higher-order modes.

A plot of equivalent or effective dielectric constant \mathcal{E}_p for the TM_{00} mode is given for the frequency-parameter range of zero to the second higher-order-mode cutoff. A second graph shows the variation with frequency of the ratio of longitudinal to radial electric fields at the dielectric boundary.

A low-frequency approximation for the dominant mode shows that \mathcal{E}_p is identical to that obtained by electrostatics. An experimental verification of \mathcal{E}_p at one frequency is included for a Pyralin composite coaxial line.

. . .

1. Introduction

A transverse section of a uniform coaxial structure with a composite dielectric \mathcal{E}_1 , \mathcal{E}_2 , is shown in Figure 1. The problem requires the following solutions:

- Field solution for the dominant mode.
- Cutoff frequencies for the lowest simple higher-order symmetrical and unsymmetrical TE and TM

* Condensation of a Master's thesis by Mr. Kostriza on deposit at the Polytechnic Institute of Brooklyn, New York.

modes as well as the unsymmetrical "mixed" TE and TM modes, thus obtaining a limit of operation for A.

C. $\lambda_p/\lambda_0 = 1/\mathcal{E}_p^{1/2}$ for the dominant mode up to the nearest higher-order-mode cutoff.

D. The effective dielectric constant \mathcal{E}_p for the composite line as the dominant mode approaches low frequency and comparison with the value obtained by electrostatics.

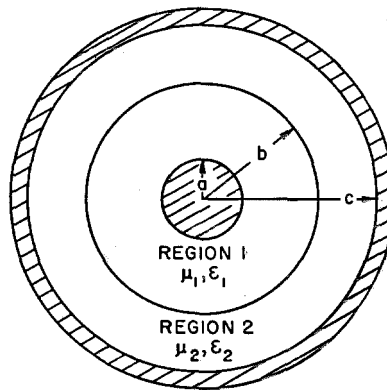


Figure 1—Transverse section of uniform coaxial structure with composite dielectric.

Comparison of C and D sets the error obtained when the composite structure is assumed to sustain the TEM mode.

1.1 ASSUMPTIONS

- Metal boundaries are perfect conductors.
- $\mu_1 = \mu_2 = \mu_0$.
- \mathcal{E}_1 and \mathcal{E}_2 are lossless; $\mathcal{E}_1 > \mathcal{E}_2 = \mathcal{E}_0$.
- The coaxial section is semi-infinite.
- Propagation constant $\gamma_1 = \gamma_2$.

1.2 GENERAL WAVE TYPES IN CYLINDRICAL COORDINATES

The wave equation for the axial component only (E_z or H_z) may be written¹

$$\nabla_t^2 E_z = \left(\frac{\partial^2}{\partial r^2} + \frac{1}{r} \frac{\partial}{\partial r} + \frac{1}{r^2} \frac{\partial^2}{\partial \phi^2} \right) E_z = -k_c^2 E_z, \quad (1)$$

¹W. Smythe, "Static and Dynamic Electricity," McGraw-Hill Book Company, Incorporated, New York, New York; First Edition, 1939; page 167.

where $k_c^2 = \gamma^2 + k^2 = \gamma^2 + \omega^2 \mu \mathcal{E}$, and ∇_t^2 is the two-dimensional transverse Laplacian.

The solution to (1) is assumed to be of the form

$$\left. \begin{aligned} E_z \text{ (for TM waves)} \\ H_z \text{ (for TE waves)} \end{aligned} \right\} = RF_\phi \quad (2)$$

where

$$\left. \begin{aligned} F_\phi &= C \cos n\phi + D \sin n\phi \\ \text{and} \\ R &= AJ_n(k_c r) + BN_n(k_c r), \\ \text{or} \\ R &= AJ_n(k_c r) + BH_n^{(1)}(k_c r); \end{aligned} \right\} (3)$$

and where J , N , and $H^{(1)}$ are Bessel functions to be defined later.

In terms of (2), the transverse components of E and H are given² by

$$\left. \begin{aligned} E_r &= -\frac{1}{k_c^2} \left(\gamma \frac{\partial E_z}{\partial r} + j \frac{\omega \mu}{r} \frac{\partial H_z}{\partial \phi} \right), \\ E_\phi &= \frac{1}{k_c^2} \left(-\frac{\gamma}{r} \frac{\partial E_z}{\partial \phi} + j \omega \mu \frac{\partial H_z}{\partial r} \right), \\ H_r &= \frac{1}{k_c^2} \left(j \frac{\omega \mathcal{E}}{r} \frac{\partial E_z}{\partial \phi} - \gamma \frac{\partial H_z}{\partial r} \right), \\ H_\phi &= -\frac{1}{k_c^2} \left(j \omega \mathcal{E} \frac{\partial E_z}{\partial r} + \frac{\gamma}{r} \frac{\partial H_z}{\partial \phi} \right). \end{aligned} \right\} (4)$$

1.3 CHOICE OF TYPES OF SOLUTION OF WAVE EQUATION

Since the problem contains two distinct regions (see Figure 1), to avoid confusion let k_c be replaced by k_1 for region 1 and by k_2 for region 2. Also, since the propagation constant is assumed to be identical for both regions, then

$$\gamma^2 = k_1^2 - \mathcal{E}_1 \mu_1 \omega^2 = k_2^2 - \mathcal{E}_2 \mu_2 \omega^2. \quad (5)$$

For unattenuated propagation, γ is a pure imaginary: $\gamma = j\beta$, and (5) then becomes

$$\beta^2 = \mathcal{E}_1 \mu_1 \omega^2 - k_1^2 = \mathcal{E}_2 \mu_2 \omega^2 - k_2^2. \quad (6)$$

Equation (6) may be written in terms of phase velocity $v_p = \omega/\beta$. Here,

$$\frac{1}{v_p^2} = \frac{1}{v_1^2} - \left(\frac{k_1}{\omega} \right)^2 = \frac{1}{v_0^2} - \left(\frac{k_2}{\omega} \right)^2, \quad (7)$$

where $v_1^2 = 1/\mathcal{E}_1 \mu_1$ and $v_0^2 = 1/\mathcal{E}_2 \mu_2 = 1/\mathcal{E}_0 \mu_0$. Also, for $\mathcal{E}_1 > \mathcal{E}_2 = \mathcal{E}_0$ and $\mu_1 = \mu_2 = \mu_0$, $v_1 < v_0$.

² S. Ramo and J. R. Whinnery, "Fields and Waves in Modern Radio," John Wiley & Sons, Incorporated, New York, New York; First Edition, 1944: page 326.

In order that the phase velocity be bounded by v_0 and v_1 , i.e., $v_0 > v_p > v_1$, if $k_1^2 > 0$ then from (7), $k_2^2 < 0$. Hence k_2 must be imaginary. For this case, the R functions become

$$\left. \begin{aligned} R \text{ (region 1)} &= A_1 J_n(k_1 r) + B_1 N_n(k_1 r), \\ R \text{ (region 2)} &= A_2 J_n(k_2 r) + B_2 H_n^{(1)}(k_2 r). \end{aligned} \right\} (8)$$

If $k_1^2 > 0$ and $k_2^2 > 0$, then $v_p > v_0 > v_1$. Here the R functions may consist of J_n and N_n :

$$\left. \begin{aligned} R_1 &= A_1 J_n(k_1 r) + B_1 N_n(k_1 r), \\ R_2 &= A_2 J_n(k_2 r) + B_2 N_n(k_2 r). \end{aligned} \right\} (9)$$

In (8) and (9), J_n is a Bessel function³ of the first kind, of order n ; N is the Neumann function, of order n ; and H is the Hankel function, of order n . The Hankel function replaces the Neumann function for imaginary arguments only because of the availability of tabulations.

2. Dominant Mode, $TM_{nr} = TM_{00}$

The boundary and continuity conditions imposed are $B_{n_1} = B_{n_2}$, $D_{n_1} = D_{n_2}$, $H_{t_1} = H_{t_2}$, $E_{t_1} = E_{t_2}$, and E_t (metal) = 0.

2.1 DETERMINANTAL EQUATION

For angular symmetry, $n=0$ in (3) and $F_\phi = 1$. Using subscripts to differentiate regions 1 and 2 as in (5), and with $k_1 = k_1 > 0$ and $k_2 = jk_0$ with $k_0 > 0$, equations (8) apply with zeroth-order functions.

If (4) are applied and the above boundary conditions are met, the following set of relationships is obtained:

$$\left. \begin{aligned} A_1 J_0(k_1 a) + B_1 N_0(k_1 a) &= 0, \\ A_2 J_0(jk_0 c) + B_2 H_0^{(1)}(jk_0 c) &= 0, \\ A_1 J_0(k_1 b) + B_1 N_0(k_1 b) \\ &= A_2 J_0(jk_0 b) + B_2 H_0^{(1)}(jk_0 b), \\ \frac{\mathcal{E}_1}{k_1} [A_1 J_1(k_1 b) + B_1 N_1(k_1 b)] \\ &= \frac{\mathcal{E}_2}{jk_0} [A_2 J_1(jk_0 b) + B_2 H_1^{(1)}(jk_0 b)]. \end{aligned} \right\} (10)$$

In order that a solution of (10) may exist, the determinant of the coefficients A_1 , B_1 , A_2 , and B_2 must be zero.⁴ A little manipulation results in

³ E. Jahnke and F. Emde, "Tables of Functions," Dover Publications, New York, New York; Fourth Edition, 1943: pages 130-133.

⁴ M. Bocher, "Introduction to Higher Algebra," The Macmillan Company, New York, New York; First Edition, 1907: chapter 3.

$$\frac{J_1(mx)N_0(x) - J_0(x)N_1(mx)}{J_0(x)N_0(mx) - J_0(mx)N_0(x)} \cdot \frac{1}{x} = \frac{\mathcal{E}_2}{\mathcal{E}_1} \cdot \frac{1}{jy} \cdot \frac{J_1(jmy)H_0^{(1)}(jmy) - J_0(jmy)H_1^{(1)}(jmy)}{J_0(jmy)H_0^{(1)}(jmy) - J_0(jmy)H_0^{(1)}(jmy)} \quad (11)$$

This equation includes the following substitutions:⁵ $x = k_1 a$, $y = k_0 a$, $mny = k_0 c$, $mx = k_1 b$, $my = k_0 b$, where $m = b/a$ and $n = c/b$.

Equation (11) will be denoted as the "determinantal equation," the solution of which is required for specific values of m , n , and $\mathcal{E}_2/\mathcal{E}_1$. In this paper, results are given for $m=2$, $n=1.25$, and $\mathcal{E}_2/\mathcal{E}_1=1/4$; the dimensions corresponding to an air-filled coaxial line of 54.9-ohm characteristic impedance.

In addition to (11), x and y must satisfy a second relationship, obtained from (6):

$$\left. \begin{aligned} y^2 &= (A\omega + x)(A\omega - x), \\ A^2 &= a^2(\mathcal{E}_1\mu_1 - \mathcal{E}_2\mu_2). \end{aligned} \right\} (12)$$

Figure 2 gives a plot of x , y , and βa for incremental values of $A\omega$ ranging from 0.001 to 1.9225.

2.2 FIELD COMPONENTS, TM_{00}

When A_2 , B_1 , and B_2 are expressed in terms of A_1 (see (10)), the field components take the following form.

$$\left. \begin{aligned} \text{In region 1, where } a \leq r \leq b, \\ E_{z_1} &= A_0 \cdot [J_0(k_1 r)N_0(k_1 a) - J_0(k_1 a)N_0(k_1 r)], \\ E_{r_1} &= \frac{\gamma}{k_1} \cdot A_0 [J_1(k_1 r)N_0(k_1 a) - J_0(k_1 a)N_1(k_1 r)], \\ A_0 &= A_1/N_0(k_1 a), \\ E_{r_1}/H_{\phi_1} &= \gamma/j\omega\mathcal{E}_1 = \beta/\omega\mathcal{E}_1. \end{aligned} \right\} (13)$$

⁵L. Pincherle, "Electromagnetic Waves in Metal Tubes Filled Longitudinally with Two Dielectrics," *Physical Review*, volume 66, pages 118-130; September 1 and 15, 1944.

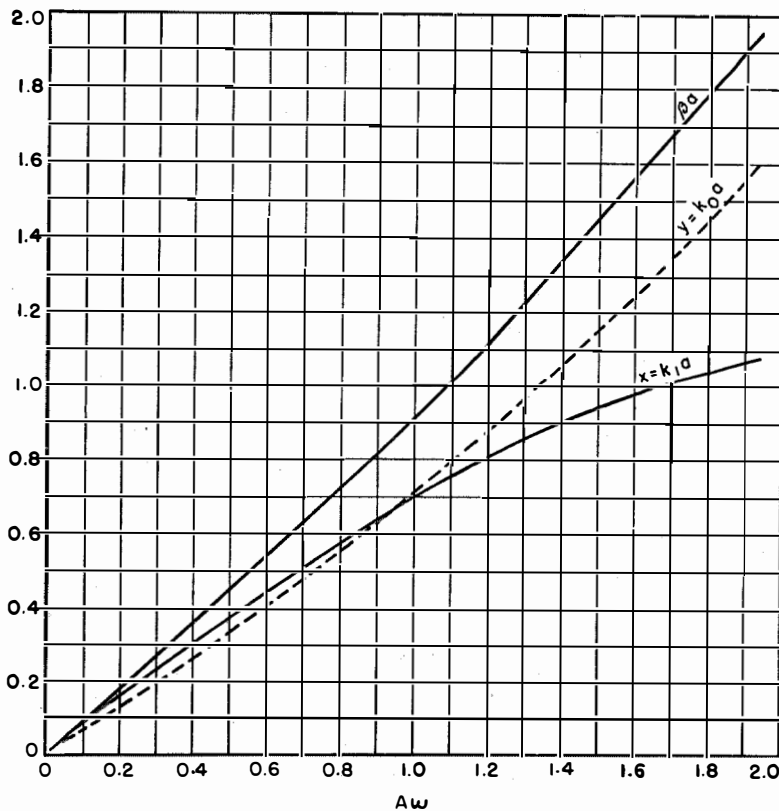


Figure 2—Values of x and y as solutions of determinantal equation (11). Phase constant βa is shown for $m=2$, $n=1.25$, and $\mathcal{E}_2/\mathcal{E}_1=1/4$.

In region 2, where $b \leq r \leq c$,

$$\left. \begin{aligned} E_{z_2} &= A_0 F \cdot [J_0(jk_0 c)H_0^{(1)}(jk_0 r) - J_0(jk_0 r)H_0^{(1)}(jk_0 c)], \\ F &= \frac{J_0(k_1 a)N_0(k_1 b) - J_0(k_1 b)N_0(k_1 a)}{J_0(jk_0 b)H_0^{(1)}(jk_0 c) - J_0(jk_0 c)H_0^{(1)}(jk_0 b)}, \\ E_{r_2} &= \frac{\gamma}{jk_0} \cdot A_0 F \cdot [J_0(jk_0 c)H_1^{(1)}(jk_0 r) - J_1(jk_0 r)H_0^{(1)}(jk_0 c)], \\ E_{r_2}/H_{\phi_2} &= \gamma/j\omega\mathcal{E}_2 = \beta/\omega\mathcal{E}_2. \end{aligned} \right\} (14)$$

Figure 3 shows a plot of γ/k , $\omega\mathcal{E}/k$, and $\gamma/j\omega\mathcal{E}$ versus $A\omega$ for each region.

2.3 RATIO OF E_z TO E_r AT BOUNDARY RADIUS b

From (13),

$$\frac{E_{z_1}(b)}{E_{r_1}(b)} = \frac{1}{\gamma k_1} \cdot \frac{J_0(k_1 b)N_0(k_1 a) - J_0(k_1 a)N_0(k_1 b)}{J_1(k_1 b)N_0(k_1 a) - J_0(k_1 a)N_1(k_1 b)} \quad (15)$$

The magnitude of (15) versus $A\omega$ is shown in Figure 4. For ready reference, Figure 5 shows frequency versus $A\omega$.

From continuity of tangential electric fields and normal displacement flux density it follows that

$$E_{z_1}(b)/E_{r_1}(b) = (\epsilon_1/\epsilon_2)[E_{z_2}(b)/E_{r_2}(b)].$$

3. Cutoff of Higher-Order TM Modes

3.1 SYMMETRICAL CASE, TM_{0r} MODES ($n=0, r=1,2,\dots$)

Only the first two higher-order modes are evaluated. As in the TM_{00} case, to obtain angular symmetry, $n=0$, and F_ϕ is unity in (3).

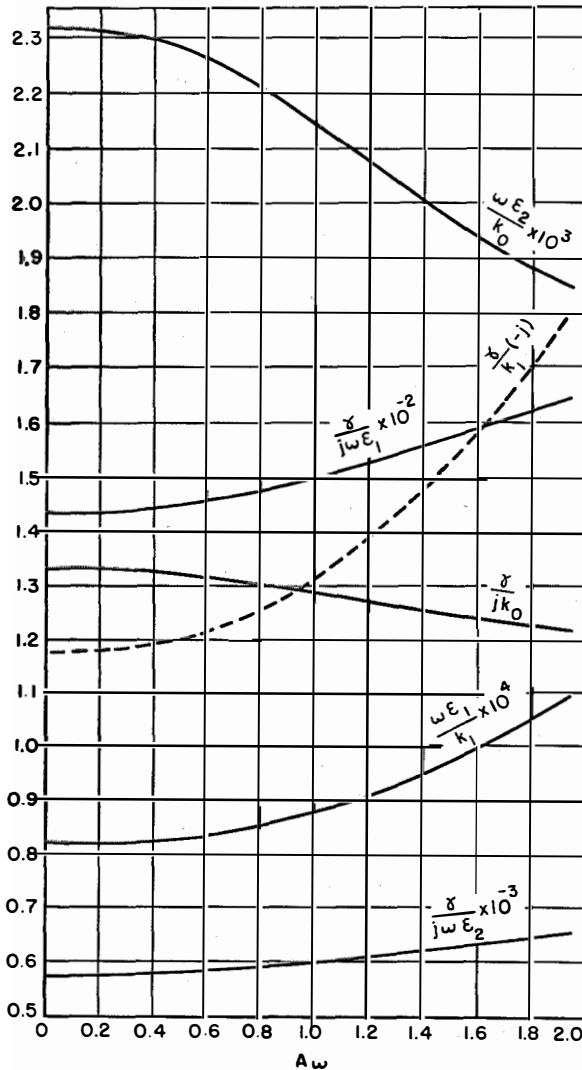


Figure 3—Values of TM_{00} coefficients in field equations (13) and (14).

Since $v_p > v_0 > v_1$, then $k_1^2 > 0$ and $k_2^2 > 0$ holds for this case so that the R functions are given by (9).

Applying (4) with appropriate boundary conditions, a set of relationships similar to (10) is obtained with the substitution of k_2 for jk_0 , N_0

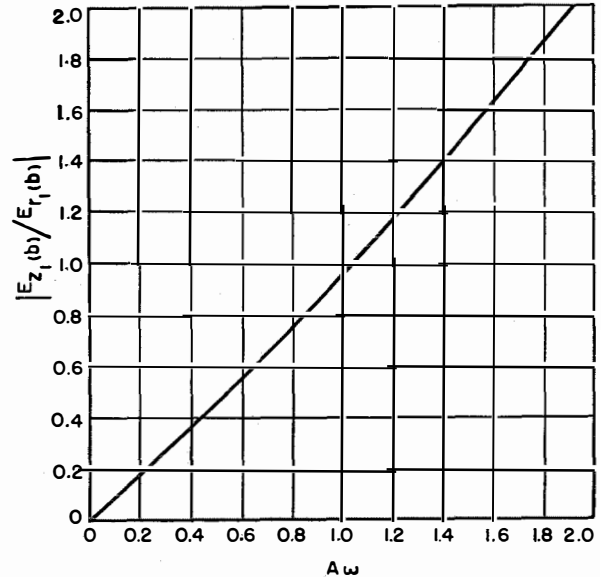


Figure 4—Magnitude of the ratio $E_{z_1}(b)$ to $E_{r_1}(b)$ for TM_{00} mode.

for $H_0^{(1)}$, and N_1 for $H_1^{(1)}$. As before, the determinant is set equal to zero. The resulting "determinantal equation" is

$$\frac{J_1(mx)N_0(x) - J_0(x)N_1(mx)}{J_0(x)N_0(mx) - J_0(mx)N_0(x)} \cdot \frac{1}{x} = \frac{\epsilon_2}{\epsilon_1} \cdot \frac{1}{y} \cdot \frac{J_1(my)N_0(mny) - J_0(mny)N_1(my)}{J_0(mny)N_0(my) - J_0(my)N_0(mny)}, \quad (16)$$

with m , n , and x as before, and with $y = k_2a$, $my = k_2b$, and $mny = k_2c$.

At cutoff, $\gamma = 0$ and from (5),

$$\left. \begin{aligned} y &= px \\ \text{where } p &= (\epsilon_2\mu_2/\epsilon_1\mu_1)^{1/2}. \end{aligned} \right\} (17)$$

Equation (16) may now be written as a function of x only:

$$\frac{J_1(mx)N_0(x) - J_0(x)N_1(mx)}{J_0(x)N_0(mx) - J_0(mx)N_0(x)} = \frac{\epsilon_2}{\epsilon_1} \cdot \frac{1}{p} \cdot \frac{J_1(mp x)N_0(mn p x) - J_0(mn p x)N_1(mp x)}{J_0(mn p x)N_0(mp x) - J_0(mp x)N_0(mn p x)}, \quad (18)$$

This is the cutoff-frequency equation for TM_{0r} modes.

A graphical solution of (18) with $m = 2$, $n = 1.25$, $p = 0.5$ yields the roots

$$x^i = 2.220 \quad \text{and} \quad x^{ii} = 4.879,$$

giving the first two cutoff frequencies.

3.1.1 TM_{0r} Field Components

Following the procedure of Section 2, the field components take the following form.

In region 1 where $a \leq r \leq b$,

$$\left. \begin{aligned} E_{z_1} &= A_0 [J_0(k_1 r) N_0(k_1 a) - J_0(k_1 a) N_0(k_1 r)], \\ E_{r_1} &= (\gamma/k_1) \cdot A_0 \cdot [J_1(k_1 r) N_0(k_1 a) - J_0(k_1 a) N_1(k_1 r)], \\ E_{r_1}/H_{\phi_1} &= -j\gamma/\omega\epsilon_1, \\ A_0 &= A_1/N_0(k_1 a). \end{aligned} \right\} (19)$$

In region 2 where $b \leq r \leq c$,

$$\left. \begin{aligned} E_{z_2} &= A_0 F \cdot [J_0(k_2 c) N_0(k_2 r) - J_0(k_2 r) N_0(k_2 c)], \\ E_{r_2} &= (\gamma/k_2) A_0 F \cdot [J_0(k_2 c) N_1(k_2 r) - J_1(k_2 r) N_0(k_2 c)], \\ E_{r_2}/H_{\phi_2} &= -j\gamma/\omega\epsilon_2, \\ F &= \frac{J_0(k_1 a) N_0(k_1 b) - J_0(k_1 b) N_0(k_1 a)}{J_0(k_2 b) N_0(k_2 c) - J_0(k_2 c) N_0(k_2 b)}. \end{aligned} \right\} (20)$$

3.2 CIRCULARLY UNSYMMETRIC CASE, $n \neq 0$

If the R functions are assumed to be given by (9) and F_ϕ by (3), then (4) yields a set of expressions for the field components in each region. It is found when boundary conditions are applied that the result leads either to a trivial solution or to a violation of the basic assumption $\epsilon_1 > \epsilon_2$ and $\mu_1 = \mu_2 = \mu_0$. Hence, it is concluded that circularly unsymmetric TM modes cannot exist for $\epsilon_1 > \epsilon_2$ and $\mu_1 = \mu_2 = \mu_0$.

4. Cutoff of Higher-Order TE Modes

4.1 SYMMETRIC CASE, TE_{0r} MODES ($n=0, r=1, 2, \dots$)

Only the first ($r=1$) higher-order mode is evaluated, although a general formula is derived.

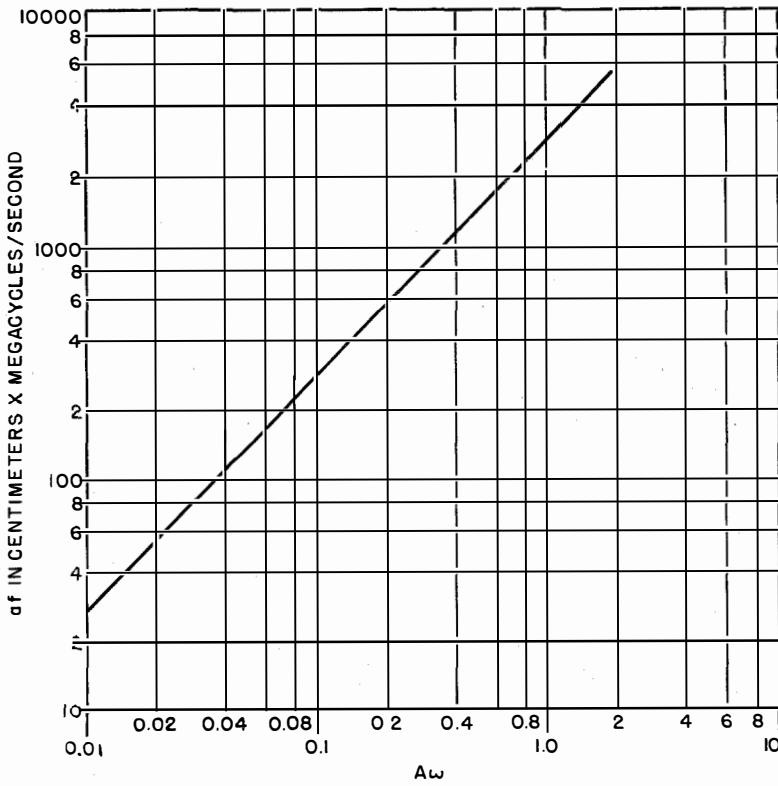


Figure 5—Conversion of $A\omega$ to af in centimeters \times megacycles per second.

H_{z_1} and H_{z_2} are given by (9) with $F_\phi = C =$ unity. Application of (4) with appropriate boundary conditions results in

$$\left. \begin{aligned} A_1 J_0(k_1 b) + B_1 N_0(k_1 b) &= A_2 J_0(k_2 b) + B_2 N_0(k_2 b), \\ A_1 J_0'(k_1 a) + B_1 N_0'(k_1 a) &= 0, \\ A_2 J_0'(k_2 c) + B_2 N_0'(k_2 c) &= 0, \\ (\mu_1/k_1) [A_1 J_0'(k_1 b) + B_1 N_0'(k_1 b)] &= (\mu_2/k_2) [A_2 J_0'(k_2 b) + B_2 N_0'(k_2 b)]. \end{aligned} \right\} (21)$$

The determinant of the coefficients of $A_1, B_1, A_2,$ and B_2 is set to zero, with $J_0' = -J_1$ and $N_0' = -N_1$, giving

$$\frac{\mu_1}{k_1} \frac{J_1(k_1 a) N_1(k_1 b) - N_1(k_1 a) J_1(k_1 b)}{J_1(k_1 a) N_0(k_1 b) - N_1(k_1 a) J_0(k_1 b)} = \frac{\mu_2}{k_2} \frac{N_1(k_2 b) J_1(k_2 c) - J_1(k_2 b) N_1(k_2 c)}{N_0(k_2 b) J_1(k_2 c) - J_0(k_2 b) N_1(k_2 c)}. \quad (22)$$

Introducing $m, n, x, y,$ etc., as in Section 3, results in (23), the fundamental determinantal

equation to be satisfied for TE_{0r} modes.

$$\frac{\mu_1}{k_1} \frac{J_1(x)N_1(mx) - J_1(mx)N_1(x)}{N_0(mx)J_1(x) - N_1(x)J_0(mx)} = \frac{\mu_2}{k_2} \frac{N_1(my)J_1(mny) - N_1(mny)J_1(my)}{J_1(mny)N_0(my) - J_0(my)N_1(mny)} \quad (23)$$

At cutoff $\gamma=0$, and using (5),

$$k_1/k_2 = x/y, \quad y = px, \quad p = (\mathcal{E}_2\mu_2/\mathcal{E}_1\mu_1)^{1/2}. \quad (24)$$

With (24) in mind, the cutoff-frequency equation is

$$\frac{J_1(x)N_1(mx) - J_1(mx)N_1(x)}{N_0(mx)J_1(x) - N_1(x)J_0(mx)} = \frac{\mu_2}{\mu_1} \frac{1}{p} \frac{N_1(mpx)J_1(mnpx) - N_1(mnpx)J_1(mpx)}{J_1(mnpx)N_0(mpx) - J_0(mpx)N_1(mnpx)}. \quad (25)$$

A graphical solution of (25) with $m=2$, $n=1.25$, and $p=0.5$, yields the first root at $x^i=2.31$.

4.1.1 TE_{0r} Field Components

In region 1, where $a \leq r \leq b$,

$$\left. \begin{aligned} H_{z_1} &= A_0 \cdot [J_0(k_1r)N_1(k_1a) \\ &\quad - J_1(k_1a)N_0(k_1r)], \\ E_{\phi_1} &= -j(\omega\mu_1/k_1)A_0 \cdot [J_1(k_1r)N_1(k_1a) \\ &\quad - J_1(k_1a)N_1(k_1r)], \\ -E_{\phi_1}/H_{r_1} &= j\omega\mu_1/\gamma; \\ A_0 &= A_1/N_1(k_1a). \end{aligned} \right\} (26)$$

In region 2, where $b \leq r \leq c$,

$$\left. \begin{aligned} H_{z_2} &= A_0F \cdot [J_0(k_2r)N_1(k_2c) \\ &\quad - J_1(k_2c)N_0(k_2r)], \\ E_{\phi_2} &= -j(\omega\mu_2/k_2)A_0F \cdot [J_1(k_2r)N_1(k_2c) \\ &\quad - J_1(k_2c)N_1(k_2r)], \\ -E_{\phi_2}/H_{r_2} &= j\omega\mu_2/\gamma, \\ F &= \frac{J_0(k_1b)N_1(k_1a) - J_1(k_1a)N_0(k_1b)}{J_0(k_2b)N_1(k_2c) - J_1(k_2c)N_0(k_2b)}. \end{aligned} \right\} (27)$$

4.2 CIRCULARLY UNSYMMETRIC CASE, $n \neq 0$

As in the circularly unsymmetric TM case, proper satisfaction of boundary conditions leads to the untenable requirement that $\mathcal{E}_1\mu_1 = \mathcal{E}_2\mu_2$. The conclusion is therefore reached that simple TE modes for $n \neq 0$ cannot exist for $\mathcal{E}_1 > \mathcal{E}_2$ and $\mu_1 = \mu_2 = \mu_0$.

5. Mixed Modes, $(E_z + H_z)_{nr}$ Modes

In the previous sections, certain symmetrical classes of solutions were found that completely satisfy the boundary conditions of the problem. These solutions may be said to be patterned after the homogeneous-regions classes of symmetrical modes, the TE and TM , where each in itself is found sufficient to provide complete satisfaction of boundary conditions. These symmetrical modes may be termed "simple" modes.⁵

"Simple" unsymmetrical modes are nonexistent in the composite coaxial line, as pointed out in Sections 3.2 and 4.2.

In nonhomogeneous regions, to satisfy the boundary conditions, the general solution for unsymmetrical modes requires simultaneous existence of E_z and H_z , or a linear combination of all solutions obtained from the wave equation. A step-by-step exposition becomes a little inelegant, therefore only a brief outline is included.

5.1 FUNDAMENTAL EQUATION

Application is made of the general equations (2) and (3).

5.1.1 For TE Modes

$$\begin{aligned} H_z &= [A_0J_n(kr) + B_0N_n(kr)] \\ &\quad \cdot [C \cos n\phi + D \sin n\phi] \\ &= [AJ_n(kr) + BN_n(kr)] \cdot \cos(n\phi - \phi_i). \end{aligned}$$

General	In Region 1	In Region 2	} (28)
k, μ	k_1, μ_1	k_2, μ_2	
A, B	A_1, B_1	A_2, B_2	
ϕ_i	$\phi_1 = 0$	ϕ_2	

where arbitrarily $\phi_1=0$ by selection of initial reference. Also, it is implicitly assumed that the periodicity in the angle ϕ is the same for both regions, identified by the single n .

5.1.2 For TM Modes

$$\begin{aligned} E_z &= [AJ_n(kr) + BN_n(kr)] \cdot \cos(n\phi - \phi_i) \end{aligned}$$

General	In Region 1	In Region 2	} (29)
k, \mathcal{E}	k_1, \mathcal{E}_1	k_2, \mathcal{E}_2	
A, B	A', B'	A^2, B^2	
ϕ^i	ϕ'	ϕ^2	

In the suppressed factor $\exp(j\omega t - \gamma z)$, in view of (5), the following is assumed to be true:

$$\begin{aligned} k_1(TE) &= k_1(TM) = k_1(\omega) = k_1, \\ k_2(TE) &= k_2(TM) = k_2(\omega) = k_2. \end{aligned}$$

The continuity of tangential components at the boundary between unlike dielectrics requires that

$$\Sigma E_{z_1}(b) = \Sigma E_{z_2}(b) \quad (30.1)$$

$$\Sigma E_{\phi_1}(b) = \Sigma E_{\phi_2}(b) \quad (30.2)$$

$$\Sigma H_{z_1}(b) = \Sigma H_{z_2}(b) \quad (30.3)$$

$$\Sigma H_{\phi_1}(b) = \Sigma H_{\phi_2}(b) \quad (30.4)$$

From (30.3), $\phi_2 = 0$ (simplest value). From (30.1), $\phi' = \phi^2 = \phi_0$; and again from (30.4), if ϕ_0 is to be independent of ϕ , then $\phi_0 = \pi/2$, again choosing the simplest value.

There then remain eight constants $(A, B)_i$ and $(A, B)^i$, where $i = 1, 2$ in (28) and (29). Applying (30) yields four relations. Satisfying the requirements of $E_t = 0$ at the metal walls gives four more. The solution of this eighth-order determinant may be expressed as:

$$\left(\frac{\gamma n}{b}\right)^2 = \frac{-\omega^2}{(1/k_1^2 - 1/k_2^2)^2} X Y, \quad (31)$$

where

$$X = \frac{\mu_1}{k_1} \cdot \frac{N'(k_1 a) J'(k_1 b) - J'(k_1 a) N'(k_1 b)}{N'(k_1 a) J(k_1 b) - J'(k_1 a) N(k_1 b)} - \frac{\mu_2}{k_2} \cdot \frac{J'(k_2 b) N'(k_2 c) - N'(k_2 b) J'(k_2 c)}{J(k_2 b) N'(k_2 c) - N(k_2 b) J'(k_2 c)}, \quad (32)$$

$$Y = \frac{\mathcal{E}_1}{k_1} \cdot \frac{N(k_1 a) J'(k_1 b) - J(k_1 a) N'(k_1 b)}{N(k_1 a) J(k_1 b) - J(k_1 a) N(k_1 b)} - \frac{\mathcal{E}_2}{k_2} \cdot \frac{J'(k_2 b) N(k_2 c) - N'(k_2 b) J(k_2 c)}{J(k_2 b) N(k_2 c) - N(k_2 b) J(k_2 c)}, \quad (33)$$

and the order n of the Bessel functions has been suppressed. Equation (31) is valid for all n exclusive of $n = 0$.

5.2 CUTOFF FOR $(E_z + H_z)_{nr}$ MODES

With $\gamma = 0$ in (31), X and Y must be zero, either jointly or independently. We cannot allow k_1 to equal k_2 , for then $\mathcal{E}_1 \mu_1 = \mathcal{E}_2 \mu_2$. Therefore, two separate cutoff equations are had in (32) and (33).

From its complexity, (32) may be said to be analogous to a TE -derived system or more simply an e mode. Similarly, (33) may be called a TM -derived or an h mode. The complete mode structure, then, is rather inadequately labeled $(E_z + H_z)_{nr}$, for to each n there is a doubly infinite set of r 's, one set for the e mode and a second set for the h mode. It seems more appropriate, therefore, to label this complex mode structure as $(E_z + H_z)_{nr(e, h)}$.

5.3 CUTOFF VALUES FOR $(E_z + H_z)_{1r}$ MODES

Equations (32) and (33) were solved graphically for $m = 2$, $n = 1.25$, $p = 0.5$, and $Z_1'(x) = Z_0(x) - (1/x)Z_1(x)$. The first two solutions to (32) are $x^i = 0.775$, and $x^{ii} = 2.45$. In terms of the frequency parameter $A\omega$, the lowest cutoff occurs at $A\omega^i = 0.671$. The first root of (33) is $x^i = 2.32$, or $A\omega^i = 2.01$.

5.4 COMPARISON OF HIGHER-ORDER CUTOFFS IN SOLID VERSUS COMPOSITE LINES

For convenience, let $a = 1$, and let c/a for the solid line be 2.5. Also, from (38), if $\omega \rightarrow 0$ then $\mathcal{E}(\text{solid}) = \mathcal{E}(\text{composite}) = 2.31$.

Ratios k_c or f_c (solid) are

TE_{11}	TM_{01}	TE_{01}	TM_{11}
1	3.54	3.67	3.67

Ratios k^i or f^i (composite) are

$(E_z + H_z)_{11(e=1)}$	TM_{01}	TE_{01}	$(E_z + H_z)_{11(h=1)}$
1	2.87	2.98	2.99

It is interesting to compare the lowest f^i (composite) with the lowest f_c (solid). These are, respectively, the $e = 1$ -mode and the TE_{11} -mode cutoff values. The ratio is

$$\begin{aligned} f^i/f_c &= (k_1^i/k_c) [\mathcal{E}(\text{solid})/\mathcal{E}_1]^{1/2} \\ &= (0.775/0.558) 0.76 = 1 \end{aligned}$$

5.5 FIELD COMPONENTS FOR $(E_z + H_z)_{1r(e, h)}$ MODES

In TE -mode region 1, where $a \leq r \leq b$,

$$H_{z1} = A_1 [J_1(k_1 r) - N_1(k_1 r) J_1'(k_1 a) / N_1'(k_1 a)] \cdot \cos \phi, \quad (34)$$

where E_r , E_ϕ , H_r , and H_ϕ are given by (4).

In TE -mode region 2, where $b \leq r \leq c$, apply (34) with $A_1 \rightarrow A_1 H$, $k_1 \rightarrow k_2$, $a \rightarrow c$, and $\mu_1 \rightarrow \mu_2$, where

$$H = \frac{N_1'(k_1 a) J_1(k_1 b) - J_1'(k_1 a) N_1(k_1 b)}{J_1(k_2 b) N_1'(k_2 c) - N_1(k_2 b) J_1'(k_2 c)} \cdot \frac{N_1'(k_2 c)}{N_1'(k_1 a)}$$

In TM -mode region 1, where $a \leq r \leq b$,

$$E_{z1} = A_1 \pi [J_1(k_1 r) - N_1(k_1 r) J_1(k_1 a) / N_1(k_1 a)] \cdot \sin \phi, \quad (35)$$

where E_ϕ , E_r , H_r , and H_ϕ are given by (4), and

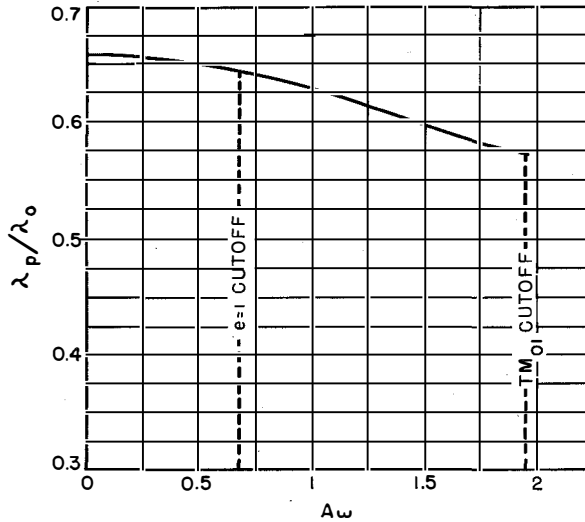


Figure 6— λ_p/λ_0 plotted against $A\omega$.

where

$$\pi = \frac{j\omega\mu_1 \left[\frac{N_1'(k_1a)J_1'(k_1b) - J_1'(k_1a)N_1'(k_1b)}{N_1'(k_1a)} \right] - j\omega\mu_2 H \left[\frac{J_1'(k_2b)N_1'(k_2c) - N_1'(k_2b)J_1'(k_2c)}{N_1'(k_2c)} \right]}{\frac{\gamma n}{b} \left[\frac{N_1(k_1a)J_1(k_1b) - J_1(k_1a)N_1(k_1b)}{N_1(k_1a)} \right] \cdot \left[\frac{1}{k_1^2} - \frac{1}{k_2^2} \right]}$$

In TM -mode region 2, where $b \leq r \leq c$, apply (35) with $\pi A_1 \rightarrow A_1 K \pi$, $k_1 \rightarrow k_2$, $a \rightarrow c$, and $\epsilon_1 \rightarrow \epsilon_2$, where

$$K = \frac{N_1(k_1a)J_1(k_1b) - J_1(k_1a)N_1(k_1b)}{J_1(k_2b)N_1(k_2c) - N_1(k_2b)J_1(k_2c)} \cdot \frac{N_1(k_2c)}{N_1(k_1a)}$$

6. Equivalent Dielectric Constant for TM_{00} Mode

The equivalent dielectric constant ϵ_p for the composite line, in analogy with a homogeneous-dielectric coaxial line is defined as

$$\lambda_p/\lambda_0 = 1/\epsilon_p^{1/2}, \quad (36)$$

where λ_p is the phase wavelength in the composite dielectric and λ_0 is the free-space wavelength. The various constants of the problem entering into (36) may be interrelated to give

$$\lambda_p/\lambda_0 = A\omega/3^{1/2}(\beta a) = 1/\epsilon_p^{1/2} \quad (37)$$

where $A = a/3^{1/2} \times 10^{10}$ seconds for the problem under consideration, with a in centimeters. A plot of λ_p/λ_0 versus $A\omega$ is shown in Figure 6.

The usable frequency limit for the TM_{00} mode alone is governed by the $(E_z + H_z)_{1,r(\epsilon=1)}$ cutoff, which was found to be at $A\omega^2 = 0.671$. As already pointed out, this is analogous to the solid-

coaxial-line behavior, where a nonsymmetrical (TE_{11}) mode is the governing factor.

Figure 6 indicates that for the assumed values of m , n , and p , the factor ϵ_p is an increasing function of frequency. At the first higher-order-mode cutoff, it increases by about 5 percent, whereas at the second cutoff it has increased by 33 percent above its low-frequency value.

7. Analytical Evaluation of ϵ_p for Composite Line as $\omega \rightarrow 0$

Equation (37) may be recast⁶ into

$$\epsilon_p = \left(\frac{\epsilon_1}{\epsilon_2} - 1 \right) \left(\frac{\beta a}{A\omega} \right)^2_{\omega \rightarrow 0} \quad (38)$$

Now,

$$\left(\frac{\beta a}{A\omega} \right)_{\omega \rightarrow 0} = \frac{\epsilon_1 \mu_1}{\epsilon_1 \mu_1 - \epsilon_2 \mu_2} - \left(\frac{x = k_1 a}{A\omega} \right)^2_{\omega \rightarrow 0} \quad (39)$$

It may be shown that

$$\left(\frac{x}{A\omega} \right)_{\omega \rightarrow 0}^2 = \frac{\epsilon_1}{\epsilon_2} \ln n / \left(\frac{\epsilon_1}{\epsilon_2} \ln n + \ln m \right). \quad (40)$$

Using (40), and (39) in (38),

$$\epsilon_p = \frac{(\epsilon_1/\epsilon_2) \ln mn}{(\epsilon_1/\epsilon_2) \ln n + \ln m}. \quad (41)$$

This is the low-frequency equivalent of the composite-line dielectric constant. It is identical to that derived on an electrostatic basis.

8. Experimental Verification of ϵ_p for a Composite Line

Actually, the measurement of equivalent propagation constant and equivalent dielectric constant of a composite coaxial section was performed before the theoretical Sections 1 through 7 were developed. The dielectric selected was a sample of Pyralin. At the time the experimental work was done, the radio-frequency characteristics of this dielectric were unknown to the writer; therefore γ (complex) and ϵ (complex) of Pyralin were measured.

⁶ Derivations of (38), (39), and (40) are too lengthy to be given here; for particulars, refer to thesis.

Two methods were used, the Q method,⁷ and the impedance method with use of existing charts.⁸ In each method, the test line consisted of a nominal 50-ohm, $\frac{5}{8}$ -inch- (1.59-centimeter-) outside-diameter coaxial line, a calibrated standing-wave detector, and the test sample. At 2200 megacycles per second, the results are given in Table 1. An "average" value of $\mathcal{E}^*/\mathcal{E}_0$ was used.

TABLE 1

MEASUREMENTS OF SOLID-PYRALIN-DIELECTRIC LINE

	Q Method	Impedance Method
γ per Centimeter	0.905/84°30'	0.905/83°45'
$\mathcal{E}^*/\mathcal{E}_0$	3.93/-11°	3.93/-12°30'
$\tan \delta$	0.194	0.222

Exactly the same procedure was followed for the Pyralin-and-air composite line. At 2200 megacycles, the results given in Table 2 were obtained.

TABLE 2

MEASUREMENTS OF COMPOSITE PYRALIN-AND-AIR LINE

	Q Method	Impedance Method
γ per Centimeter	0.677/87°15'	0.680/87°40'
$\mathcal{E}_p^*/\mathcal{E}_0$	2.20/-5°30'	2.22/-4°40'

The composite line had the following dimensions:

$a=0.3175$ centimeter, $b=0.579$ centimeter, $c=0.7125$ centimeter, $m=1.824$, and $n=1.23$.

The following information for Pyralin has been given:⁹

$f=2.2 \times 10^9$, $\mathcal{E}'=3.9$, and $\tan \delta=0.16$.

The measured values were:

$f=2.2 \times 10^9$, $\mathcal{E}'=3.93$, and $\tan \delta$ (average) = 0.208.

⁷ J. C. Slater, "Microwave Transmission," McGraw-Hill Book Company, Incorporated, New York, New York; First Edition, 1942: page 35.

⁸ Roberts and Van Hippel, "New Method for Measurement of Dielectric Constant and Loss in the Range of Centimeter Waves," Massachusetts Institute of Technology, Cambridge, Massachusetts; March, 1941.

⁹ "Tables of Dielectric Materials," Report V, Laboratory for Insulation Research, Massachusetts Institute of Technology, Cambridge, Massachusetts; February, 1944.

Which data are the more reliable is impossible to determine, although it must be mentioned that precision apparatus was not employed, nor was the standing-wave-detector compensated for the presence of the slot. The discrepancy, however, is quite small.

As regards the composite dielectric, measurements did not take into account the possible presence of any discontinuity susceptance. Further errors could be introduced if a higher-order mode were sustained in the composite line, together with the TM_{00} mode. However, for the dimensions used ($m=1.824$ (≈ 2), $n=1.23$ (≈ 1.25), and $a=0.3175$ centimeters), the cutoff of the lowest higher-order mode occurs at $A\omega^i=0.67$.

From Figure 5, the approximate value of af is 1800 centimeters \times megacycles per second, or $f=5660$ megacycles; almost a 3:1 frequency safety margin as regards actual propagation of the next mode.

The low-frequency approximation of \mathcal{E}_p for the experiment is $2.26/-5^\circ$. From Figure 5, with $af=700$, we have $A\omega=0.26$. Figure 6 shows that this corresponds to a matter of a few percent increase in \mathcal{E}_p , well within the experimental error, so that $\mathcal{E}_p(2200)=\mathcal{E}_p(0)=2.26$. The measured value, $\mathcal{E}_p=2.21$, is then in error by some 3 percent.

9. Conclusions

It has been demonstrated that the composite line may be treated as a homogeneous coaxial structure whose effective dielectric constant is readily computed from electrostatic considerations to within a 5-percent error at the cutoff frequency of the next higher-order mode.

Furthermore, the rather complex equations derived for the cutoff of the first higher-order mode need not be used since its cutoff frequency is identical to the homogeneous-line TE_{11} -mode cutoff when the dielectric constant of the homogeneous line is the electrostatic equivalent of the composite line.

It has been shown that even for moderately lossy dielectrics and for a limited frequency range, the composite line may be replaced by an equivalent homogeneous coaxial line sustaining a TEM mode.

New Linear Passive Nonreciprocal Microwave Circuit Component*

By LADISLAS GOLDSTEIN† and M. A. LAMPERT

Federal Telecommunication Laboratories, Incorporated; Nutley, New Jersey

STUDIES of propagation of guided microwave through an anisotropic electron gas have been in progress at Federal Telecommunication Laboratories since the summer of 1950. In the course of these studies, particular attention was paid to the case where the anisotropy was produced by a uniform constant magnetic field permeating the electron-gaseous medium in a direction parallel to the waveguide axis.

The study of propagation of electromagnetic waves through a dielectric medium made anisotropic in this way goes back quite far in the history of electromagnetism. Faraday, by sending plane-polarized light waves through a transparent medium of reasonably high refractive index with a magnetic field across it in the direction of propagation, discovered the effect bearing his name, which consists of rotation of the polarization plane of the light waves. Furthermore, he noted that the sense of rotation is the same for the reflected wave as for the incident wave. Thus, for example, a fixed observer noting a clockwise rotation of the incident wave would note an equal additional clockwise rotation of the reflected wave on its return

through the medium. If the Faraday experiment is translated into radio and microwave frequencies, a behavior may be observed that produces nonreciprocity when the signal traverses the magneto-anisotropic medium between input and output terminals. Indeed, the failure of the various reciprocity theorems when electrons in a magnetic field are involved is a fact long familiar to students of electromagnetic phenomena in the ionosphere.

We have performed Faraday-type experiments with waves launched in the linearly polarized TE_{11} mode in a circular waveguide at frequencies in the range of 4600 to 5500 megacycles, the dielectric being the electrons present in the plasma of a gas discharge. The composite element, consisting of a section of waveguide with an electron-gas generating tube inside it and with a magnetic field generator surrounding the whole, may be referred to as a "magneto-optic" component. For magnetic fields not too near that field corresponding to electron gyroresonance with the signal frequency, not only were the expected Faraday rotations obtained, but they were of quite large magnitude. The results of our experiments were summarized in two brief publications.^{1,2} It is evident, in view of the preceding discussion, that the magneto-optic component that produces these rotations constitutes a linear passive³ nonreciprocal microwave circuit element, which is furthermore an electronic element. This was pointed out by us in our

* Reprinted from *Proceedings of the IRE*, volume 41, pages 295-296; February, 1953. The work discussed in this letter was sponsored by the Signal Corps Engineering Laboratories, Fort Monmouth, New Jersey.

Since this letter was written and the necessary clearance obtained for publication, an article by C. L. Hogan, titled, "Ferromagnetic Faraday Effect at Microwave Frequencies and its Applications," appeared in the *Bell System Technical Journal*, volume 31, pages 1-31; January, 1952. This article describes a realization of Tellegen's gyration by means of the Faraday effect in a ferromagnetic medium. The Faraday rotations are produced in such a medium by interaction of the radio-frequency magnetic field with the medium. In mathematical terms, the permeability is a second-order tensor and the dielectric constant is a scalar. In the dielectric Faraday effect studied by us, the rotations are produced by interaction of the radio-frequency electric field with a free-electron gas; that is, the dielectric constant is a second-order tensor and the permeability is a scalar. A very considerable practical advantage in the dielectric Faraday effect, as obtained in our experiments, is that the electron gas medium may itself be modulated or pulsed. In the ferromagnetic Faraday effect, only the magnetic field can practically be modulated.

† Now with the University of Illinois.

¹L. Goldstein, M. A. Lampert, and J. F. Heney, "Magneto-Optics of an Electron Gas with Guided Microwaves," *Electrical Communication*, volume 28, pages 233-234; September, 1951; also, *Physical Review*, volume 82, pages 956-957; June 15, 1951.

²L. Goldstein, M. A. Lampert, and J. F. Heney, "Magneto-Optics of an Electron Gas for Guided Microwaves: Propagation in Rectangular Waveguides," *Electrical Communication*, volume 28, page 322; December, 1951; also, *Physical Review*, volume 83, page 1255; September 15, 1951.

³Although power is required for production of a free-electron gas, the device is passive insofar as interaction of the free electrons, which lack any significant drift velocity, and the propagating microwave signal is concerned.

presentations of these results at the Eleventh Annual Conference on Physical Electronics at the Massachusetts Institute of Technology in March, 1951 and at the Electron Devices Conference of the Institute at the University of New Hampshire in June, 1951. In addition, we pointed out a particularly cogent application of such a component exploiting its nonreciprocal nature, namely, as a lossless buffer between a signal source and its load, completely independent of reflections at the load (this being accomplished by a 45-degree rotation of the plane of polarization of the signal in the component).

Recently our attention has been called to two articles by Tellegen^{4,5} bearing on the general problem of constructing linear passive nonreciprocal network elements. To relate his work to ours, we may note that the Maxwell equations,

⁴ B. D. H. Tellegen, "The Gyrator, a New Electric Network Element," *Philips Research Reports*, volume 3, pages 81-101; April, 1948.

⁵ B. D. H. Tellegen, "The Synthesis of Passive Resistanceless Fourpoles that May Violate the Reciprocity Relation," *Philips Research Reports*, volume 3, pages 321-337; October, 1948.

as modified by the presence of electrons in a constant magnetic field, are contained implicitly in his equations (33) of the gyrator article. The modification of the Maxwell equations are precisely the replacement of the scalar dielectric constant by a second-order tensor dielectric "constant," the "new" parts of which depend on the magnetic flux density. Tellegen, however, did not pursue the case of anisotropy in a dielectric because voltage step-up is unobtainable in such a medium.⁶

Though, indeed, our magneto-optic component is simply a one-to-one voltage transformer, it still is an eminently realizable linear passive nonreciprocal microwave circuit component. It is furthermore a completely electronic element in that the electron-gaseous medium can itself be modulated or pulsed on and off. Furthermore, one can visualize the nonreciprocal character of the device directly from its rotation properties without recourse to mathematical discussion.

⁶ He discusses this on page 99 of reference 4.

Contributors to This Issue



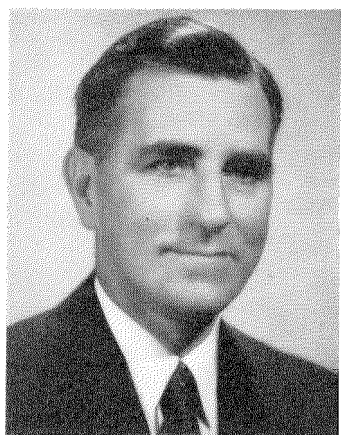
LADISLAV GOLDSTEIN

LADISLAV GOLDSTEIN was born in 1906 in Hungary. He received from the University of Paris a bachelor's degree in 1924, master's in 1928, and doctor of science in 1937.

Dr. Goldstein is an author of the article in this issue on a new microwave circuit component.

He was employed as a research physicist in the Curie Laboratory of the Institute of Radium of the University of Paris from 1928 to 1940. During the following year, he was with the Institute of Atomic Physics of the University of Lyon.

In 1941, he came to New York City where from 1942 to 1944 he was employed as a research physicist by the Canadian Radium and Uranium



HENRY F. HERBIG

Corporation. Since 1945, he was with Federal Telecommunication Laboratories as a senior project engineer. He recently joined the electrical engineering department of the University of Illinois.

Dr. Goldstein is a member of the American Physical Society.

• • •

HENRY FRANK HERBIG was born in Atlanta, Georgia on July 17, 1898. He received the B.S. degree with honors in electrical engineering from Georgia Institute of Technology in 1921.

A paper in this issue reports some of his work on the use of selenium rectifiers for contact protection.

From 1921 to 1923, he was employed by the Western Electric Company.

In 1923, he was placed in charge of the engineering laboratory of the Commercial Cable and Postal Telegraph Companies by Professor Pupin of Columbia University, who was a consultant to that company. His association with that physicist also included postgraduate work at Columbia and continued until the death of Doctor Pupin in 1935.

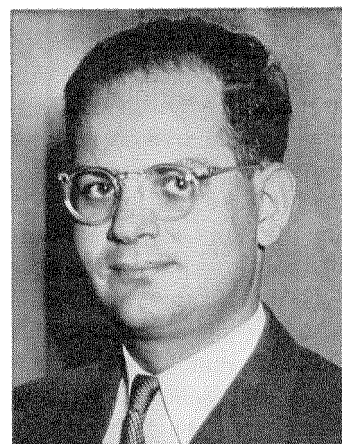
From 1935 to 1938, Mr. Herbig maintained a consulting practice. During the following four years, he was with the North Electric Company, reporting to the president on research and development work.

Rejoining the International System in 1942 as head of the telephone laboratory of International Standard Electric Corporation, he is now assigned to special technical duties at Federal Telecommunication Laboratories.

Mr. Herbig is a member of the American Institute of Electrical Engineers. A number of patents have been granted to him.

• • •

J. A. KOSTRIZA. A photograph and biography of Mr. Kostriza, author of the paper on composite-dielectric coaxial lines, appears on pages 78-79 of the March, 1953, issue.



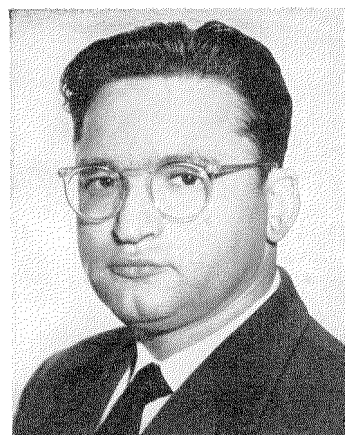
MURRAY A. LAMPERT

MURRAY A. LAMPERT was born in New York City in 1921. He received the B.A. and M.A. degrees from Harvard University.

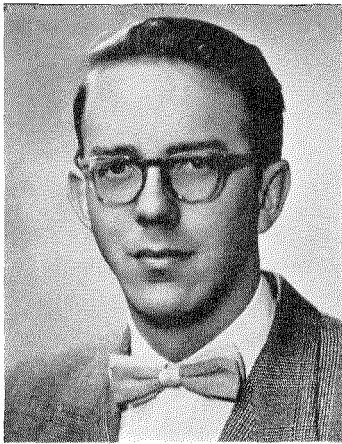
Two papers in this issue report some of Mr. Lampert's studies on gaseous discharges.

During the second world war, he taught in the Army-Navy Officers Electronics Training School at Harvard for two years and spent another year doing optical design work for the Harvard Observatory optical research project.

After the war, he worked for three years at the radiation laboratory of the University of California at Berkeley on the interaction of high-energy particles with nuclei.



PHILIP PARZEN



JOHN T. PEDERSON

From 1949 to 1952, Mr. Lampert was in the vacuum-tube department of Federal Telecommunication Laboratories, where he worked on microwave amplifiers and microwave propagation through electron gases.

In August of 1952, Mr. Lampert joined the staff of the RCA Laboratories Division at Princeton, New Jersey, and has since been engaged in the problems of generating millimeter and submillimeter radiation.

• • •

PHILIP PARZEN was born on June 28, 1916, in Poland. He received the B.S. degree in physics from the College of the City of New York in 1939 and the M.S. degree in physics from New York University in 1946.

Mr. Parzen is the author of two papers in this issue on noise in traveling-wave tubes.

During the second world war, he was employed at the Westinghouse Research Laboratories. Since 1947, he has been with Federal Telecommunication Laboratories and has worked on microwave tubes and electromagnetic-wave propagation.

Mr. Parzen is a member of the American Physical Society.

• • •

JOHN T. PEDERSON was born on August 29, 1931, in Bottineau, North Dakota.

Mr. Pederson wrote the well-illustrated article on production-line paint-

ing. He came to The Coolerator Company in 1951 under a cooperative work-study program set up by the University of Minnesota, where he is working for his degree in mechanical engineering.

• • •

JACQUES VAN CAUWENBERGHE was born in Paris on May 5th, 1915. He studied electrical and mechanical engineering at Brussels University and, after performing his military service in the Belgian Army from 1935 to 1936, obtained his engineering degree in 1939. He then served as an assistant in the physical laboratory of the university.

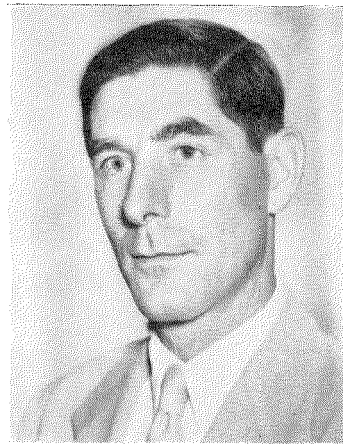
During the first part of the second world war, Mr. Van Cauwenberghe served as a liaison and observation officer in the army, and from 1940 to 1942, he did special measurement and research work at the Monceau-Fontaine colliery.

From 1942 to 1944, he was attached to the signaling department of the Ateliers de Constructions Electriques de Charleroi. In 1944, he rejoined the army as head of the radio section of the Belgian Parachute Regiment. He was injured during parachute training and was then attached to a section dealing with special telephone questions.

Since 1945, Mr. Van Cauwenberghe has been head of the signaling department at Bell Telephone Manufacturing Company in Antwerp. In this issue, he is author of the article on the application of remote signaling and control to electric railways.



J. VAN CAUWENBERGHE



A. J. WARNER

Mr. Van Cauwenberghe is a member of the Association of American Railroads.

• • •

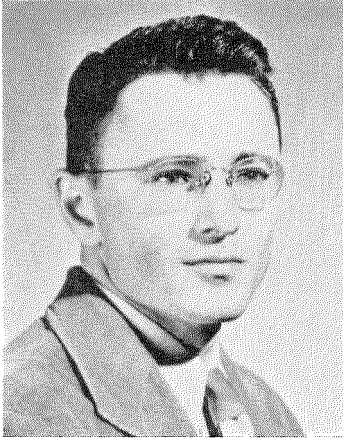
A. J. WARNER was born in London, England, on March 25, 1913. He received the B.Sc. degree in chemistry in 1935 from the University of London.

Mr. Warner is the author of the paper on the new dielectric *IN-420*.

He joined the staff of Standard Telephones and Cables, Limited, as a metallurgical chemist in 1930 and attended college on a leave of absence from 1932 to 1935. He was assigned in 1940 to the new insulants factory at Enfield, Middlesex.

In 1941, he was transferred to the United States to the International Telephone and Radio Manufacturing Company in Newark, New Jersey. In 1945, he became manager of the dielectrics laboratory of Federal Telecommunication Laboratories and in 1949 was appointed technical director of the chemical and physical laboratories. At present, Mr. Warner is technical director of the research and development laboratories.

Mr. Warner is a Fellow of the Chemical Society, London, the Society of Chemical Industry in Great Britain, and the Society of Plastics Engineers in the United States; as well as being a member of the American Chemical Society, American Society for Testing Materials, American Institute of Electrical Engineers, and the American



ALAN D. WHITE

Association for the Advancement of Science. He is also an American delegate to the International Standards Organization TC/61 on Plastics.

• • •

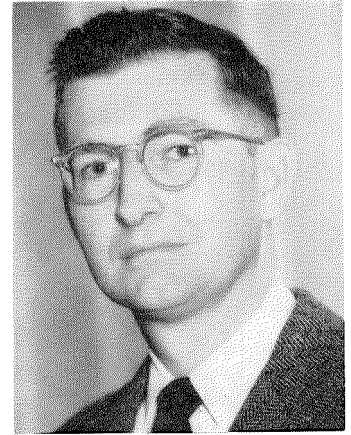
ALAN D. WHITE was born in 1923 in Rahway, New Jersey. He received the B.S. degree in Physics in 1949 from Rutgers University and the M.S. degree

in Physics from Syracuse University in 1952. From 1949 to 1951, he was employed part time as a teaching assistant in the physics department at Syracuse University.

Since 1951, Mr. White has been employed at Federal Telecommunication Laboratories doing research work on the behavior of gas discharges in microwave fields. Some of this work is reported in this issue.

Mr. White is a Member of Phi Beta Kappa and Sigma Xi.

• • •



JOHN D. WINTERS

JOHN D. WINTERS was born in Spokane, Washington, on August 16, 1921. He served in the United States Navy as an electronic technician. The B.S. degree was given him by Stanford University in 1947.

Mr. Winters is coauthor of the paper on the use of selenium rectifiers for contact protection.

He joined the International System in 1947 as a student management trainee, and received diversified training at Federal Telephone and Radio Corporation, International Standard Electric Corporation, and the Cuban

Telephone Company. In 1948 he was transferred to the International Standard Electric Corporation, where he worked on the development of telephone switching systems.

In 1949, he was transferred to Federal Telecommunication Laboratories, where he has been engaged in work on telephone switching systems and more recently on radio transmitters.

Mr. Winters is presently completing work for the M.S.E.E. degree at Newark College of Engineering.

INTERNATIONAL TELEPHONE AND TELEGRAPH CORPORATION

Associate Manufacturing and Sales Companies

United States of America

Capehart-Farnsworth Corporation, Fort Wayne, Indiana
Flora Cabinet Company, Inc., Flora, Indiana
Thomasville Furniture Corporation, Thomasville, North Carolina
The Coolerator Company, Duluth, Minnesota
Federal Telephone and Radio Corporation, Clifton, New Jersey
Federal Electric Corporation, Clifton, New Jersey
International Standard Electric Corporation, New York, New York
International Standard Trading Corporation, New York, New York
I. T. & T. Distributing Corporation, New York, New York
Kellogg Switchboard and Supply Company, Chicago, Illinois

British Commonwealth of Nations

Standard Telephones and Cables, Limited, London, England
Creed and Company, Limited, Croydon, England
International Marine Radio Company Limited, Croydon, England
Kolster-Brandes Limited, Sidcup, England
Standard Telephones and Cables Pty. Limited, Sydney, Australia
Silovac Electrical Products Pty. Limited, Sydney, Australia
Austral Standard Cables Pty. Limited, Melbourne, Australia
New Zealand Electric Totalisators Limited, Wellington, New Zealand
Federal Electric Manufacturing Company, Ltd., Montreal, Canada

North America

Standard Electrica de Mexico, S.A., Mexico City, Mexico.

South America

Compañía Standard Electric Argentina, Sociedad Anónima, Industrial y Comercial, Buenos Aires, Argentina
Standard Electrica, S.A., Rio de Janeiro, Brazil
Compañía Standard Electric, S.A.C., Santiago, Chile

Continental Europe

Vereinigte Telephon- und Telegraphenfabriks Aktiengesellschaft Ozeja, Nissi & Co., Vienna, Austria
Bell Telephone Manufacturing Company, Antwerp, Belgium
Standard Electric Aktieselskab, Copenhagen, Denmark
Compagnie Générale de Constructions Téléphoniques, Paris, France
Le Matériel Téléphonique, Paris, France
Les Téléimprimeurs, Paris, France
C. Lorenz, A.G. Stuttgart, Germany
Mix & Genest Aktiengesellschaft and Subsidiaries, Stuttgart, Germany
G. Schaub Apparatebau G.m.b.H., Pforzheim, Germany
Stüdeusche Apparatefabrik Gesellschaft m.b.H., Nuremberg, Germany
Fabbrica Apparechiature per Comunicazioni Elettriche, Milan, Italy
Nederlandsche Standard Electric Maatschappij N.V., The Hague, Netherlands
Standard Telefon og Kabelfabrik A/S, Oslo, Norway
Standard Electrica, S.A.R.L., Lisbon, Portugal
Compañía Radio Aérea Marítima Española, Madrid, Spain
Standard Eléctrica, S.A., Madrid, Spain
Aktiebolaget Standard Radiofabrik, Stockholm, Sweden
Standard Telephone et Radio S.A., Zurich, Switzerland

Telephone Operating Companies

Companhia Telefônica Nacional, Rio de Janeiro, Brazil
Compañía de Teléfonos de Chile, Santiago, Chile
Cuban American Telephone and Telegraph Company, Havana, Cuba
Cuban Telephone Company, Havana, Cuba
Compañía Peruana de Teléfonos Limitada, Lima, Peru
Porto Rico Telephone Company, San Juan, Puerto Rico

Radiotelephone and Radiotelegraph Operating Companies

Compañía Internacional de Radio, Buenos Aires, Argentina
Compañía Internacional de Radio Boliviana, La Paz, Bolivia
Companhia Radio Internacional do Brasil, Rio de Janeiro, Brazil
Compañía Internacional de Radio, S.A., Santiago, Chile
Radio Corporation of Cuba, Havana, Cuba
Radio Corporation of Porto Rico, San Juan, Puerto Rico

Cable and Radiotelegraph Operating Companies

(Controlled by American Cable & Radio Corporation, New York, New York)

The Commercial Cable Company, New York, New York¹
Mackay Radio and Telegraph Company, New York, New York²
All America Cables and Radio, Inc., New York, New York³
Sociedad Anónima Radio Argentina, Buenos Aires, Argentina⁴

¹Cable service. ²International and marine radiotelegraph services.
³Cable and radiotelegraph services. ⁴Radiotelegraph service.

Laboratories

Federal Telecommunication Laboratories, Inc., Nutley, New Jersey
International Telecommunication Laboratories, Inc., New York, New York
Laboratoire Central de Télécommunications, Paris, France
Standard Telecommunication Laboratories, Limited, London, England

Associate Licensee, Manufacturing, and Sales Companies in Japan

Nippon Electric Company, Limited, Tokyo
Sumitomo Electric Industries, Limited, Osaka